Aus der Medizinischen Klinik und Poliklinik II

der Ludwig-Maximilians-Universität München

Direktorin: Prof. Dr. med. Julia Mayerle

Tumor-specific delivery of 5FU incorporated EGFR targeted aptamers induce cytotoxicity in pancreatic cancer cells

Dissertation

zum Erwerb des Doktorgrades Medizin

an der Medizinische Fakultät

der Ludwig-Maximilians-Universität München

vorgelegt von

Qi Li

aus Beijing, China

2021

Mit Genehmigung der Medizinischen Fakultät

der Universität München

Berichterstatter:	Prof. Dr. med. Julia Mayerle
Mitberichterstatter:	Prof. Dr. Christiane J. Bruns Priv.-Doz. Dr. Michael Haas
Mitbetreuung durch den promovierten Mitarbeiter:	Dr. rer. med. Ujjwal Mukund Mahajan
Dekan:	Prof. Dr. med. dent. Reinhard Hickel
Tag der mündlichen Prüfung:	20.05.2021

Table of contents

Zusammenfassung

Das duktale Pankreasadenokarzinom (PDAC) ist eine der tödlichsten Krebsarten mit einer äußerst schlechten Prognose. Das Fehlen einer Früherkennung und begrenzte therapeutische Möglichkeiten sind die wichtigsten Gründe für die sehr schlechten Verlaufsaussichten. Derzeit wird modifiziertes FOLFIRINOX (mFOLFIRINOX, 5-Fluorouracil / Leucovorin in Kombination mit Irinotecan und Oxaliplatin) als adjuvante, neoadjuvante und palliative Standardbehandlung für Patienten mit PDAC empfohlen. Obwohl dieser Therapieansatz bereits drei Chemotherapeutika enthält, die hocheffizient und stark zytotoxisch sind, können die Tumorpatienten Chemoresistenzen entwickeln die zu einem unbefriedigenden klinischen Ergebnis führen. Darüber hinaus trägt das Fehlen gezielter Therapien bei fortgeschrittenem PDAC weiter zur therapeutischen Missständen bei. Die Entwicklung neuartiger Strategien für die Gabe von Chemotherapeutika oder gezielte Behandlungsansätze sind für das Pankreaskarzinom dringend erforderlich.

In der vorliegenden Studie habe ich RNA-Aptamere mit eingebautem 5-Fluorouracil (5FU) synthetisiert und charakterisiert. Spezifisch-synthetisierte Aptamere binden an den epidermalen Wachstumsfaktorrezeptor (EGFR) von Tumorzellen und werden darüber in die Tumorzelle aufgenommen. Hierbei habe ich den Wirkmechanismus der 5FU-Aptamere untersucht und deren Einsatz als neue zielgerichtete Therapie für das PDAC überprüft. EGFR-bindende Aptamere, die 5FU enthalten (EGFR-5FU-Aptamere), wurden durch in-vitro Transkription synthetisiert. Die Bindung der Aptamere an EGFR wurde mit Hilfe von in-silico Analysen und Bindungsaffinitätsmessungen charakterisiert. Im Anschluss wurde die Anreicherung der Aptamere in den Tumorzellen nachgewiesen und untersucht, welcher Mechanismus für die Endozytose der Aptamere verantwortlich ist. Weiterhin habe ich mittels Immunblot-Analyse überprüft, welchen Einfluss die EGFR-bindenden Aptamere auf den EGFR/ERK-Signalweg von humanen und murinen PDAC Zelllinien haben. In funktionellen Analysen habe ich anschließend die Zytotoxität der Aptamere bestimmt, die Ausbildung von Zellkolonien unter Aptamer-Behandlung getestet und mittels

Durchflusszytometrie die Wirkung der Aptamere auf den Zellzyklus untersucht. Um die Spezifität der Aptamere zu bestimmen habe ich mit dem CRISPR/Cas9 System EGFR-Knockout (KO) Tumorzellen erzeugt und das Zellüberleben von Kontroll- und EGFR-KO Zellen, sowie von 5FU-resistenten Tumorzellen, nach Aptamer-Behandlung gemessen.

Meine Ergebnisse zeigen, dass ich erfolgreich EGFR-5FU-Aptamere erzeugen konnte. Der Einbau von 5FU in die Aptamere beeinträchtigte nicht die Bindungsaffinität zu humanem EGFR. Weiterhin konnte ich nachweisen, dass die Internalisierung von EGFR-5FU-Aptameren in die Tumorzellen EGFR-abhängig war und über eine Clathrin-vermittelte Endozytose erfolgte. Ähnlich wie EGFR-Inhibitoren können die Aptamere den EGFR-Signalweg in humanen PDAC-Zelllinien blockieren. Funktionell führte die EGFR-5FU-Aptamer Behandlung der Tumorzellen zu einer verringerten Ausbildung von Tumorkolonien und induzierte einen Zellzyklusstopp in der G1-Phase. Darüber hinaus konnte ich nachweisen, dass die EGFR-5FU-Aptamere ebenfalls zytotoxisch für Kontroll- und 5FU-resistente PDAC-Zellen waren, aber keinen Einfluss auf EGFR-KO Tumorzellen hatten.

Zusammenfassend konnte ich in meinem Projekt erfolgreich EGFR-5FU-Aptamere synthetisieren, die effektiv an EGFR binden und internalisiert werden. Die gezielte Abgabe von 5FU direkt in die Tumorzelle hat ein enormes Potenzial für eine erfolgreiche Tumortherapie, welche unabhängig von Chemoresistenz-Mechanismen ist.

Summary

Pancreatic ductal adenocarcinoma (PDAC) is one of the deadliest cancers with an extremely poor prognosis. Lack of early detection and limited therapeutic options are the most important reasons for the devastating outcome. Currently, modified FOLFIRINOX (mFOLFIRINOX, 5-fluorouracil/leucovorin combined with irinotecan and oxaliplatin) is recommended as standard treatment for patients with PDAC in an adjuvant, neoadjuvant or palliative setting. Even though the regimen contains already three highly cytotoxic chemotherapeutic agents, the development of chemoresistance leads to an unsatisfactory clinical outcome. Furthermore, the lack of targeted therapies for advanced pancreatic cancer contributes further to therapeutic indecision. Thus, developing novel drug delivery systems or targeted therapy strategies is urgently required for PDAC therapy.

In the present study, I generated and characterized epidermal growth factor receptor (EGFR)-targeted aptamers with intrinsically incorporated 5-fluorouracil (5FU). I analyzed their application in PDAC treatment and investigated the working mechanism for targeted therapy. 5FU-incorporated EGFR-targeted aptamers (EGFR-5FU aptamers) were synthesized by in-vitro transcription and were characterized by in-silico docking and binding affinity measurement. Time-lapsed live cell imaging recorded the uptake of aptamers by PDAC cells and identified the mechanism of endocytosis. I furthermore explored the influence of aptamers on EGFR/ERK signaling by immunoblot analysis using human and mouse PDAC cell lines. To investigate the functional relevance of aptamers, I exhibited colony-forming capabilities of the tumor cells and the influence of the EGFR-5FU aptamers on cell cycle using flow cytometry analysis. Moreover, the CRISPR/Cas9 gene-editing system was implemented to generate *EGFR* knockout (KO) PDAC cells. The impact of aptamers on cell viability was tested on control, *EGFR* KO and 5FU-resistant PDAC cells.

My results demonstrated that I successfully generated EGFR-5FU aptamers. 5FU incorporation into the aptamers did not interfere with their binding affinity to human EGFR. The internalization of EGFR-5FU aptamers into cancer cells was EGFR-

dependent and the mechanism of uptake was based on clathrin-mediated endocytosis. The aptamers blocked the EGFR signaling pathway similarly as EGFR inhibitors in human PDAC cell lines. Furthermore, tumor cell treatment with EGFR-5FU aptamers decreased colony formation and induced cell cycle arrest at the G1 phase. Moreover, EGFR-5FU aptamers reduced the viability of control and 5FU-resistant PDAC cells, but not of *EGFR* KO PDAC cells.

In summary, I successfully synthesized EGFR-5FU aptamers, which displayed effective EGFR targeting and 5FU delivery in PDAC cells. EGFR-5FU aptamers have the potential to improve PDAC therapy and might suspend chemoresistance in the future.

List of abbreviations

Abbreviations	Full name
%	Percent
°C	Grad celsius
5FdU	5-fluoro-2'-deoxyuridine
5FdUTP	5-fluorouracil triphosphate
5FU	5-fluorouracil
aa	amino acid
ALPPL2	Alkaline phosphatase placental-like 2
ANOVA	Analysis of variance
Anti-miRNAs	microRNAs inhibitors
ApDCs	Aptamer-drug conjugates
APS	Ammonium persulfate
ASOs	Antisense oligonucleotides
ATP	Adenosine triphosphate
BCA	Bicinchoninic acid
Bp	Base pair
BSA	Bovine serum albumin
CDA	Cytidine deaminase
cDNA	Complementary DNA
CRC	Colorectal cancer
CRISPR	Clustered Regularly Interspaced Short Palindromic Repeats
CT	Computer tomography
CTP	Cytidine triphosphate
Cy3	Cyanin 3
DAPI	4'6-diamidino-2-phenylindile
dCK	Deoxycytidine kinase
dFdCTP	Gemcitabine triphosphate
DMEM	Dulbecco's Modified Eagle Medium
DMF	Dimethylformamid
DMSO	Dimethylsulfoxide
DNA	Deoxyribonucleic acid
DPD	Dihydropyrimidine dehydrogenase
dTMP	Deoxythymidine monophosphate
DTT	Dithiothreitol
dUMP	Deoxyuridinemonophosphate
ECL	Enhanced chemiluminescene
EDTA	Ethylenediamine tetraacetate
EGF	Epidermal growth factor
EGFR	Epidermal growth factor receptor
ELISA	Enzyme-linked immunosorbent assay

EMT	Epithelial mesenchymal transition
E-value	Expected value
ERK	Extracellular signal regulated kinase
FACS	Fluorescence activated cell sorting
FBS	Fetal bovine serum
FdUMP	5-fluoro-2'-deoxyuridine-5'-monophosphate
FdUTP	5-fluoro-2'-deoxyuridine-5'-triphosphate
FOLFIRINOX	5-fluorouracil/leucovorin combined with irinotecan and oxaliplatin
FUTP	5-fluorouridine-5'triphosphate
g	gram
x g	Gravitation force g (9,897 m/s^2)
GAPDH	Glyceraldehyde 3-phosphate dehydrogenase
gRNA	Guide RNA
GTP	Guanosine triphosphate
h	Hours
HDR	Homology directed repair
HEPES	Hydroxyethyl piperazine N'-2-ethane sulfonic acid
HER	Human epidermal growth factor receptor
IC_{50}	Half maximal inhibitory concentration
IgG	Immunoglobulin G
K_D	Equilibrium dissociation constant
kDa	Kilo Dalton = 10^3 Dalton
KO	Knock-out
M	Molar
mA	Milliampere = 10^{-3} Ampere
mAbs	Monoclonal antibodies
MAPK	Mitogen activated phosphokinases
mFOLFIRINOX	Modified FOLFIRINOX
mg	Milligram = 10^{-3} Gram
min	Minutes
miRNA	microRNAs
ml	Milliliter = 10^{-3} Liter
mM	Millimolar
mRNA	Messenger RNA
MRPs	Multidrug resistance-associated proteins
ms	Millisecond
MW	Molecular weight
ng	Nanogram = 10^{-9} Gram
Ni-NTA	Nickel-nitrilotriacetic acid
nM	Nanometer = 10^{-9} Meter
NSCLC	Non-small cell lung cancer

NTP	Nucleoside triphosphate
OD	Optical density
OPRT	Orotate phosphoribosyl transferase
OS	Overall survival
P/S	Penicillin / Streptomycin
PAGE	Polyacrylamide gel electrophoresis
PAMPA	Parallel artificial membrane permeability assay
PAUF	Pancreatic adenocarcinoma up-regulated factor
PBS	Phosphate buffered saline
PCA	Protocatechuic acid
PCR	Polymerase chain reaction
PDAC	Pancreatic ductal adenocarcinoma
pH	Pondus Hydrogenii
PI	Propidium iodide
pmol	Picomole = 10^{-12} Mole
PRPP	Phosphoribosyl pyrophosphate
PVDF	Polyvinylidene fluoride
RCTs	Randomized controlled trials
RFU	Relative fluorescence units
RNA	Ribonucleic acid
Rpm	Revolutions per minute
RT	Room temperature
s	Second
SCCHN	Squamous cell carcinoma of the head and neck
SD	Standard deviation
SDS	Sodium deodecyl sulfate
SELEX	Systematic Evolution of Ligands by EXponential enrichment
SEM	Standard error of mean
siRNA	Small interfering RNA
TAE	Tris acetate EDTA
TBE	Tris borate EDTA
TBST	Tris buffer saline Tween 20
TCA	Trichloroacetic acid
TEMED	Tetramethylethylenediamine
TK	Thymidine kinase
TKIs	Tyrosine kinase inhibitors
TP	Thymidine phosphorylase
Tris	Trishydroxymethylaminomethane
TS	Thymidylate synthase
U	Units
UDPK	Uridine diphosphate kinase
UK	Uridine kinase

UMPK	Uridine monophosphate kinase
UP	Uridine phosphorylase
UTP	Uridine triphosphate
UV	Ultraviolet
V	Volt
v/v	Volume/volume
w/v	Weight/volume
WB	Western blot
WT	Wild type
µg	Microgram = 10^{-6} Gram
µl	Microliter = 10^{-6} Liter
µM	Micromolar = 10^{-6} Molar

1. Introduction

1.1 Pancreatic ductal adenocarcinoma and chemotherapy

Pancreatic ductal adenocarcinoma (PDAC), originating from the exocrine compartment of the pancreas, constitutes for 90 % of pancreatic cancers [1]. It is the seventh most common malignancy and the fourth leading cause of cancer-related death in developed countries [2]. Only in 2018, 458,918 new cases (2.5 % of cancer cases) were diagnosed and 432,242 deaths (4.5 % of all deaths caused by cancer) were counted worldwide [3]. In addition, the prognosis of PDAC is the worst among all types of solid tumors, and the 5-year survival rate remains as low as 9 % [4].

The poor prognosis is considered mainly because of late diagnosis and limited therapeutic options. Due to unspecific symptoms and an absence of effective early screening methods, over 80 % of patients are diagnosed at advanced tumor stages, where metastases are already present [5]. Although surgical resection is described as a potentially curative therapy for PDAC, only 10–20 % of PDAC patients have resectable tumors [6]. However, surgery alone is not enough. Adjuvant treatment after resection has a clear benefit on survival when choosing the best-fitted therapy [7]. Based on the results from the PRODIGE 24-PA6 (NCT01526135) trial, the median disease-free survival was 21.6 months in the modified FOLFIRINOX (mFOLFIRINOX, folinic acid, fluorouracil, irinotecan and oxaliplatin) group and 12.8 months in the gemcitabine group ($p < 0.0001$) [8]. Therefore, the recommendation for adjuvant standard treatment after tumor resection changed from gemcitabine to mFOLFIRINOX.

For most patients in an advanced metastatic tumor stage, systematic chemotherapy is the mainstay of treatment to prolong survival [9]. In the past, the administration of gemcitabine was the standard of care. However, in recent years new therapy regimens were established. The PRODIGE 4/ACCORD 11 (NCT00112658) trial demonstrated that in comparison to gemcitabine (median overall survival (OS) of 6.8 months), FOLFIRINOX could obviously improve the survival of PDAC patients (median OS of 11.1 months, $p < 0.001$) [10]. The MPACT (NCT00844649) trial revealed a survival advantage for gemcitabine in combination with nab-paclitaxel over gemcitabine alone

(median OS 8.5 versus 6.7 months, $p < 0.001$) [11]. Both of the combination regimens, as first-line therapy for metastatic pancreatic cancer, are associated with a substantial toxicity profile and are only available for patients with good general conditions. For those with poor performance status, the optional regimens are gemcitabine with or without nab-paclitaxel, nanoliposomal irinotecan plus 5-fluoruracil (5FU) or oxaliplatin plus 5FU [12].

Although systematic chemotherapy can help to improve the prognosis, the outcome of metastatic PDAC is still unsatisfying. Even for the fittest patients who can tolerate triple therapy (FOLFIRINOX protocol), which is the most effective regimen, the median OS is only 11 months [13]. Therefore, uncovering new therapeutic options to increase efficiency and to overcome chemoresistance are urgently needed for the treatment of PDAC.

1.2 PDAC and chemoresistance

Although several therapeutic drugs are sufficient among patients with PDAC, the development of tumor resistance limits their efficacy significantly. Resistance to chemotherapy is a multifactorial process [14]. A better understanding of the PDAC chemoresistance is required to overcome this effect. Until now, many PDAC chemoresistance-related studies focused on insufficient drug delivery and inadequate drug biotransformation in cancer cells.

Indeed, administered drugs should be able to reach the tumor sites to display therapeutic effects. However, a rapid drug elimination, degradation, or inactivation by biotransforming enzymes prevent drug targeting within efficient concentration and activity ranges. In addition, cellular drug uptake is a prerequisite for drug cytotoxicity. The downregulation of uptake transporters on the cell membrane and an increased drug efflux from cancer cells make therapeutic drugs less effective [15]. Besides drug availability and cellular uptake, the stromal barrier is another problem for drug delivery. PDAC is characterized by an abundant desmoplastic stroma, which accounts for up to 90 % of the tumor volume [16]. This stromal architecture creates a stiffness of PDAC tissue preventing anticancer agents to penetrate the tumor tissue, which results in

treatment failure.

Changes in cellular drug metabolism are also involved in PDAC chemoresistance [17]. For example, the strongly reduced expression of deoxycytidine kinase (dCK), which is the main rate-limiting enzyme for intracellular gemcitabine activation, is linked with gemcitabine resistance in vitro [18, 19]. Whereas overexpression of dCK promotes gemcitabine sensitivity in orthotopic pancreatic tumor mouse models [20]. Moreover, the protein expression level of dCK in pancreatic cancer tissue from patients treated with gemcitabine alone correlates significantly with progression-free survival [21]. Therefore, dCK is a potential biomarker of gemcitabine sensitivity and provides valuable prognostic indication for PDAC patients treated adjuvant with gemcitabine [22]. Apart from the activating enzyme, the inactivating enzyme also influences drug resistance. The mRNA expression levels of cytidine deaminase (CDA), which catalyzes the metabolic inactivation of gemcitabine, is upregulated in PDAC tumor tissues, compared to healthy tissues [23]. CDA inhibition decreases gemcitabine inactivation and increases the levels of gemcitabine active metabolites in PDAC cells [24]. As I mentioned before, nab-paclitaxel plus gemcitabine are more effective in comparison with gemcitabine alone in PDAC treatment. One explanation for this higher efficiency is that the level of CDA is reduced by nab-paclitaxel, resulting in increased intratumoral gemcitabine levels and promoted tumor regression [25].

As one of the major challenges in PDAC therapy, overcoming chemoresistance is an urgent need to improve the prognosis. Exploring chemoresistance-related mechanisms improved our understanding and revealed novel directions to make anticancer agents more effective. Additional efforts are still required to achieve more advancements in PDAC treatment.

1.3 5-fluorouracil in the treatment of PDAC

5-fluorouracil (5FU) is a fluoropyrimidine and was one of the first chemotherapeutic drugs with anticancer activity. It was first generated by Heidelberger et al. in 1957 and the authors replaced hydrogen with fluorine at the C-5 position of uracil [26]. As a pyrimidine analog, 5FU itself indicates no cytotoxic effects [27]. The anti-tumor effects

are introduced after conversion into several active metabolites, such as 5-fluorouridine-5'triphosphate (FUTP), 5-fluoro-2'-deoxyuridine-5'-triphosphate (FdUTP) and 5-fluoro-2'-deoxyuridine-5'-monophosphate (FdUMP) via several enzymatically catalyzed reactions in cancer cells. The active metabolites FUTP/FdUTP are incorporated into RNA/DNA, which leads to RNA/DNA damage, whereas FdUMP inhibits the activity of thymidylate synthase (TS). As a result, deoxythymidine monophosphate (dTMP) synthesis is inhibited, which induces the blocking of DNA synthesis [28]. The 5FU anabolism and catabolism are shown in **Figure 1.1**.

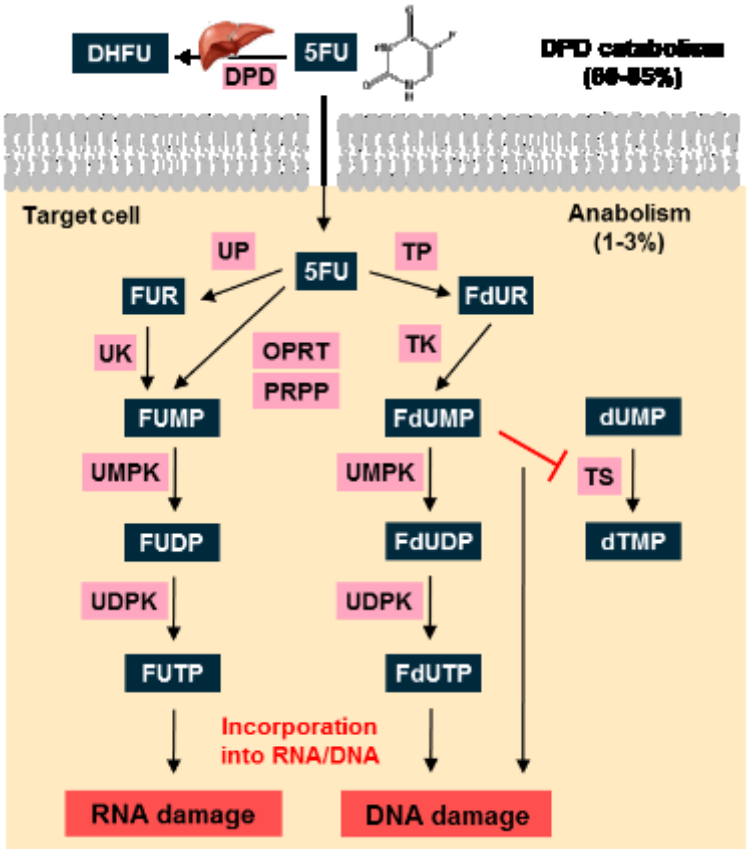

Figure 1.1 5FU anabolism and catabolism. Abbreviations: DPD, dihydropyrimidine dehydrogenase; dTMP, deoxythymidine monophosphate; dUMP, deoxyuridine monophosphate; FdUMP, fluorodeoxyuridine monophosphate; OPRT, orotate phosphoribosyltransferase; PRPP, phosphoribosyl pyrophosphate; TK, thymidine kinase; TP, thymidine phosphorylase; TS, thymidylate synthase; UDPK, uridine diphosphate kinase; UK, uridine kinase; UMPK, uridine monophosphate kinase; UP, uridine phosphorylase. Adopted from references: [28, 29]

5FU is widely used in the treatment of PDAC as the backbone of adjuvant and neoadjuvant therapy [7, 30]. As described above (Chapter 1.1), FOLFIRINOX has

become a standard of care in metastatic PDAC [10]. Recent clinical trials have shown that gemcitabine plus capecitabine (an orally active prodrug of 5-fluorouracil) or mFOLFIRINOX performed better than gemcitabine monotherapy after surgery [8, 31]. Furthermore, the combination of gemcitabine and S1 (an orally active fluoropyrimidine) as neoadjuvant therapy improved the R0 resection rate and overall survival (OS) [32]. However, PDAC is extremely resistant to prototypical 5FU monotherapy. For 5FU-treated patients with advanced PDAC, the median OS rate is 4.41 months and one-year survival rate is 2 %. The overall clinical response rate to 5FU monotherapy is merely 4.8 % [33].

Several studies provide insights into 5FU resistance mechanisms [34]. A deficit in drug uptake is considered as one of the most notable reasons. After administration of 5FU, more than 80 % of the injected dose is degraded in the liver, where dihydropyrimidine dehydrogenase (DPD) is abundantly expressed (**Figure 1.1**). Therefore, less than 20 % of 5FU reaches target sites [35]. As the rate-limiting enzyme in the catabolic cascade of 5FU, DPD influences the circulating concentration of 5FU, which further affects drug delivery. High expression of DPD allows fewer 5FU available in the bloodstream so that no sufficient 5FU can be uptake by cancer cells. As a result, it leads to poor response to 5FU-based chemotherapy for PDAC [36]. Another explanation for inefficient 5FU uptake is increased efflux of 5FU from cancer cells. Multidrug resistance-associated protein 5 (MRP5), which controls the efflux of nucleotides and nucleoside analogs, is overexpressed in PDAC cells [37]. MRP5 inhibition increased significantly the accumulation of 5FU and its metabolites, resulting in enhanced 5FU cytotoxicity in PDAC cells in-vitro. Hence, developing a novel strategy for continuous delivery of stable chemotherapeutics is necessary to increase the efficiency of 5FU treatment and reduce 5FU efflux. A strategy of targeted drug delivery to cancer cells will boost the uptake efficiency, in addition. This will not only help to overcome chemoresistance, but will also diminish the side effects of chemotherapy medications.

1.4 EGFR targeted therapy in PDAC

Epidermal growth factor receptor (EGFR), also known as ErbB-1, is the prototype of

the EGFR family that also includes ErbB-2/HER2, ErbB-3/HER3, and ErbB-4/HER4 [38]. In PDAC, EGFR is overexpressed in over 90 % of the cases and the elevated expression is associated with a higher rate of mortality, substantial tumor growth and the appearance of metastases [39, 40]. EGFR is also associated with multiple cancer-related signaling pathways, playing a role in chemoresistance, angiogenesis and apoptosis [41]. Therefore, EGFR-targeted therapy is considered to be a promising therapeutic strategy for PDAC patients. EGFR-targeted therapies contain monoclonal antibodies (mAbs) and tyrosine kinase inhibitors (TKIs). Anti-EGFR mAbs as EGFR competitive inhibitors can block ligand binding and prevent further receptor dimerization and downstream signaling. EGFR TKIs compete with the adenosine triphosphate (ATP) for binding to the kinase domain of EGFR and inhitibit its phosphorylation, subsequently stopping the activation of downstream signal transduction cascades [42].

Unfortunately, unlike patients with other cancers such as non-small cell lung cancer (NSCLC), colorectal cancer (CRC), squamous cell carcinoma of the head and neck (SCCHN), who can benefit from anti-EGFR mAbs and EGFR TKIs [43-45], EGFR-targeted therapies did not show the expected results for PDAC patients. One meta-analysis including twenty-eight studies (7 randomized controlled trials (RCTs) and 21 cohort studies) reported that the additional EGFR-targeted treatment to chemotherapy did not improve progression-free or overall survival (OS) [46]. Similarly, another meta-analysis including 4564 patients showed that there was no significant improvement in survival for patients with metastatic disease using targeted drugs. The target therapies were erlotinib, cetuximab, rigosertib, elpamotide, bevacizumab, aflibercept, axitinib, masitinib and ganitumab [47].

The failure of EGFR-targeted therapies is probably because of widespread *KRAS* mutation (95 %) in pancreatic cancer (**Figure 1.2**). It is believed that RAS signaling can be stimulated by upstream activation involving EGFR [48]. However, direct blockage of EGFR or an inhibition of the EGFR kinase activity merely prevents the downstream signaling of wild type (WT) RAS. Mutant *KRAS* signaling is not affected resulting in PDAC progression [49]. Thus, EGFR inhibition may not be an encouraging direction

for PDAC therapy.

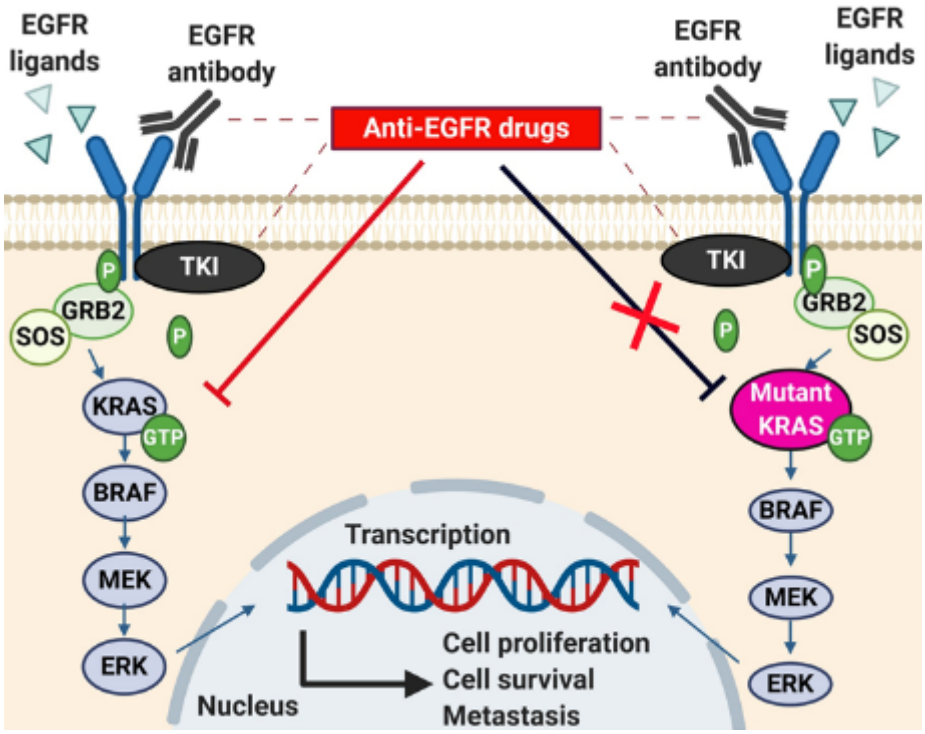

Figure 1.2 Mechanism of response to anti-EGFR drugs in PDAC therapy. Stimulation of epidermal growth factor receptor (EGFR) results in the activation of the RAS/RAF/MAK/ERK signaling cascade. This activation improves cell proliferation and metastasis. Anti-EGFR drugs, including monoclonal antibodies (mAbs) and tyrosine kinase inhibitors (TKIs), inhibit the EGFR/wild-type (WT) KRAS signaling pathway. However, blocking the upstream signaling by anti-EGFR drugs can not inhibit mutant KRAS related signaling cascade in PDAC cells.

Although additional EGFR-targeted therapy cannot improve the survival, EGFR still can be an eligible target for drug delivery because of its high expression on the membrane of PDAC cells. Several EGFR-targeted nanoparticular systems have been designed for PDAC. Amit and colleagues presented their formulation of redox-responsive EGFR-targeting peptide-modified type B gelatin nanoparticles as a carrier for gemcitabine in PDAC treatment [50]. These novel EGFR-targeted gemcitabine loaded nanoparticles displayed a significant cytotoxic profile in-vitro and in-vivo. Ana and colleagues developed erlotinib (anti-EGFR antibody) -conjugated parvifloron D-loaded albumin nanoparticles (BSA NPs) and uncovered increased cytotoxicity in the treatment of pancreatic cancer [51]. Moreover, William and coworkers investigated

cetuximab (anti-EGFR antibody) as a targeting agent for camptothecin-loaded polymeric nanoparticles (NPs). The cetuximab-coupled camptothecin-loaded NPs successfully delivered camptothecin into *KRAS* mutant cetuximab-resistant PDAC cells in-vivo and reduced tumor growth [52]. These results demonstrated that EGFR-targeted drug delivery increased the therapeutic effectiveness for PDAC. Therefore, an EGFR-targeted drug delivery strategy is a remarkable option for PDAC therapy.

1.5 Novel treatment approaches with aptamers in PDAC

Aptamers are a class of single-stranded RNA or DNA ligands selected from Systematic Evolution of Ligands by EXponential enrichment (SELEX, see also **Figure 1.4**), which target specific proteins by their unique three-dimensional structures [53]. Compared to antibodies, which are widely used in many cancers, aptamers have the advantage of higher tissue penetrability, rapid production, low generation cost, less immunogenicity, satisfying thermal stability, and ease of labeling [54, 55]. Thus, aptamers are increasingly popular in the area of cancer diagnostics and therapeutics. The comparison between aptamers and antibodies are shown in **Table 1**.

Table 1 Comparison between nucleic acid aptamers and antibodies.

	Aptamers	Antibodies
Chemical property	Nucleic acids	Protein
Size	Small	Large
Target range	Wide	Limited to antigenic target
Manufacture	In-vitro	In-vivo
Synthesis time	Weeks	Months
Batch	Uniform	Varies
Cost	Cheap	Expensive
Specificity	Higher	High
Affinity	High	High
Stability	Good	Bad
Shelf-life	Long	Limited
Immunogenicity	None or low	High
Modification	Easy	Difficult
Clinical application	Immature	Mature

Adopted from references: [56, 57]

Several studies have already explored the possibility of aptamer-based targeted therapy in PDAC [58]. After SELEX selection and aptamer characterization, some aptamers were confirmed for specifically targeting certain molecules, and for being used as targeted inhibitors. As a result, these aptamers can impede the proliferation of cancer cells by blocking cancer-related signaling pathways, similarly as antibodies. Aptamers are internalized specifically into cells upon binding to their target and work as powerful drug carriers. Various aptamer-based drug delivery systems with easily incorporated oligonucleotides, nucleoside analogs and other chemotherapy drugs were designed and developed [59-61]. These systems displayed their excellent drug delivery efficiency in cancer treatment, which indicated that aptamers could also be optional guides for targeted therapy. The applications of aptamers in targeted therapy are shown in **Figure 1.3**.

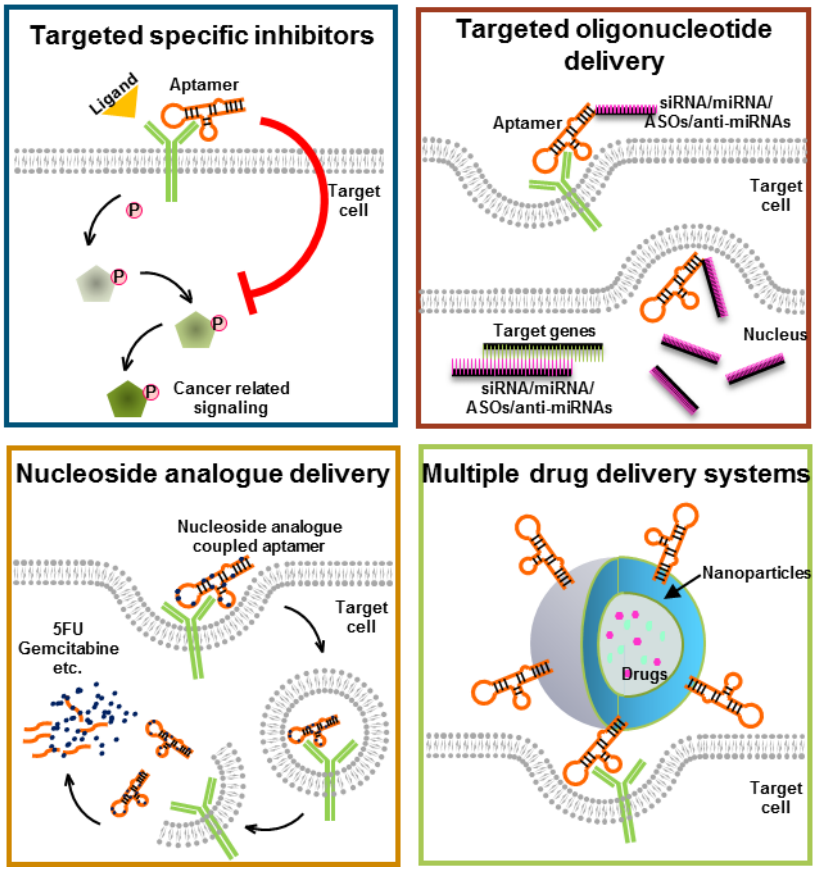

Figure 1.3 The applications of aptamers in targeted therapy. Aptamers are used as specific inhibitors and therapeutic drug carriers in cancer treatment. As carriers, aptamers can have incorporated different kinds of oligonucleotides, nucleotide analogs, or are bound to nanoparticle drug delivery systems. Abbreviations: Anti-miRNAs,

microRNAs inhibitors; ASOs, antisense oligonucleotides; miRNA, microRNAs; siRNA, short interfering RNAs.

Several aptamers were developed as inhibitors for PDAC treatment. For example, Sorah and colleagues generated a RNA aptamer P15 targeting intermediate filament vimentin on the membrane of PDAC cells. Vimentin is a biomarker of epithelial-to-mesenchymal transition (EMT), which plays a crucial role in cancer invasion. Thus, it is not surprising that Vimentin-targeted aptamer P15 has inhibitory effects and significantly impedes PDAC cell invasion [62]. Kim and colleagues created a RNA aptamer (P12FR2) directed against pancreatic adenocarcinoma up-regulated factor (PAUF), which is overexpressed in pancreatic cancer. Aptamer P12FR2 not only inhibits PAUF-induced migration of PDAC cells in-vitro, but also decreases tumor growth in a subcutaneous pancreatic cancer mouse model [63]. These exciting results display that aptamers as inhibitors have the potential to be effective in PDAC therapy.
Among all therapeutics, nucleoside analogs are very special for aptamer-based targeted treatment because of their similar structure with nucleotides, which means they can be incorporated into aptamers in different ways. For example, Pooja Dua et al. integrated five repeats of 5 fluoro 2' deoxyuridine (5FdU) to the 3' end of ALPPL2 (alkaline phosphatase placental like 2)-targeted RNA aptamer. As a result, this drug-loaded ALPPL2-targeted aptamer successfully delivered multiple 5FdU into ALPPL2-expressing pancreatic cancer cells and inhibited cell proliferation in-vitro [64]. Sorah Yoon and co-workers developed a PDAC-targeted RNA aptamer P19, which was synthesized with gemcitabine. They used gemcitabine triphosphate (dFdCTP) to replace cytidine triphosphate (CTP) in RNA aptamers. These aptamer-drug conjugates (ApDCs) not only obviously inhibited cell proliferation in PDAC cells, but also impeded cell proliferation in the gemcitabine-resistant PDAC cells in-vitro [65]. Thus, gemcitabine-incorporated aptamers are an attractive cell-specific drug delivery system in PDAC therapy.
The first human EGFR-targeted RNA aptamer was selected in 2011 using the Systematic Evolution of Ligands by EXponential enrichment (SELEX) assay [66]. The process is summarized in **Figure 1.4**. Briefly, the single-stranded RNA library was

incubated with recombinant human EGFR-Fc (hEGFR) fusion protein. The library was a pool of 10^{14} single-stranded RNA nucleotides, which contains 106 nucleotides including a random region in the middle and fixed sequences on both ends. Then, unbound sequences were washed away, and bound sequences were extracted and used for DNA reverse transcription. The reversed DNA pool was amplified by PCR following in-vitro transcription to generated a new single-stranded RNA library. After 10 cycles of iterative binding, partitioning and amplification, each DNA template was sequenced and each candidate aptamer was characterized.

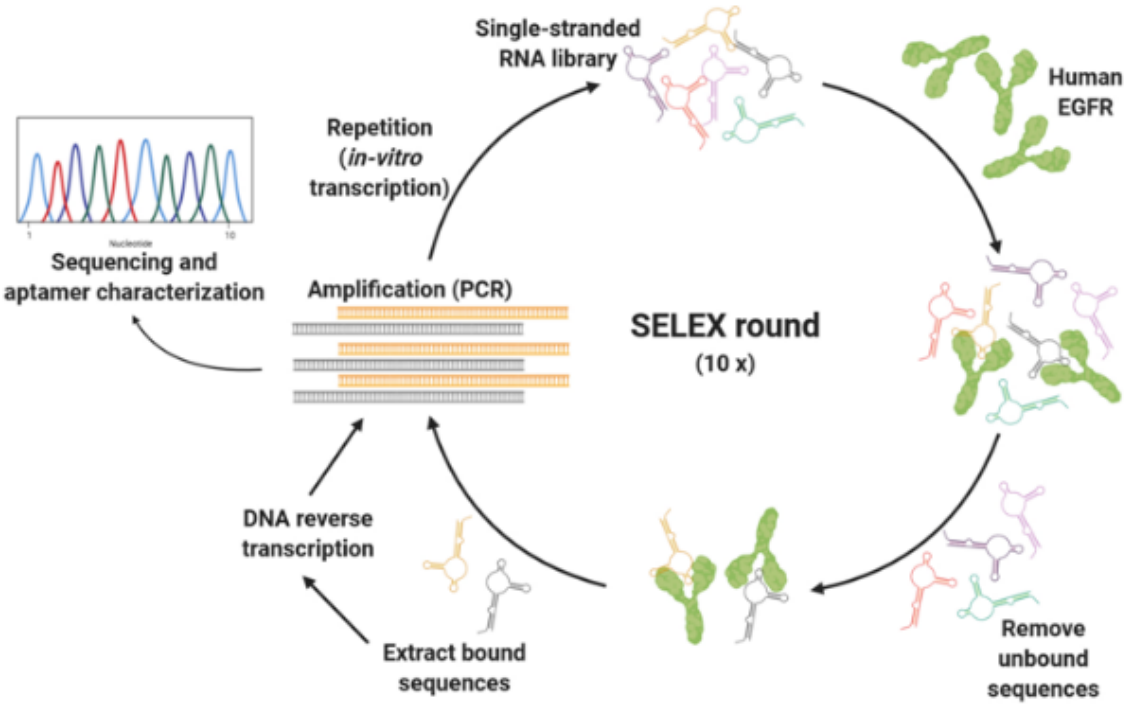

Figure 1.4 The SELEX process for the generation of human EGFR-targeted RNA aptamers. The process of SELEX mainly includes iterative binding, partitioning and amplification. After 10 rounds of selection, the DNA template was sequenced and candidate aptamers were characterized.

Among all selected aptamers, E07 exhibited the best affinity with human EGFR [66]. In addition, it could also target mouse Egfr. Moreover, after binding to the protein, it could be internalized into EGFR-expressing cells. These features made E07 as a promising guide to targeted escort anti-tumor agents into EGFR-expressing cancer cells. Therefore, I chose E07 as a drug carrier in my study. The unmodified EGFR-targeted RNA aptamer E07 is named as EGFR aptamer throughout my study.

2. Aim of the study

Developing novel drug delivery systems or targeted therapy strategies are an urgent need in the treatment of PDAC. Aptamers, which can specifically target proteins by their unique three-dimensional structures, are very promising tools to deliver anti-cancer drugs to specific target sites. Considering EGFR overexpression in 90 % of all PDAC cases, I chose EGFR as the target and designed a novel 5FU-incorporated aptamer (EGFR-5FU aptamer). This new aptamer could be working as an EGFR-targeting 5FU deliverer in EGFR overexpressed pancreatic cancer cells and as an EGFR inhibitor which could block the cancer-related signaling pathway. The hypothesis of EGFR-5FU aptamer working system is shown in **Figure 2**.

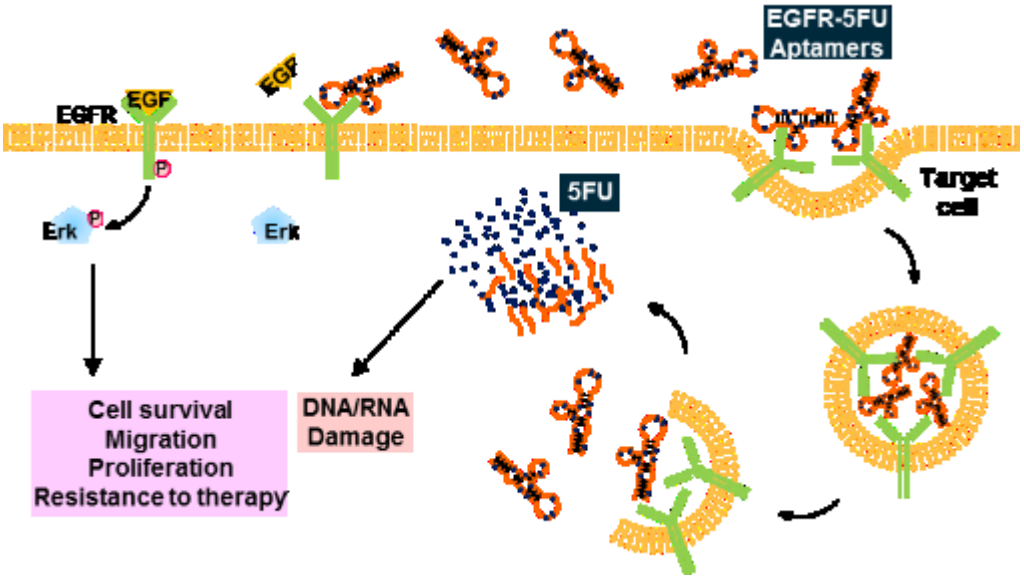

Figure 2. The hypothesis of EGFR-5FU aptamer working system. EGFR is highly abundant on the membrane of PDAC cancer cells. EGF activates EGFR signaling pathway which induces cell survival, migration, proliferation and therapy resistance. EGFR-5FU aptamers bind specifically with the extracellular domain of EGFR and block the EGF-activated EGFR signaling pathway, comparable to EGFR inhibitors. After EGFR-5FU aptamers bind to EGFR, they are internalized by cancer cells via endocytosis. Subsequently, EGFR-5FU aptamers are released from the vesicles and are digested by intracellular lyases, which are setting free a substantial amount of 5FU to induce DNA/RNA damage.

In the project, I addressed the following points:

1. Generating 5FU-incorporated EGFR-targeted aptamer (EGFR-5FU aptamer) and exploring its characteristics.

2. Investigating whether EGFR-5FU aptamer can be internalized into EGFR high expression cancer cells and its uptake mechanism.
3. Determining the influence of aptamer-based 5FU delivery on viability, colony-forming and cell cycle of cancer cells.
4. Identifying whether EGFR-5FU aptamers have an inhibitory effect on EGFR signaling in cancer cells.

3. Materials and methods

3.1 Materials

3.1.1 Antibodies

Table 3.1 Antibodies

Antibody	Type	Host	Application / Dilution	Manufacturer / Reference
Anti-EGFR	Primary	Rabbit	WB / 1:1000	Cell Signaling, Danvers, USA / #4267
Anti-*phospho*-EGFR	Primary	Rabbit	WB / 1:1000	Cell Signaling, Danvers, USA / #3777
Anti-p44/42 MAPK (Anti-Erk1/2)	Primary	Rabbit	WB / 1:1000	Cell Signaling, Danvers, USA / #4695
Anti-*phospho*-p44/42 MAPK (Anti-pErk1/2)	Primary	Rabbit	WB / 1:1000	Cell Signaling, Danvers, USA / #4376
Anti-GAPDH	Primary	Mouse	WB / 1:1000	Meridian Life Science, Memphis, USA / H86504M
Anti-Mouse IgG	Secondary	Mouse	WB / 1:15000	Cell Signaling, Danvers, USA / #7076
Anti-Rabbit IgG	Secondary	Rabbit	WB / 1:15000	Cell Signaling, Danvers, USA / #93702
Anti-Egfr	Primary	Goat	In vitro cells	R&D systems, Minneapolis, USA / #AF1280
Cetuximab (Anti-EGFR)	Primary	Mouse / Human	In vitro cells	Eli lilly, Cambridge, USA

3.1.2 Enzymes and kits

Table 3.2 Enzymes and kits

Enzyme or kit	Manufacturer
RNAse A	Qiagen, Hilden, Germany
RNase free DNase I	Thermo Fisher Scientific, Waltham, USA
T7 RNA polymerase	Thermo Fisher Scientific, Waltham, USA
DNeasy blood & tissue kit	Qiagen, Hilden, Germany
Mini Elute PCR purification kit	Qiagen, Hilden, Germany
Pierce BCA Protein Assay Kit	Thermo Fisher Scientific, Waltham, USA
QUIAEX II (Gel Extraction Kit)	Qiagen, Hilden, Germany

3.1.3 Plasmids

Table 3.3 Plasmids

Plasmid	Manufacturer / Reference
EGFR CRISPR-Cas9 KO Plasmid (human)	Santa Cruz, Dallas, USA / sc-400015
EGFR HDR Plasmid (human)	Santa Cruz, Dallas, USA / sc-400015-HDR
EGFR CRISPR-Cas9 KO Plasmid (mouse)	Santa Cruz, Dallas, USA / sc-420131
EGFR HDR Plasmid (mouse)	Santa Cruz, Dallas, USA / sc-420131-HDR

3.1.4 Chemicals and reagents

Table 3.4 Chemicals and reagents

Chemical or reagent	Manufacturer
5Fluoro-UTP (5FU-TP)	Jena bioscience, Jena, Germany
Agarose SERVA for DNA electrophoresis	SERVA, Heidelberg, Germany
Albumine fraction V, Bovine serum albumin (BSA)	Carl Roth GmbH, Karlsruhe
Ammonium acetate	Sigma-Aldrich, St. Louis, USA
Ammonium persulfate (APS)	Sigma-Aldrich, St. Louis, USA
Boric acid	Sigma-Aldrich, St. Louis, USA
Bromophenol blue	Sigma-Aldrich, St. Louis, USA
Calcium chloride ($CaCl_2$)	Sigma-Aldrich, St. Louis, USA
Crystal violet	Sigma-Aldrich, St. Louis, USA
Cyanin-3-hydrazid	Lumiprobe, Hannover, Germany
DAPI (4′,6-Diamidino-2-phenylindole dihydrochloride)	Sigma-Aldrich, St. Louis, USA
Dimethylformamid (DMF)	Carl Roth GmbH, Karlsruhe, Germany
Dimethyl sulfoxide (DMSO)	Sigma-Aldrich, St. Louis, USA
Disodium hydrogen phosphate (Na_2HPO_4)	Carl Roth GmbH, Karlsruhe, Germany
DNA Loading Dye (6X)	Thermo Fisher Scientific, Waltham, USA
Dulbecco's Modified Eagle's Medium (DMEM), high glucose with L glutamine	Sigma-Aldrich, St. Louis, USA
Dynasore	Sigma-Aldrich, St. Louis, USA
EDTA Solution (0.5 M), pH 8.0	Thermo Fisher Scientific, Waltham, USA
EGFR Recombinant Human Protein, His Tag, Active	Thermo Fisher Scientific, Waltham, USA
Epidermal growth factor (EGF, human)	BD Biosciences, Franklin Lakes, USA
Epidermal growth factor (EGF, mouse)	R&D systems, Minneapolis, USA

Ethanol	Merck, Darmstadt, Germany
Ethylenediaminetetraacetic acid disodium salt dihydrate (EDTA)	Sigma-Aldrich, St. Louis, USA
Fetal Bovine Serum (FBS)	Sigma-Aldrich, St. Louis, USA
Filipin III	Sigma-Aldrich, St. Louis, USA
GeneRuler 100 bp Plus DNA Ladder	Thermo Fisher Scientific, Waltham, USA
GeneRuler Low Range DNA Ladder (10 - 1000 bp)	Thermo Fisher Scientific, Waltham, USA
Genistein	Sigma-Aldrich, St. Louis, USA
Glacial acetic acid	Carl Roth GmbH, Karlsruhe, Germany
Glucose	SERVA, Heidelberg, Germany
Glycerol	Carl Roth GmbH, Karlsruhe, Germany
Glycine	Carl Roth GmbH, Karlsruhe, Germany
HEPES (4-(2-hydroxyethyl)-1-piperazineethanesulfonic acid)	Pan-Biotech, Aidenbach, Germany
Herbimycin A	Sigma-Aldrich, St. Louis, USA
Low Range ssRNA Ladder (50 – 1000 bp)	New England Biolabs, Frankfurt, Germany
Magnesium acetate tetrahydrate	Sigma-Aldrich, St. Louis, USA
Magnesium chloride ($MgCl_2$)	Carl Roth GmbH, Karlsruhe, Germany
Methanol	Merck, Darmstadt, Germany
MTT, (3-(4,5–Dimethylthiazol–2-yl)-2,5-diphenyl tetrazolium bromide)	Sigma-Aldrich, St. Louis, USA
NTPs set (ATPs, CTPs, GTPs, UTPs)	Thermo Fisher Scientific, Waltham, USA
Nuclease free water	Ambion, Naugatuck, USA
PageRuler™ Plus prestained Protein Ladder (10 to 180 kDa)	Thermo Fisher Scientific, Waltham, USA
Penicillin / Streptomycin (P/S) solution	Sigma-Aldrich, St. Louis, USA
Phosphate-buffered saline (1X) (PBS)	Sigma-Aldrich, St. Louis, USA
Pierce™ ECL Western Blotting Substrate	Thermo Fisher Scientific, Waltham, USA
Pierce™ Phosphatase Inhibitor Tablets	Thermo Fisher Scientific, Waltham, USA
Pierce™ Protease Inhibitor Tablets	Thermo Fisher Scientific, Waltham, USA
Plasmid Transfection Medium	Santa Cruz, Dallas, TX, USA
Ponceau S	Sigma-Aldrich, St. Louis, USA
Potassium chloride (KCl)	Carl Roth GmbH, Karlsruhe, Germany
Potassium dihydrogen phosphate (KH_2PO_4)	Carl Roth GmbH, Karlsruhe, Germany
Propidium iodode (PI)	Sigma-Aldrich, St. Louis, USA

Puromycin	Sigma-Aldrich, St. Louis, USA
Reaction buffer for *in-vitro* transcription (5X)	Thermo Fisher Scientific, Waltham, USA
ReadyMix™ REDTaq® PCR Reaction Mix with $MgCl_2$	Sigma-Aldrich, St. Louis, USA
RNA loading dye (2X)	Thermo Fisher Scientific, Waltham, USA
Rotiphorese® NF-Acrylamid / Bis solution 30 %	Carl Roth GmbH, Karlsruhe, Germany
Sodium Acetate	Carl Roth GmbH, Karlsruhe, Germany
Sodium Acetate Solution (3 M), pH 5.2	Thermo Fisher Scientific, Waltham, USA
Sodium azide (NaN_3)	Carl Roth GmbH, Karlsruhe, Germany
Sodium chloride (NaCl)	Carl Roth GmbH, Karlsruhe, Germany
Sodium dihydrogen phosphate (NaH_2PO_4)	Merck, Darmstadt, Germany
Sodium dodecyl sulfate (SDS) pellets	Carl Roth GmbH, Karlsruhe, Germany
Sodium orthovanadate	Sigma-Aldrich, St. Louis, USA
Sodium periodate ($NaIO_4$)	Honeywell, Charlotte, USA
SYBR™ Safe DNA Gel Stain	Thermo Fisher Scientific, Waltham, USA
SYBR™ Safe Green II RNA Gel stain	Thermo Fisher Scientific, Waltham, USA
Tetramethylethylenediamine (TEMED)	Carl Roth GmbH, Karlsruhe, Germany
Trichloroacetic acid (TCA)	Carl Roth GmbH, Karlsruhe, Germany
Tris base	Carl Roth GmbH, Karlsruhe, Germany
Triton™ X-100	Sigma-Aldrich, St. Louis, USA
Trypsin-EDTA solution (10X)	Sigma-Aldrich, St. Louis, USA
Tween®20	Carl Roth GmbH, Karlsruhe, Germany
β-mercaptoethanol	Sigma-Aldrich, St. Louis, USA

3.1.5 Solutions and buffers

Table 3.5 Solutions and buffers

Component	Amount
APS, 10 %	
APS	1 g, 10 % (w/v)
Distilled water	to 10 ml
Blotting buffer for western blot	
BSA	5 g, 5 % (w/v)
TBS-T	to 100 ml
Cell lysis buffer (1X) for protein isolation, pH 8.0	
Tris base	0.3 g, 50 mM

SDS	1 g, 2 % (w/v)
Pierce™ Phosphatase Inhibitor	5 tablets
Pierce™ Protease Inhibitor	1 tablet
Distilled water	to 50 ml
Crystal violet staining solution	
Crystal violet	0.5 g, 0.5 % (w/v)
Methanol	25 ml, 25 % (v/v)
Distilled water	to 100 ml
Diffusion buffer for RNA isolation	
Ammonium acetate	3.85 g, 0.5 M
Magnesium acetate tetrahydrate	214.5 mg, 10 mM
EDTA	29.2 mg, 1 mM
SDS	0.1 g, 0.1 % (w/v)
Distilled water	to 100 ml
FACS Buffer	
BSA	1 g, 1 % (w/v)
Sodium azide	0.05 g, 0.05 % (w/v)
PBS	to 100 ml
Laemilli Buffer (4X), pH 6.8	
Tris base	0.15 g, 125 mM
SDS	0.2 g, 2 % (w/v)
Glycerol	1 ml, 10 % (v/v)
Bromophenol blue	0.05 g, 0.5 % (w/v)
β-mercaptoethanol	500 µl, 2 % (v/v)
Distilled water	to 10 ml
Live cell imaging buffer, pH 7.2	
NaCl	0.91 g, 155 mM
KCl	0.037 g, 5 mM
$CaCl_2$	0.022 g, 2 mM
$MgCl_2$	0.0095 g, 1 mM
NaH_2PO_4	0.024 g, 2 mM
HEPES	0.24 g, 10 mM
Glucose	0.18 g, 10mM
Distilled water	to 100 ml
Phosphate Buffer Saline (PBS, 1X), pH 7.4	
NaCl	8 g, 0.14 M
KCl	0.2 g, 2.7 mM
Na_2HPO_4	0.24 g, 7.1 mM
KH_2PO_4	0.24 g, 0.15mM
Distilled water	to 1000 ml
PI Staining solution I for FACS	
Triton™ X-100	0.1 ml, 0.1 % (v/v)
Dnase-free RNaseA	0.02 g, 0.02 % (w/v)

Propidium iodode	0.002 g, 0.002 % (w/v)
PBS	to 100 ml
Ponceau S staining solution	
Ponceau S	2.5 g, 0.5 % (w/v)
TCA	15 ml, 3% (v/v)
Distilled water	to 500 ml
Sodium acetate, 0.1 M, pH 4.5	
Sodium acetate	0.12 g, 0.1 M
Distilled water	to 10 ml
Sodium acetate, 1 M, pH 6.0	
Sodium acetate	1.2 g, 1 M
Distilled water	to 10 ml
Stripping Buffer, pH 2.0	
Glycine	15 g, 0.1 M
SDS	1 g, 0.1 % (w/v)
Tween®20	10 ml, 1 % (v/v)
Distilled water	to 1000 ml
TAE buffer (10X)	
Tris base	48.5 g, 0.4 M
EDTA	2.9 g, 10 mM
Glacial acetic acid	11.4 ml, 0.2 M
Distilled water	to 1000 ml
TBE buffer (10X), pH 8.3	
Tris base	54.5 g, 450 mM
EDTA	2.9 g, 10 mM
Boric acid	27.8 g, 450 mM
Distilled water	to 1000 ml
TBS-T (10X) (washing buffer for western blot), pH 7.3	
Tris base	12.1 g, 0.1 mM
NaCl	87.7 g, 1.5 M
Tween®20	5 ml, 0.5 % (v/v)
Distilled water	to 1000 ml
Towbin transfer buffer (1X) for western blot	
Tris base	3.03 g, 25 mM
Glycine	14.4 g, 192 mM
SDS	1 g, 0.1 % (v/v)
Methanol	200 ml, 20 % (v/v)
Distilled water	to 1000 ml
Tris-Glycine-SDS (10X) (running buffer for western blot), pH 8.0	
Tris base	30.3 g, 0.25 M
Glycine	144 g, 1.92 M
SDS	10 g, 1% (v/v)
Distilled water	to 1000 ml

Washing buffer for binding affinity measurement	
$MgCl_2$	0.48 g, 5 mM
PBS	to 1000 ml

3.1.6 Cell lines

Table 3.6 Cell lines

Cell line	Characteristics
PaTu-8988T	Cancer cell line (human pancreatic adenocarcinoma)
5FU resistant PaTu-8988T	Cancer cell line (human pancreatic adenocarcinoma), extremely resistant to 5FU
MCF-7	Cancer cell line (human breast adenocarcinoma)
DT6606PDA	Cancer cell line (murine pancreatic adenocarcinoma)

3.1.7 Consumables

Table 3.7 Consumables

Material	Manufacturer
µ-Slide Chamber Slide (8-well)	Ibidi, Gräfelfing, Germany
Cell culture flasks (25 cm, 75 cm)	Sarstedt, Nürnbrecht, Germany
Cell culture plates (6-well, 24-well)	Greiner Bio-One, Kremsmünster, Austria
Cell culture plates (96-well)	Eppendorf, Berzdorf, Germany
Cell culture plates, TC dish (100 mm)	Sarstedt, Nürnbrecht, Germany
Cryogenic tube (2 ml)	STARLAB, Hamburg, Germany
MultiScreen® IP Filter Plate (96-well)	Merck, Darmstadt, Germany
Ni-NTA HIS sorb plates (96-well)	Qiagen, Hilden, Germany
Nitrocellulose blotting membrane	GE Healthcare, Little Chalfont, UK
PCR reaction tube	Biozym, Oldendorf, Germany
Pipette filter tips (10 µl, 200 µl, 1000 µl)	Sarstedt, Nürnbrecht, Germany
Pipette tips (10 µl, 200 µl, 1000 µl)	Sarstedt, Nürnbrecht, Germany
Reaction tubes (0.5 ml, 1.5 ml, 2 ml)	Eppendorf, Berzdorf, Germany
Reaction tubes (15 ml, 50 ml)	Sarstedt, Nürnbrecht, Germany
Scalpel, Feather disposable scalpel	Feather, Osaka, Japan
Serological pipettes, sterile (5 ml, 10 ml, 25 ml)	Sarstedt, Nürnbrecht, Germany
Xtra-Clear Advanced Polyolefin Starseal	STARLAB, Hamburg, Germany

3.1.8 Equipment

Table 3.8 Equipment

Equipment	Manufacturer
Analytical balance	Kern, Göggingen, Germany

BD Accuri™ C6 Plus personal flow cytometer	BD Biosciences, Franklin Lakes, USA
Beach scale	Kern, Göggingen, Germany
Biological safety cabinet, HeraSafe™	Thermo Fisher Scientific, Waltham, USA
Centrifuge 5417R	Eppendorf, Hamburg, Germany
Centrifuge 5418	Eppendorf, Hamburg, Germany
Centrifuge 5702R	Eppendorf, Hamburg, Germany
FLUOstar® Omega Microplate Reader	BMG Labtech, Ortenberg, Germany
Fusion Fx Vilber Lourmat	Vilber Lourmat GmbH, Eberhardzell, Germany
Heracell 240 CO_2 Incubator	Marshall Scientific, Hampton, USA
inoLab pH 720	WTW, Weilheim, Germany
IX50 Phase contrast inverted microscope	Olympus, Shinjuku, Japan
Leica Fluorescence microscope	Leica, Wetzlar, Germany
Mastercycler® pro vapo.protect	Eppendorf, Hamburg, Germany
Mini PROTEAN® Tetra Cell	Bio-Rad, Herkules, USA
Mini Trans-Blot® Module	Bio-Rad, Herkules, USA
Pipetboy acu 2	Integra, Biebertal, Germany
PIPETMAN® classic	Gilson, Middleton, USA
PowerPac™ Basic Power Supply	Bio-Rad, Herkules, USA
Sonoplus HD2070 with MS72 microtip	Bandelin, Berlin, Germany
SpectraMax® Plus 384 Microplate Reader	Molecular Devices, San José, USA
TS1 ThermoShaker	Biometra GmbH, Göttingen, Germany
Vortex mixer	Neolab, Heidelberg, Germany

3.1.9 Softwares and graphical user interface

Table 3.9 Softwares and graphical user interfaces

Program	Producer
Affinity Designer	Serif (Europe) Ltd., Nottingham, UK
EndNote X8	Thomson Reuters, New York City, USA
FCS Express 6 plus Reader	De Novo, Pasadena, USA
FusionCaptAdvance (7.17.02a)	Vilber Lourmat GmbH, Eberhardzell, Germany
GraphPad Prism 5	GraphPad Software, Inc., La Jolla, USA
ImageJ	By Wayne Rasband, NIH, Bethseda, USA
Leica MM AF 1.5	Leica, Wetzlar, Germany
Microsoft Office (Word, Excel, PowerPoint)	Microsoft, Redmond, USA
Omega-Data Analysis	BMG Labtech, Ortenberg, Germany
R (version 3.5.2)	Open-source software
R studio (version 1.1.442)	Open-source software
Softmax Pro 7.0	Molecular Devices, San José, USA

3.2 Methods

3.2.1 Aptamers synthesis

Based on the reported sequence of a RNA aptamer targeting human EGFR (E07 aptamer) [66], I designed a single-strand DNA template including starting sequence, T7 promoter sequence and E07 aptamer sequence. The T7 promoter sequence assured the generation of RNA aptamers in in-vitro transcription by T7 RNA polymerase. The starting sequence improved the efficiency of the promoter. E07 aptamer sequence was the template for aptamers' creation. Firstly, the DNA template was amplified by polymerase chain reaction (PCR). The sequences of the DNA template and PCR primers are provided in **Table 3.10**. The PCR reaction was prepared as described in **Table 3.11**. The PCR program is listed in **Table 3.12**. Then, the PCR products were purified by the Mini Elute PCR purification kit (see Chapter 3.2.2). The DNA concentration was measured by SpectraMax® Plus 384 Microplate Reader. The successful DNA amplification was confirmed by agarose gel electrophoresis (3 % (w/v) agarose in TAE buffer (1X) containing 0.02 % of SYBR™ Safe DNA Gel Stain). After adding DNA loading dye (6X) to the DNA sample, the mixture was loaded on a 3 % agarose gel. In addition, a DNA standard (Low Range DNA Ladder, 10 bp plus) was administered to compare the lengths of DNA fragments. For separation, 70 V was applied for 45 min and the separated DNA was visualized under UV light exposure in Fusion Fx Vilber Lourmat.

Table 3.10 Sequences of the DNA template and PCR primers

Name	Sequence (5'→3')
EGFR targeted DNA template	AGCGAATTC*TAATACGACTCACTATA*GGGTGC CGCTATAATGCACGGATTTAATCGCCGTAGAA AAGCATGTCAAAGCCG (sequence in italic represents T7 promoter sequence and underlined sequence depicts aptamer sequence)
Primer, E07-Forward	AGCGAATTCTAATACGACTC
Primer, E07-Reverse	CGGCTTTGACATGCTTTTC

Table 3.11 DNA template PCR reaction (per 20 µl)

Component	Amount
ReadyMix™ REDTaq® PCR Reaction Mix with $MgCl_2$	10 µl
Forward primer (10 µM)	0.5 µl
Reverse primer (10 µM)	0.5 µl
DNA template (100 pM)	2 µl
Nuclease-free water	7 µl
	Total volume 20 µl

Table 3.12 DNA template PCR program

Step		Temperature	Duration	Cycle
Initial denaturation		95 °C	10 min	1X
Amplification cycles	Denaturation	95 °C	30 s	35X
	Annealing	60 °C	45 s	
	Elongation	72 °C	50 s	
Final elongation		72 °C	5 min	1X
Storage		4 °C	∞	1X

After that, 5 pmol purified DNA template (see **3.2.2**) was applied in 100 µl in-vitro transcription systems which are provided in **Table 3.13** and **Table 3.14**. Notably, equal amounts of ATPs, CTPs, GTPs and UTPs were used for the generation of EGFR aptamers. Equal amounts of ATPs, CTPs, GTPs and 5FU-TPs were used for the generation of EGFR-5FU aptamers. Thus, 5FU-TPs replaced all UTPs and were intrinsically incorporated into EGFR-5FU aptamers. The reactions were incubated at 37 °C overnight. For DNA template degradation, 5 µl RNase-free DNase I (1 U/µl) was added and the reaction was incubated at 37 °C for another 30 min. To terminate the reaction, 5 µl 0.5 M EDTA solution was added and the reaction was incubated at 72 °C for 5 min. Then, 10 µl sodium acetate (3 M, pH 5.2) and 250 µl 100 % ethanol were added to precipitate the RNA. The reaction was stored at -80 °C for 30 min and centrifuged at full speed for 30 min at 4° C. After drying the RNA pellet, 50 µl nuclease-free water was added to get the desired aptamers solutions.

Table 3.13 Reaction system for generation of EGFR aptamers

Ingredient	Volume
5X reaction buffer	20 µl
NTPs (20 mM) (ATPs, CTPs, GTPs, UTPs)	10 µl

DNA template	5 pmol
T7 RNA polymerase (20 U/µl)	3 µl
Nuclease free water	to 100 µl

Table 3.14 Reaction system for generation of EGFR-5FU aptamers

Ingredient	Volume
5X reaction buffer	20 µl
5FU-NTPs (4mM) (ATPs, CTPs, GTPs, 5FU-TPs)	50 µl
DNA template	5 pmol
T7 RNA polymerase (20 U/µl)	3 µl
Nuclease free water	to 100 µl

The successful generation of aptamers was confirmed by 6 M urea polyacrylamide gel electrophoresis (PAGE). The gel was prepared as described in **Table 3.15**. Urea was used for denaturing secondary and tertiary RNA structures.

Table 3.15 Pipetting scheme of 6 M urea polyacrylamide gel

Ingredient	Volume
NF-Acrylamid / Bis solution 30 %	9.3 ml
TBE (10X)	2 ml
Nuclease free water	8.5 ml
Urea	7.3 g
10% APS (w/v)	100 µl
TEMED	30 µl

The same amount of RNA loading dye (2X) was added to the RNA sample. The mixture was loaded on the 6 M urea polyacrylamide gel, which was pre-run for 30 min, 150 V in TBE buffer (1X). A RNA standard (Low Range RNA Ladder, 50 bp plus) was administered to compare the lengths of RNA fragments. For separation, 150 V was applied for 60 min and the gel was stained with Sybr Green II RNA Gel stain (0.02 % (v/v) in TBE buffer (1X)) for 30 min. The RNA bands were visualized in UV light and the desired bands were cut by RNase free surgical blades. Finally, the purified aptamers were extracted by the QUIAEX II gel extraction kit (see 3.2.3). The RNA concentration was measured by SpectraMax® Plus 384 Microplate Reader. All RNA samples were stored at -80 °C for further applications.

3.2.2 Purification of PCR templates

After the PCR reaction, the DNA products were purified by the Mini Elute PCR purification kit according to the manufacturer's protocol. Firstly, 5 volumes of Buffer PB (binding buffer) were added in 1 volume of the PCR sample and mixed well. Then, the mixture was transferred into a MiniElute column. DNA was selectively bound to the MiniElute membrane (centrifugation 1 min, 6000 x g, RT) and washed one time with Buffer PE (washing buffer). Finally, DNA was eluted and resuspended in 50 µl nuclease-free water (incubation 1 min, centrifugation 1 min, 6000 x g, RT).

3.2.3 RNA extraction from gels

To extract RNA from polyacrylamide gels, the QUIAEX II gel extraction kit was utilized according to the manufacturer's protocol. Firstly, gels were weighed and 2 volumes of diffusion buffer were added in 1 volume of gel (200 µl for each 100 mg of gel). Then, the sample was incubated at 50 °C for 30 min. After centrifugation at 10000 x g for 1 min at RT, the supernatant was removed and its approximate volume was calculated. 6 volumes of Buffer QX1 (binding buffer) were added to 1 volume of sample. Subsequently, 10 µl of QIAEX II (binding particles) was added and mixed well. RNA was selectively bound to the QIAEX II (incubation 10 min, RT) and washed twice with Buffer PE (washing buffer). Finally, RNA was eluted (incubation 5 min after vortexing, centrifugation 1 min, 10000 x g, RT) and resuspended in 20 µl nuclease-free water.

3.2.4 3'-labeling of aptamers

For all fluorescence measurements, aptamers were labeled with Cy3. In brief, 25 µl aptamers were added into 65 µl sodium acetate (0.1 M, pH 4.5). The final concentration of the RNA sample should not be higher than 0.25 mM (4590 ng/µl). To 90 µl of the aptamers, fresh 10 µl of $NaIO_4$ solution (100 mM, 21.4 mg/ml, dissolved in nuclease-free water) was added and the reaction mixture was incubated at 4 °C in the dark for 2 h. Then, the oxidized aptamers were precipitated from the reaction by adding 10 µl sodium acetate (3 M, pH 5.2) and 250 µl 100 % ethanol. After incubation for 30 min at -80 °C and centrifugation at full speed for 30 min at 4 °C, the RNA pellet was dried and

aptamers were resuspended in 70 µl of water. Next, 2 µl of Cy3 hydrazide (30 mM, 16.3 mg/ml, dissolved in dimethylformamide (DMF)) and 10 µl sodium acetate (1 M, pH 6.0) was added to the oxidized aptamers and the reaction was incubated overnight at 4 °C in the dark. Next day, 10 µl sodium acetate (3 M, pH 5.2) and 250 µl 100% ethanol were added and the reaction mixture was stored at -80 °C for 30 min. The reaction mixture was centrifuged at full speed for 30 min at 4° C. After drying the pellet, 50 µl nuclease-free water was added to get a Cy3-labeled aptamer solution. The concentration of Cy3-labeled aptamers was measured by SpectraMax® Plus 384 Microplate Reader.

3.2.5 In-silico characterization

The RNA secondary structure of the aptamer was predicted using the RNAfold web server (ViennaRNA, rna.tbi.univie.ac.at/cgi-bin/RNAWebSuite/RNAfold.cgi), with default settings. The output prediction was based on the input of RNA sequence:GGGTGCCGCTATAATGCACGGATTTAATCGCCGTAGAAAAGCATGTCA AAGCCG. The RNA tertiary structure of the aptamer was predicted in RNAcomposer (rnacomposer.cs.put.poznan.pl/) from previously obtained secondary structure dot-bracket notation. All the settings during predictions were kept constant with the default server settings. The protein FASTA sequences were obtained from the Protein Data Bank (PDB, www.rcsb.org, for human EGFR) and SWISS-MODEL (swissmodel.expasy.org, for mouse Egfr). The corresponding crystal structures were saved as PDB files for further docking analysis. The sequence homology of the extracellular domain of human EGFR (PDB ID: 4UIP) and mouse Egfr (Swiss-model repository ID: Q01279), was obtained using UVA FASTA Server (fasta.bioch.virginia.edu/fasta_www2/fasta_list2.shtml). All the analysis parameters were kept constant on default server settings.

To identify non-homology-based prediction of RNA binding pockets in the extracellular domain of the EGFR protein, the crystal structures (PDB files) were processed in BindUP (bindup.technion.ac.il/index.html). For human and mouse EGFR protein, the top three candidate pockets for RNA binding were obtained in an automated way.

The dockings of the protein-RNA complex were performed using the multibody interface of the HADDOCK server (haddock.science.uu.nl/services/HADDOCK2.2/haddockserver-multi.html). All docking approaches were performed for targeted binding pockets obtained from BindUP. The interface information was converted into AIRs via the setup page of the HADDOCK. The generated AIR files, together with the input structures, were then subjected to the multibody server as input for docking. Default settings were used for all parameters. The models were evaluated according to the CAPRI criteria [67]. For each docking combination between patches and aptamers, the HADDOCK score was measured according to the website algorithm (depending on several parameters). In general, the lower the score, the less energy is needed for binding, which meant the docking combination is more stable. Thus, the candidate pocket with the lowest HADDOCK score represented the best possible pocket for aptamer binding.

After identifying the best possible pocket on the EGFR protein (or Egfr protein) for aptamer binding, I identified overlap and hindrance of aptamers binding with EGF binding pocket using in-silico docking on the HADDOCK server. The EGF binding pocket in EGFR protein (or Egfr protein) was obtained from Ogiso and Hideo, et al. [68].

3.2.6 Binding affinity of aptamers-protein complexes

The kinetics of aptamer binding to EGFR protein was determined by binding affinity measurements, which was performed like a direct enzyme-linked immunosorbent assay (ELISA) [69]. Firstly, a 96-well Ni-NTA HIS sorb plate was washed with washing buffer (PBS with 5 mM $MgCl_2$) for two times. Next, 25 ng of His-tagged EGFR recombinant human protein (2.5 ng/µl, dissolved in PBS with 5 mM $MgCl_2$) was added in each well. Following 2 h of incubation at room temperature (RT), wells were washed to remove unbound protein. Different concentrations of Cy3-conjugated EGFR aptamers and EGFR-5FU aptamers were added and the Cy3 fluorescence was measured in a FLUOstar® omega microplate reader. After incubation at 37 °C for 30 min, the plate was washed three times with washing buffer. Subsequently, the washing

buffer was added again (100 µl/well) and Cy3 fluorescence was measured again. Obtained relative fluorescence units (RFU) were normalized as a percentage to the highest RFU concentration. The design of the 96-well plate for binding affinity measurement is shown in **Figure 3.1**.

Binding affinity is typically reported by the equilibrium dissociation constant (K_d). It is calculated by the formula K_d = (aptamers concentration)*(EGFR protein concentration)/(aptamers-EGFR complex concentration). Aptamer concentration is represented by the RFU value before incubation. Aptamers-EGFR complex concentration is represented by the RFU value after incubation and washing.

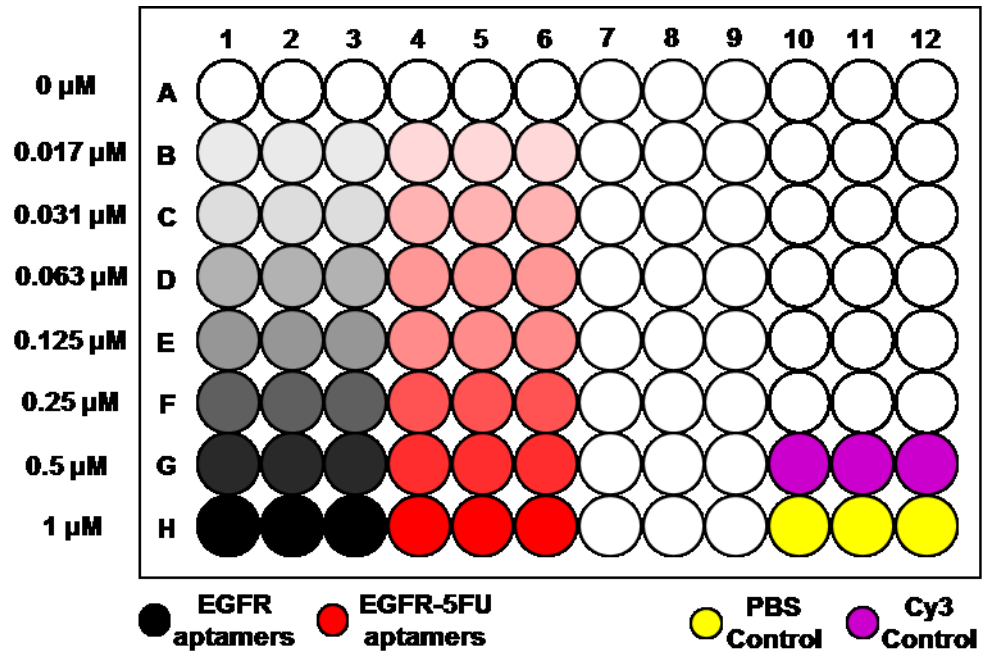

Figure 3.1 Design of binding affinity measurement. Design of 96-well sample plate for measurement of Cy3 coupled aptamers after incubation with EGFR protein at 37 °C for 30 min.

3.2.7 Cell culture

All human cell lines (PaTu-8988T, MCF-7, *EGFR* KO PaTu-8988T, 5FU-resistance PaTu-8988T) and mouse cell lines (DT6606PDA, *Egfr* KO DT6606PDA) were cultured in DMEM with 10 % FBS and 1 % penicillin-streptomycin (P/S) and incubated at 37 °C in a humidified chamber with a saturated atmosphere containing 5 % CO_2. All cell culture experiments were performed under sterile conditions in a biological safety

cabinet. Cells were passaged at a confluency of 80 - 90 % with 0.05 % trypsin (v/v) and 0.2 % EDTA (w/v) in Dulbecco's Phosphate-Buffered Saline (PBS). After incubation at 37 °C for 15 min, trypsin activity was stopped through the addition of cell culture medium. The cell suspension was centrifuged (5 min, 215 x g, RT) and the cell pellet was resuspended in the fresh culture medium. Cells were split in a ratio of 1:20 to 1:100.

To cryopreserve cells, the cell pellet was resuspended in the freezing medium (70 % DMEM, 20 % FBS, 10 % DMSO) and transferred to cryotubes. Cells were stored at -150 °C until use.

3.2.8 DNA isolation from cultured cells

To extract DNA from cultured cells, the DNeasy blood & tissue kit was utilized according to the manufacturer's protocol. The cell pellet (about 2 x 10^6 cells) was subjected to 200 µl PBS with an additional 20 µl proteinase K (20 mg/ml). After adding 200 µl Buffer AL (lysis buffer), the sample was incubated at 56 °C for 10 min. Then, 200 µl 100 % ethanol was added and the mixture (620 µl) was transferred into the DNeasy Mini spin column. DNA was selectively bound to the DNeasy membrane (centrifugation 1 min, 6000 x g, RT) and washed with washing buffer (buffer AW1 for 1 time, buffer AW2 for 1 time). Finally, DNA was eluted (incubation 1 min, centrifugation 1 min, 6000 x g, RT) and resuspended in 200 µl nuclease-free water.

3.2.9 Immunoblotting

Adherent cell samples (in 6-well plates) for immunoblotting were scraped, sonicated and homogenized in 100 µl ice-cold lysis buffer, followed by centrifugation of lysate at 10000 x g at 4 °C for 15 min. The supernatant contained the protein and was transferred into a new 1.5 ml tube. The protein concentration was determined according to the protocol from the Pierce BCA Protein Assay Kit. Immunoblotting was performed as follows: in brief, samples of 40 µg of total protein prepared in laemalli buffer (4X) were loaded on a 10 % SDS-polyacrylamide separating gel complemented with 4 % stacking gel, which was cast in a Peqlab SDS PAGE apparatus. In addition,

a PageRuler™ Plus prestained Protein Ladder (10 to 180 kDa) was administered to compare the lengths of protein fragments. The gels were subjected to electrophoresis at constant 70 V current for 30 min and 125 V for 60 min in Tris-Glycine-SDS running buffer. After completion of the run, gels were transferred to nitrocellulose membranes for immunoblotting using wet transfer methods at constant 100 V current at 4 °C for 2.5 h in transfer buffer. After completion of the transfer, nitrocellulose membranes were stained with ponceau S staining solution to check for transfer. Nitrocellulose membranes were blocked for 1 h using 5 % BSA in TBS-T (1X) and incubated with primary antibody (diluted in 5 % BSA in TBS-T (1X)) overnight at 4 °C. Primary antibodies are listed here: anti-phospho-EGFR (1:1000 dilution), anti-EGFR (1:1000 dilution), anti-phospho-p44/42 MAPK (phospho-ERK1/2) (1:1000 dilution), anti-p44/42 MAPK (ERK1/2) (1:1000 dilution) and anti-GAPDH (1:1000 dilution) as loading control. After washing the membranes with TBS-T three times for 15 min at RT, the membranes were incubated with respective secondary antibodies (1:15000 dilution in TBS-T (1X)) for 1 h at RT, followed by 15 min washes with TBS-T for three times. Afterward, blots were incubated in Pierce™ ECL Western Blotting Substrate (mixing equal parts of the Peroxide Solution and the Luminol Enhancer Solution before use) for 1 minute at room temperature. Finally, blots were visualized in Fusion Fx Vilber Lourmat for chemiluminescence.

3.2.10 Influence of EGFR signaling

PaTu-8988T and DT6606PDA cells were seeded in a 6-well plate at a density of 2.5 x 10^5 cells/well. After culturing for 24 h in DMEM/10 % FBS with 1 % (P/S), cells were serum-starved (culture medium without serum) for 6 h. Then, cells were treated with PBS, 100 ng/ml EGF, 30 nM of EGFR aptamers and a combination of 100 ng/ml EGF with 30 nM of EGFR-aptamers at 37 °C for 0 min (control without treatment), 5 min, 10 min, 20 min, 30 min and 60 min. Subsequently, cells were washed two times with PBS and the protein was harvested and subjected to immunoblotting as described above.
The status of EGFR signaling was detected by the phosphorylation of EGFR and ERK1/2. The bands were quantified with ImageJ. After automatic calculation, the

software gave each band a number based on its intensity and size. The ratio between the number of phospho-EGFR (pEGFR) bands and EGFR bands (pEGFR/EGFR), as well as the ratio between the number of phospho-ERK1/2 (pERK1/2) bands and ERK1/2 bands (pERK1/2/ERK1/2), represented the phosphorylation status of proteins. All the ratio numbers were normalized according to the time point of 0 min.

3.2.11 Time-lapsed live cell imaging and elucidation of the uptake mechanism

To observe the uptake of EGFR-5FU aptamers into PDAC cells, fluorescence time-lapsed live cell imaging was performed. To assess possible uptake mechanisms, I checked the availability of specific inhibitors to block different uptake pathways separately (**Figure 3.2**) [70-72].

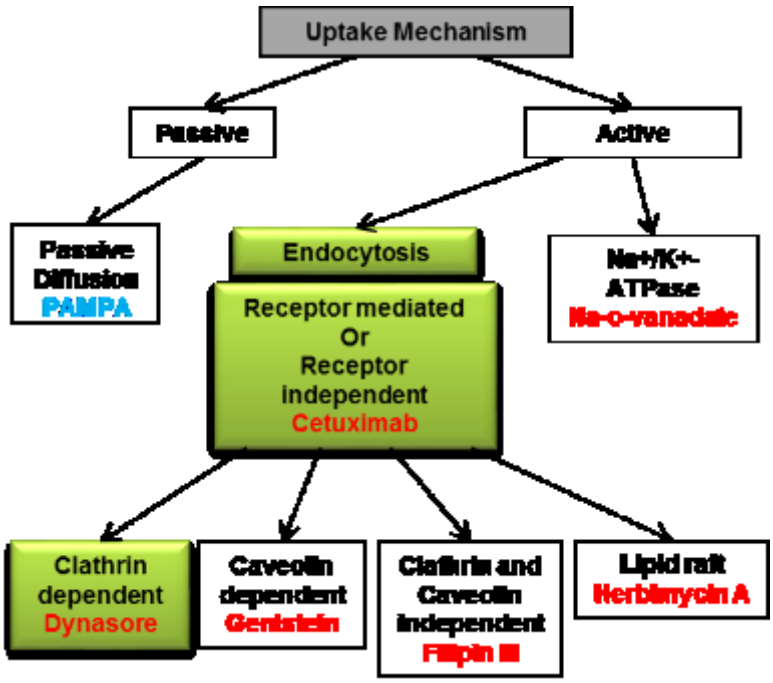

Figure 3.2 Illustration of uptake mechanism. Different uptake pathway can be inhibited by several inhibitors (red). Parallel artificial membrane permeability assay (PAMPA) is the method to confirm passive diffusion (blue).

PDAC cells were seeded in µ-Dish 8-well chamber slides at a density of 5000 cells/well. Following 24 h of incubation, cells were preincubated either with cetuximab (50 µg/ml, 12 h), dynasore (10 µM, 30 min), sodium orthovanadate (10 µM, 30 min), herbimycin

A (1 μM, 1 h), genistein (100 μM, 2 h), filipin (5 μg/mL, 1 h) or PBS (as control). Following incubation, cells were washed with PBS and nuclei were tagged by DAPI (1 μg/ml) in live cell imaging buffer for 15 min at 37 °C. Cells were subsequently washed and subjected to live cell imaging. Cells were treated with 50 nM of Cy3-conjugated EGFR-5FU aptamers and time-lapsed live cell fluorescence microscopy was carried out for 120 min at 37 °C under controlled atmosphere with 5 % CO_2 supply and in heated chambers on a Leica DM6000B microscope (Duration: 120 min, interval time: 2.5 min, camera exposure time for Cy3 channel: 5 ms, camera exposure time for DAPI channel: 20 ms). Quantification of Cy3 fluorescence reflected the accurate uptake of aptamers. The calculation was performed by Leica MM AF 1.5 software. When cells were depicted manually, the average intensity of Cy3 fluorescence was obtained. The mean of average intensity in different areas (cells) represented the quantity of EGFR-5FU aptamers. All numbers of average intensity were normalized as a percentage to the highest average intensity.

3.2.12 Parallel artificial membrane permeability assay (PAMPA)

To evaluate whether EGFR-5FU aptamers can go through the cell membrane by passive diffusion, parallel artificial membrane permeability assay (PAMPA) was performed. MultiScreen® IP Filter Plate (96-well) and Cy3-conjugated EGFR-5FU aptamers were used in this assay. The 96-well MultiScreen® IP Filter Plate contains a 96-well filtration plate with a hydrophobic polyvinylidene fluoride (PVDF) membrane on the bottom of the wells and an underdrain. As the PVDF membrane imitates the biological membranes, such as cell membranes, the spaces on both sides of the membrane mimic the pattern of inside and outside of the cell. Since this PVDF membrane is artificial, and no energy is needed to complete any active transport, the molecule passes the PVDF membrane is able to diffuse throughout the biological membrane, too.

The 96-well MultiScreen® IP Filter Plate was washed by PBS with 5mM $MgCl_2$ buffer. Following washing, different concentrations of Cy3-conjugated EGFR-5FU aptamers were added into the wells. During incubation at RT for 24 h in the dark, Cy3

fluorescence was measured at the prescribed times (0 min, 5 min, 10 min, 30 min, 60 min, 240 min, 24 h) in FLUOstar® omega microplate reader. Obtained relative fluorescence units (RFU) were corrected for bleaching and autofluorescence. A decrease in fluorescence compared to the corresponding control depicted the amount of EGFR-5FU aptamers passing through the artificial membrane by diffusion.

3.2.13 MTT assay

To assess cell viability under various conditions, MTT assay was performed. Briefly, cells were plated in triplicate in 96-well plates at a density of 5000 cells/well and allowed to adhere for 24 h. The next day, cells were subjected to different concentrations of 5FU and EGFR-5FU aptamers. After 72 h, 3-(4,5-methylthiazol-2-yl)-2,5-diphenyl-tetrazolium bromide (MTT) (20 µl/well, 2.5 mg/ml stock concentration) was added into the wells and the plates were incubated at 37 °C for 4 h. Following incubation, the medium was removed and DMSO was added (200 µl/well) and the plate was incubated at 30 min in the dark to solubilize formazan crystals. The optical density (OD) value was then measured at a wavelength of 570 nm (SpectraMax Plus 384 Microplate Reader) and the cell viability was calculated as a percentage compared to no treatment control.

For selective inhibition of EGFR, cells were plated in triplicate in 96-well plates at a density of 5000 cells/well and allowed to adhere for 24 h. Cells were incubated with 250 nM of anti-human EGFR monoclonal antibody (cetuximab) or 1 ug/ml of anti-mouse Egfr monoclonal antibody for 12 h. After incubation, cells were subjected to 30 nM 5FU and EGFR-5FU aptamers. After 72 h of incubation, cells were subjected to MTT incubation followed by quantification of viability as described above.

3.2.14 Colony-forming assay

The colony-forming assay was performed following the protocol from L.C. Crowley et al [73]. PaTu-8988T and DT6606PDA cells were plated in 96-well plates at a density of 5000 cells/well and allowed to adhere for 24 h. The next day, cells were subjected to different concentrations of EGFR-5FU aptamers or an equal amount of 5FU. After

24 h, cells from each well in 96-well plates were counted. 200 cells from each well were plated in 6-well plates. After 10 days, colonies were fixed with 100% methanol for 20 min at RT. Following washing with PBS for two times, the colonies were stained with crystal violet (0.5% (w/v), dissolved in 25% methanol) for 5 min at RT. After washing with PBS for three times, the colonies were visually and photographed in Fusion Fx Vilber Lourmat (ordinary light). The percent of area occupied by colonies was analyzed for each well and recorded by ImageJ. The obtained results were normalized as a percentage compared to no treatment control.

3.2.15 Cell cycle analysis

For cell cycle analysis, cells were treated for 24 h with 5FU (100 μM), EGFR aptamers (50 nM), EGFR-5FU aptamers (50 nM). PBS served as a control. Cell cycle analysis was performed as described previously [74]. Briefly, cells were trypsinized, washed twice with PBS, and 1 × 10^6 cells were fixed in 70 % ice-cold ethanol. The next day, cells were washed twice with PBS and the cell pellet was resuspended in 1ml of propidium iodide (PI) staining solution I and incubated for 30 min at RT. After washing the cells with PBS for another two times, the cell pellet was resuspended in 500 μl FACS buffer. Cell-cycle stages were determined using BD Accuri™ C6 Plus Flow Cytometer. The fluorescence signal was detected through the FL2 channel (Laser Excitation 488nm, Emission Detection 585/40 nm) and the percentage of cells in sub G_1, G_1, S or G_2/M phase was analyzed with the FCS Express 6 plus software.

3.2.16 Generation of *EGFR* knockout (KO) cell lines

By applying the CRISPR/Cas9 (Clustered Regularly Interspaced Short Palindromic Repeats/CRISPR-associated protein 9) system via plasmids, the target gene *EGFR* was specifically knocked out (KO) in the human PDAC cell line PuTu-8988T. The target gene *Egfr* was specifically KO in the murine PDAC cell line DT6606PDA.

The EGFR CRISPR-Cas9 KO Plasmid contains guide RNA (specifically targeting EGFR exon) and the prokaryotic nuclease Cas9. When the plasmid is successfully transfected into cells, the enzyme introduces DNA double-strand breaks where the

guide RNA binds. With the help of EGFR HDR plasmid, DNA repair is mainly committed through homology-directed repair (HDR) mechanisms and precise DNA insertion is introduced at the cleaved target sides [75]. In addition, the puromycin resistance gene (in the EGFR HDR plasmid) is incorporated into DNA cleavage sites. Thus, only positively manipulated cells can survive the puromycin selection.

Human EGFR CRISPR-Cas9 KO Plasmid consists of a pool of 3 plasmids (A, B and C), each contains a different guide RNA (gRNA). Mouse EGFR CRISPR-Cas9 KO Plasmid also consists of a pool of 3 plasmids (D, E and F) with different single-guide RNAs. The DNA sequences and positions for guide RNA (gRNA) binding are listed in **Table 3.16** and **Table 3.17.**

Table 3.16 DNA sequences and positions for gRNA binding in human *EGFR* gene

Plasmid	The DNA sequence for guide RNA binding (5'→3')	Binding position in the human EGFR gene
A	TGAGCTTGTTACTCGTGCCT	Reverse sequencing, Exon 3
B	GAGTAACAAGCTCACGCAGT	Forward sequencing, Exon 3
C	ATAGTTAGATAAGACTGCTA	Reverse sequencing, Exon 4

Table 3.17 DNA sequences and positions for gRNA binding in mouse *Egfr* gene

Plasmid	DNA sequence for guide RNA binding (5'→3')	Binding position in the human EGFR gene
D	CGGTCAGAGATGCGACCCTC	Forward sequencing, Exon 1
E	ACTGCCCATGCGGAACTTAC	Forward sequencing, Exon 2
F	CGCGCTTACAACTGCTCGGA	Reverse sequencing, Exon 3

Plasmid transfection was performed according to the protocol from Santa Cruz, Dallas, USA. Briefly, tumor cells grew to an 80 % confluency in the 6-well plate and were kept within an antibiotic-free cell culture medium for 24 hours. Then, 1 µg EGFR CRISPR-Cas9 KO Plasmid and 1 µg EGFR HDR Plasmid were diluted into plasmid transfection medium (Solution A, 150 µl). In parallel, UltraCruz® transfection reagent (10 µl per 2 µg of plasmid DNA) was diluted into plasmid transfection medium (Solution B, 150 µl). Solution A was added dropwise into Solution B, the mixture was vortexed immediately and incubated for 30 min at RT. After that, the mixture was added to the 6-well plate for co-transfection. Notably, human EGFR CRISPR-Cas9 KO Plasmid and human

EGFR HDR Plasmid were used for the generation of human *EGFR* KO PDAC cell lines, whereas mouse EGFR CRISPR-Cas9 KO plasmid and mouse EGFR HDR plasmid were used for generation of mouse *Egfr* KO PDAC cell lines.

The transfection was performed for 24 h, followed by puromycin selection (10 µg/ml) for another 120 h. Afterwards, cells were seeded as single cells in a 96-well plate. About 15 days later, colonies derived from one single cell were isolated and transferred to a 24-well plate. The surviving colonies were seeded onto 10 cm dishes. From each single human *EGFR* KO cell clone or mouse Egfr KO cell clone, DNA and protein were isolated. Cell clones were frozen in freezing medium (see 3.2.7) and stored at -150 °C for further applications.

To confirm a homozygous KO of *EGFR (Egfr)* in tumor cell clones, a multiplex PCR was performed. In this experiment, one forward primer and two reverse primers were added into one reaction. The forward primer was designed 5' end upstream of the gRNA binding sites. Reverse primers were designed 3' end downstream of the guide RNA binding site. However, control reverse primers were designed on the EGFR gene, whereas insertion reverse primers were designed on the insertion sequence. The multiplex PCR primers are provided in **Table 3.18** and **Table 3.19**.

Table 3.18 Multiplex PCR primers for human *EGFR* KO cell lines

Primer	Sequence forward (5'→3')	Sequence reverse (5'→3')	Product
Control-A	CAGGCCTTTCT	TGTGTGGAGAGAGTGAAGAAAC	363 bp
Insertion-A	CCACTTAGATT	TAACGGCGCAGAACAGAAA	678 bp
Control-B	TGTGTGGAGAG	AATCTAAGTGGAGAAAGGCCTG	331 bp
Insertion-B	AGTGAAGAAAC	GACCTGAGCTTTAAACTTACCTAGA	614 bp
Control-C	CAGCCTCTCAC	CATGACTGCAATCGTCTACCT	329 bp
Insertion-C	CCTGTAAAT	TAACGGCGCAGAACAGAA	665 bp

Table 3.19 Multiplex PCR primers for mouse *Egfr* KO cell lines

Primer	Sequence forward (5'→3')	Sequence reverse (5'→3')	Product
Control-D	AGCCTCCCTCCT	GACACGCCCTTACCTTTCTT	321 bp
Insertion-D	CTTCTTC	TCGACCTGAGCTTTAAACTTACC	695 bp
Control-E	GGAGAGAATCCC	CTGGCTCAAGTTTCCTTCCTAT	325 bp
Insertion-E	TTTGGAGAAC	GACGTAGAGTTGAGCAAGCA	690 bp

Control-F	CCACCAGAGGAT	CAGGTCTTCTACAGGGTCTTG	325 bp
Insertion-F	CTGAAGATAATAA	GACGTAGAGTTGAGCAAGCA	612 bp

Genomic DNA isolation from cultured cells was performed as described above (see 3.2.8). The DNA concentration was measured by SpectraMax® Plus 384 Microplate Reader. The PCR reactions were prepared as described in **Table 3.20**. The PCR program is listed in **Table 3.21**.

Table 3.20 PCR reaction for *EGFR (Egfr)* gene (per 20 µl)

Component	Amount
ReadyMix™ REDTaq® PCR Reaction Mix with $MgCl_2$	10 µl
Forward primer (10 µM)	0.5 µl
Reverse primer-control (10 µM)	0.25 µl
Reverse primer-insertion (10 µM)	0.25 µl
DNA template	50 ng
Nuclease free water	to 20 µl

Table 3.21 PCR program for *EGFR (Egfr)* gene

Step		Temperature	Duration	Cycle
Initial denaturation		95 °C	10 min	1X
Amplification cycles	Denaturation	95 °C	30 s	35X
	Annealing	60 °C	30 s	
	Elongation	72 °C	45 s	
Final elongation		72 °C	5 min	1X
Storage		4 °C	∞	1X

Afterwards, 2 µl DNA loading buffer (6X) was added to 10 µl of the PCR reaction mix. The samples were loaded on an agarose gel for electrophoresis (1 % (w/v) agarose in TAE buffer (1X) containing 0.02 % of SYBR™ Safe DNA Gel Stain). Additionally, a DNA standard (DNA Ladder, 100 bp plus) was administered to compare the lengths of DNA fragments. For separation, 70 V was applied for 45 min and the separated DNA was visualized under UV light exposure in Fusion Fx Vilber Lourmat.

The protein of every single clone was also collected. Western blot analysis was performed to confirm the loss of EGFR protein expression in human *EGFR* KO cell lines. The western blot was performed as described above (see 3.2.9).

3.2.17 Statistical analysis

Data are expressed as mean ± SEM unless otherwise stated and analyzed and plotted in R and R studio. IC_{50} (half-maximal inhibitory concentration) calculations were performed using the Bioconductor package, GRmetrics. The dose-response analyses were performed using the add-on package, drc. Normally distributed two-grouped data were analyses using the unpaired t-test. Multigroup data were analyzed by a one-way ANOVA test followed by Dunn's multiple comparison post-hoc test. Statistical correlations were analyzed using the Pearson test. $p < 0.05$ was considered as statistically significant.

4. Results

4.1 Generation of EGFR-targeted aptamers (EGFR aptamers) and 5FU-incorporated EGFR-targeted aptamers (EGFR-5FU aptamers)

Developing novel chemotherapeutic delivery platforms to elicit tumor-targeted therapeutic responses and elucidating its basis in averting chemoresistant tumors are clinical needs for PDAC therapy. Considering EGFR overexpression in 90 % of PDAC cases [39], EGFR-targeted drug delivery strategies are promising to improve the drug delivery into cancer cells. Aptamers are single-strand oligonucleotides, which can specifically target a protein by their unique three-dimensional structure. In addition, they have the potential to load high amounts of drugs for targeted delivery [55]. To improve the efficiency of drug delivery for the treatment of PDAC, I generated a novel EGFR-targeted RNA aptamer with intrinsically incorporated 5FU (EGFR-5FU aptamer) to deliver an abundant amount of active 5FU metabolites into cancer cells. As control, I generated also normal EGFR aptamers without any modifications. The sequence of aptamer was acquired from the published EGFR-targeted RNA aptamer E07 (named EGFR aptamer throughout my study), which was selected by targeting a recombinant human EGFR-Fc receptor fusion protein [66].

The generation process of aptamers comprised DNA template amplification, RNA transcription and RNA purification (**Figure 4.1 A**). Firstly, the designed single-stranded DNA template (80 bp) was ordered and amplified by PCR. Successful amplification of the DNA was checked by gel electrophoresis showing the desired 80 bp band (**Figure 4.1 B**). For RNA in-vitro transcription, T7-RNA polymerase requires double-stranded DNA templates, thus, the 80 bp PCR product (double-strand DNA) was used for RNA synthesis. To generate 5FU-incorporated EGFR-targeted aptamers, uridine triphosphates (UTPs) were substituted with 5-fluorouracil triphosphates (5FU-TPs) in the RNA synthesis reaction. Moreover, T7 polymerase transcribes only the DNA downstream of the T7 promoter, meaning the length of the RNA product obtained from in-vitro transcription is shorter than the length of the DNA template. The starting and T7 promoter sequence in the DNA template were 26 bp, the synthesized EGFR

targeted aptamer was 54 bp. Urea polyacrylamide gel electrophoresis (PAGE) confirmed the successful generation of aptamers showing the desired 54 bp band for EGFR aptamers and EGFR-5FU aptamers (**Figure 4.1 C**). However, the gel also displayed other bands. The bands below 54 bp represented for example uncompleted transcription products. The bands over 54 bp (e.g. 108 bp, 162 bp) represented RNA dimers and tetramers. The reason for RNA dimerization and tetramerization are hydrophobic interactions. Since RNA has hydrophobic pockets, it easily aggregates in aqueous solution. The last step in the aptamer synthesis process was RNA aptamer purification. The desired 54 bp aptamer bands were cut and extracted from the polyacrylamide gel.

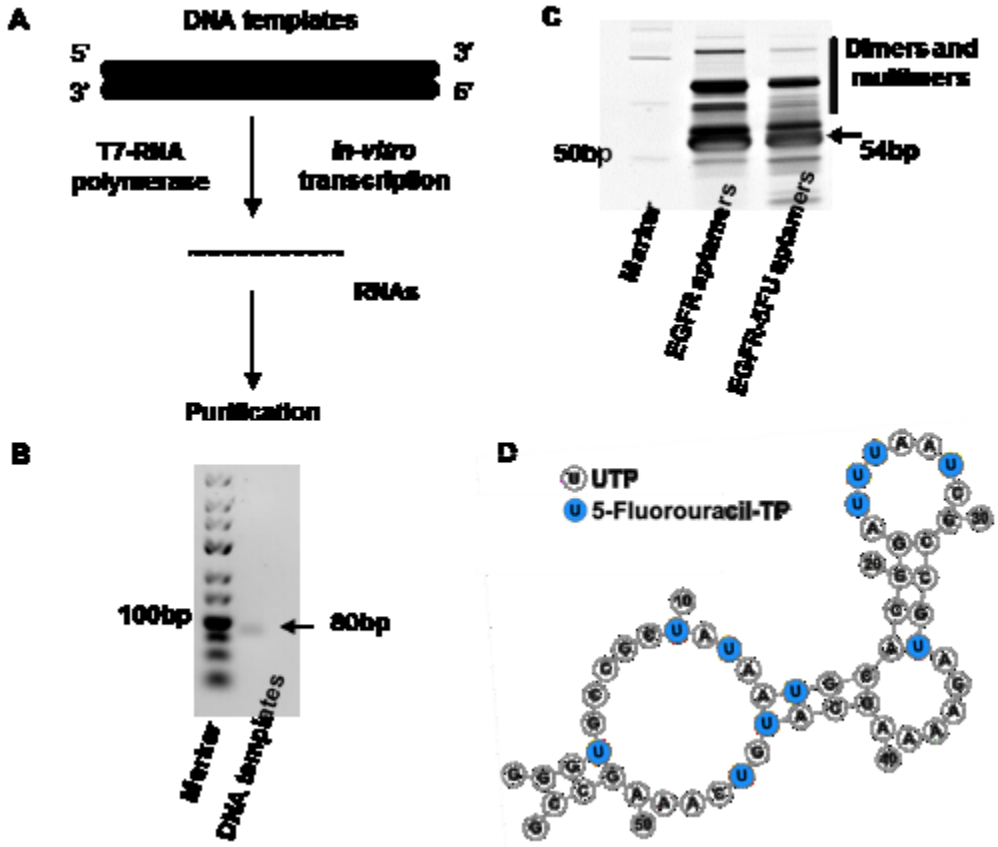

Figure 4.1: Prototype of EGFR-targeted oligonucleotide aptamers. **(A)** Scheme of EGFR-targeted aptamers synthesis. **(B)** 3% agarose gel electrophoresis depicting amplification of the DNA template (80 bp). **(C)** 6M urea PAGE gel electrophoresis depicting synthesis of EGFR aptamers (54 bp) and EGFR-5FU aptamers (54 bp) after in-vitro transcription. **(D)** The secondary single-stranded RNA structure of EGFR-5FU aptamers. Blue nucleotides depict the replacement of UTP with 5FU-TP.

To visualize the newly designed EGFR-5FU aptamer, I entered the RNA sequence in the website of ViennaRNA Web Services. The output displayed the prediction of the secondary single-stranded RNA structure. The sequence of the EGFR aptamer contained 11 UTPs, which were substituted with 5FU-TPs in EGFR-5FU aptamers (**Figure 4.1 D**). Conclusively, one molar EGFR-5FU aptamer incorporates 11 molar 5FU-TPs. In addition, the secondary structure of EGFR aptamers and EGFR-5FU aptamers form a unique cloverleaf shape that is necessary for specific EGFR targeting (**Figure 4.1 D**). Overall, abundant 5FU was incorporated in a small EGFR targeted agent, which implied the possibility of improving drug delivery into cancer cells.

4.2 In silico characterization of EGFR aptamers and EGFR-5FU aptamers

In the previous report, EGFR aptamer was found to be internalized by EGFR expressing human cancer cells and mouse cancer cells [66]. To understand its binding across species, I checked the protein sequences of human and mouse EGFR on the website of Protein Data Bank and SWISS-MODEL. The length of the extracellular domain was 621 amino acids (aa) for human EGFR and 623 aa for mouse Egfr. The UVA FASTA Server was used to compare the protein sequence of the extracellular domain between human and mouse EGFR.

In the matrix plot (**Figure 4.2.1**). The x-axis displays the length of the extracellular domain of human EGFR (positions of Receptor L-domain (Rcpt_L-dom) and Furin-like repeat (Furin_repeat) are on the right side). The y-axis exhibits the length of the extracellular domain of mouse Egfr (positions of Rcpt_L-dom and Furin_repeat are on the top). The lines in the plot represent identical sequences, and the colors demonstrate the strength of concordance as depicted in the legends of the figure. As underlined in red in the figure legend, I observed a 96.8 % sequence homology (**Figure 4.2.1**) between human and mouse variants of EGFR in 623 aa overlap (1-621:1-623). The result of a nearly 97 % similarity implies that the extracellular domain of human and mouse EGFR may have a similar binding site for the EGFR aptamer.

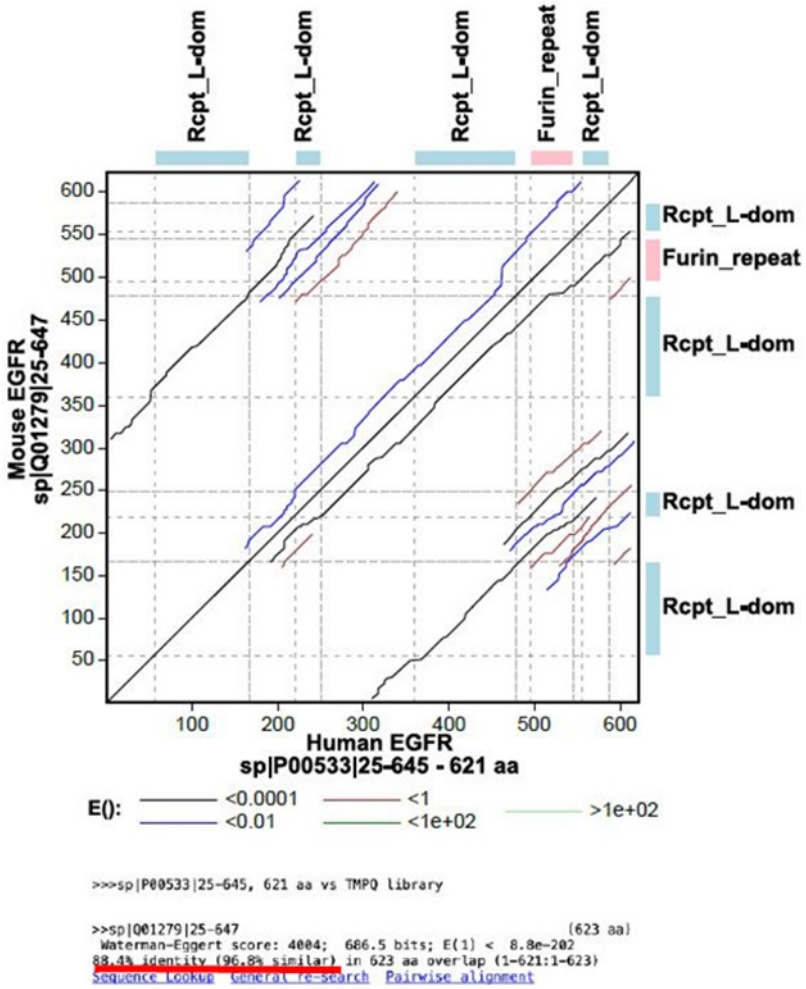

Figure 4.2.1: Sequence homology of the extracellular domain of human EGFR and mouse Egfr. The protein sequences of human EGFR (P00533) and mouse Egfr (Q01279) were acquired from Protein Data Bank and SWISS-MODEL.

Next, I investigated the possible binding sites of EGFR aptamer and EGFR-5FU aptamer in the extracellular domain of human EGFR. The analysis with BindUP identified three possible protein pockets (patch A, patch B and patch C) (**Figure 4.2.2 A**). Afterwards, six protein-RNA docking combinations (patch A - EGFR aptamer, patch B - EGFR aptamer, patch C - EGFR aptamer, patch A - EGFR-5FU aptamer, patch B - EGFR-5FU aptamer and patch C - EGFR-5FU aptamer) were tested on the HADDOCK website. For each docking combination between patch and aptamer, a HADDOCK score was calculated. The lower the score, the lesser energy is needed for binding, which meant the aptamer binding is more stable. The pocket, who showed the lowest HADDOCK score, is the pocket with the highest likelihood of aptamer binding. The results showed that the likeliest pocket for EGFR aptamer and EGFR-5FU aptamer

binding was patch A. Thus, I concluded that EGFR aptamer and EGFR-5FU aptamer share the same binding pocket in the extracellular domain of human EGFR.

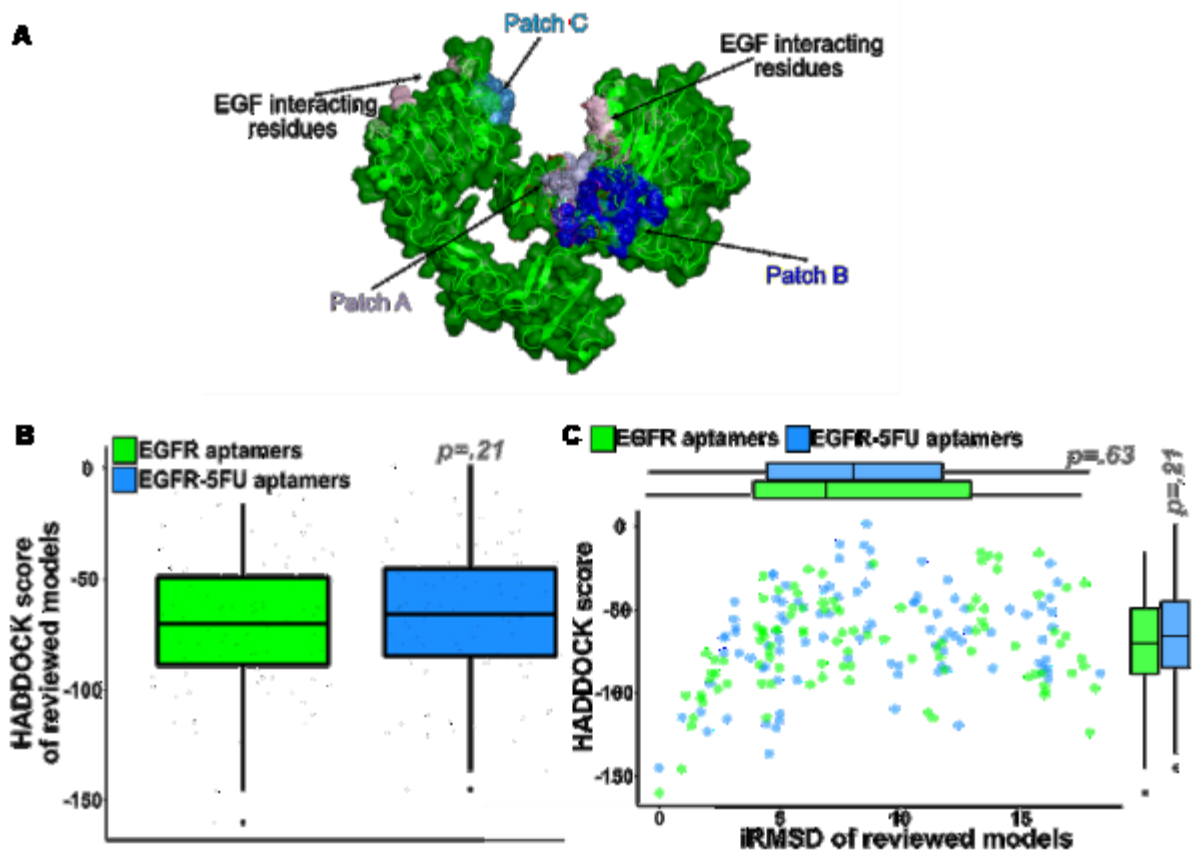

Figure 4.2.2: In silico binding analysis of aptamers with the extracellular domain of human EGFR. (A) 3D structure of the extracellular domain of human EGFR (green) and 3 possible RNA binding pockets (Patch A, Patch B, and Patch C). EGF interacting residues were labeled by pink color. **(B)** Comparison plot of the HADDOCK scores between EGFR aptamers (green) and EGFR-5FU aptamers (blue) docking to patch A (top 200 docking possibilities). **(C)** Distribution of HADDOCK scores (y-axis) in **Figure B** and related interfacial RMSD (iRMSD, root mean square distance) (x-axis). P-value was calculated by two-tailed, unpaired *t*-test.

Since EGFR aptamer and EGFR-5FU aptamer share the same binding site (patch A), I wanted to check the binding stability, which is also represented by the HADDOCK scores (**Figure 4.2.2 B**). In the top 200 docking possibilities, I identified no difference of the HADDOCK scores between EGFR aptamer and EGFR-5FU aptamer (p = 0.21). This points to the fact that the EGFR-5FU aptamer was equally efficient in binding as the EGFR aptamer. **Figure 4.2.2 C** depicts more details about the distribution of these

top 200 HADDOCK scores and the related iRMSD (interfacial root mean square distance) values. iRMSD is the RMSD of the Cα atoms of interfacial residues detected in a native structure concerning their positions in a docking model. iRMSD value increases exponentially as the interface size rise. Lower iRMSD depicts stronger binding. Thus, each dot represents a given score of HADDOCK (y-axis) and iRMSD (x-axis) in one possible binding scenario. iRMSD values of the top 200 selected models did not show significant alteration in EGFR-5FU aptamers docking structures compared to EGFR aptamers (p = 0.63), which further indicates that both aptamers were equally efficient in binding with human EGFR.

Moreover, I performed another analysis in BindUP for the identification of possible protein binding sites in mouse Egfr. Patch a, patch b and patch c were selected (**Figure 4.2.3 A**). The protein-RNA docking analysis of 6 combinations (patch a - EGFR aptamer, patch b - EGFR aptamer, patch c - EGFR aptamer, patch a - EGFR-5FU aptamer, patch b - EGFR-5FU aptamer and patch c - EGFR-5FU aptamer) revealed that EGFR aptamer and EGFR-5FU aptamer shared the same binding pocket (patch b) in the extracellular domain of mouse Egfr. Notably, the aptamer binding pocket differs in human and mouse EGFR. The comparison of HADDOCK scores in the top 200 docking possibilities demonstrated a significant increase in the binding efficiency of EGFR-5FU aptamer compared to EGFR aptamers (p = 0.01) (**Figure 4.2.3 B**). Thus, mouse Egfr binds the EGFR-5FU aptamer more efficiently than EGFR aptamer. **Figure 4.2.3 C** displayed more details about the distribution of these 200 HADDOCK scores and the related iRMSD values. The significant difference in iRMSD values (p < 0.001) confirmed that EGFR-5FU aptamer showed more efficient Egfr binding.

Although the extracellular domain of human and mouse EGFR share around 97 % sequence homology, the aptamer binding location varies between the species (patch A versus patch b). Aptamer binding to human EGFR is equally efficient between EGFR aptamer and EGFR-5FU aptamer. In contrast, mouse Egfr binds EGFR-5FU aptamer more efficiently than EGFR aptamer.

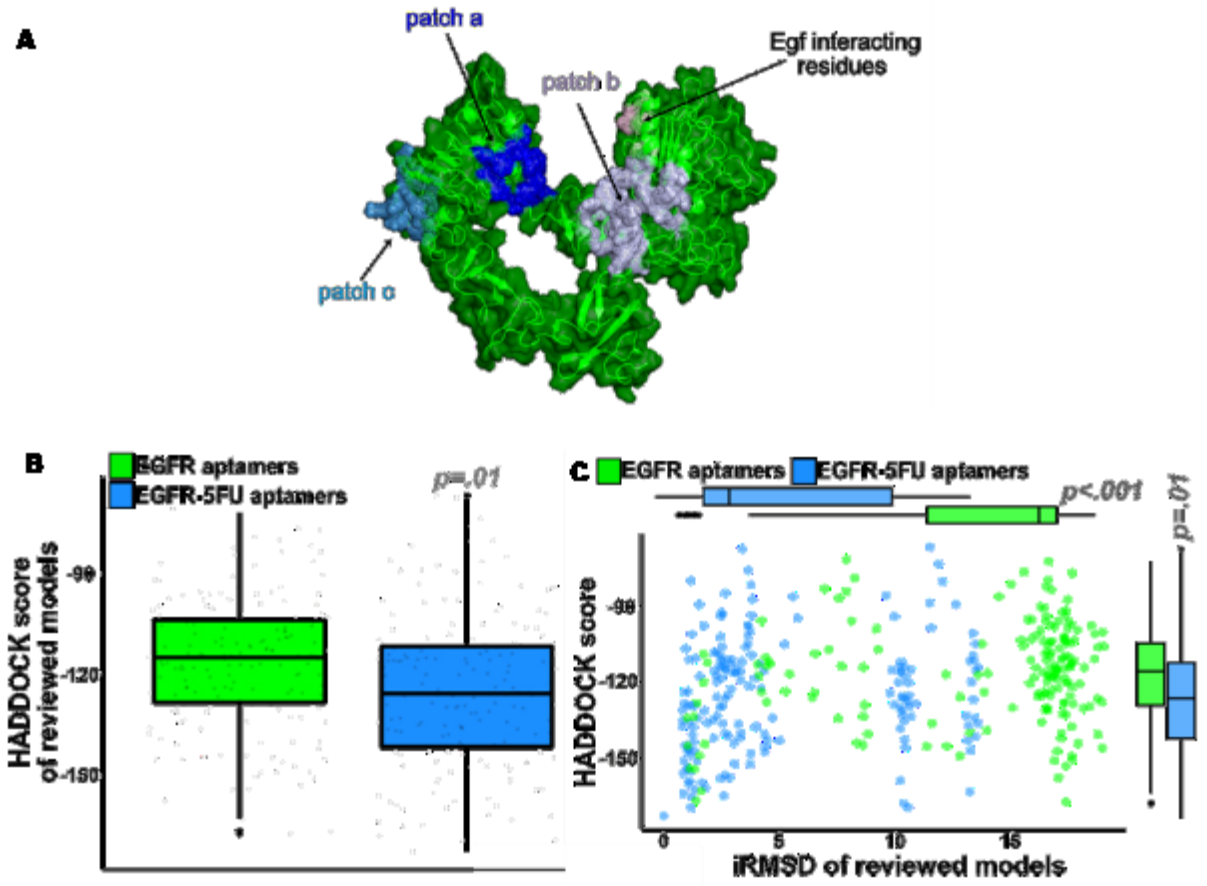

Figure 4.2.3: In silico binding analysis of aptamers with the extracellular domain of mouse Egfr. (A) 3D structure of the extracellular domain of human EGFR (green) and 3 possible RNA binding pockets (patch a, patch b, and patch c). Egf interacting residues were labeled by pink color. **(B)** Comparison plot of the HADDOCK scores between EGFR aptamers and EGFR-5FU aptamers docking to patch b (top 200 docking possibilities). **(C)** Distribution of HADDOCK scores (y-axis) in **Figure B** and related iRMSD scores (x-axis). P-value was calculated by two-tailed, unpaired *t*-test.

4.3 EGFR aptamers and EGFR-5FU aptamers interfere EGF binding with human EGFR

EGFR signaling pathways play a supportive role in the growth and spread of cancer cells. EGF, the ligand of EGFR protein, can bind to the extracellular domain of EGFR, followed by the activation of EGFR signaling. Since EGFR aptamers and EGFR-5FU aptamers also target the extracellular domain of EGFR, there is an apprehension of the competitive binding of aptamers with EGF to EGFR protein. I visualized the EGF binding sites in the extracellular domain of EGFR from published data [68] (**Figure 4.2.2 A, Figure 4.2.3 A**) and checked whether the EGFR aptamer and EGFR-5FU

aptamer blocks the EGF interaction site (**Figure 4.3**).

I observed that the binding of EGFR aptamers or EGFR-5FU aptamers with human EGFR (patch A) blocked the EGF binding site in the extracellular domain (**Figure 4.3 A**). Thus, the occupied location in principle has the possibility to impede the EGF target. However, the binding of EGFR aptamers or EGFR-5FU aptamers with the extracellular domain of mouse Egfr (patch b) did not interfere with Egf (**Figure 4.3 B**). Therefore, these aptamers cannot inhibit the Egf-stimulated EGFR signaling in mouse. In summary, EGFR aptamers and EGFR-5FU aptamers could be human EGFR inhibitors, but not mouse Egfr inhibitors.

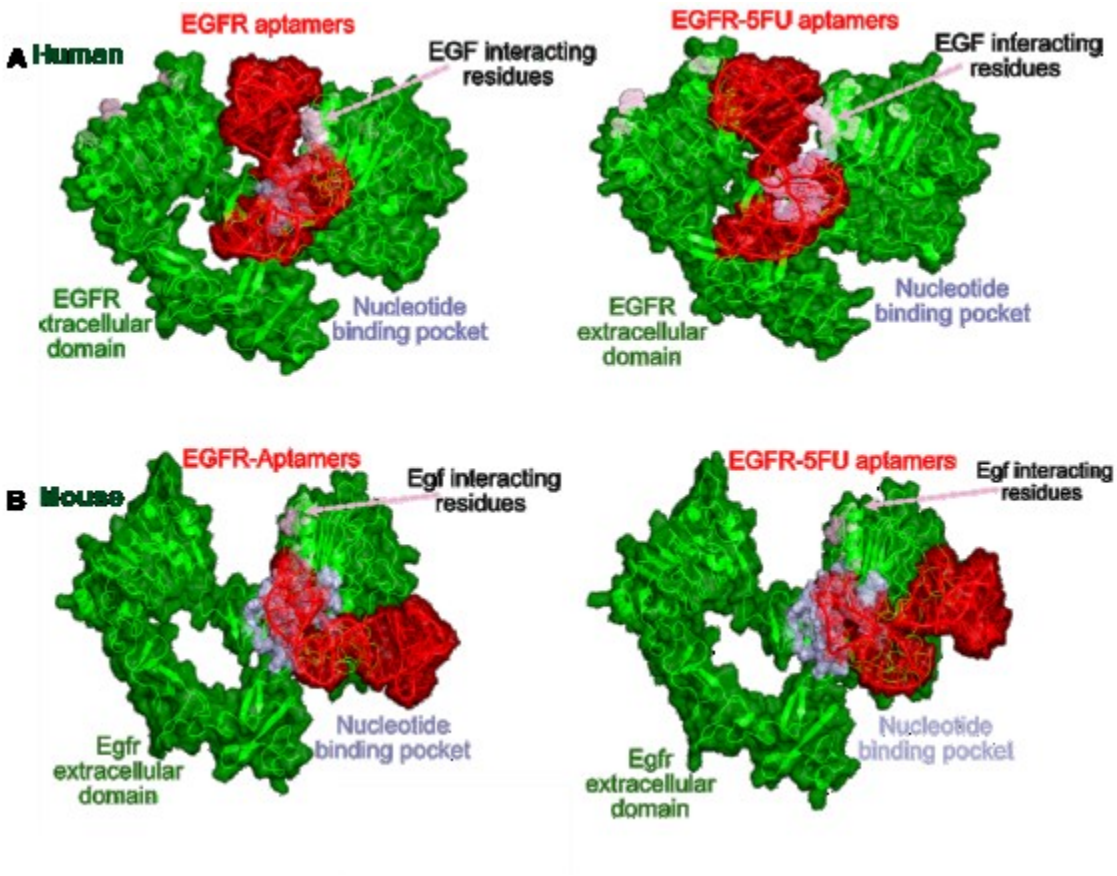

Figure 4.3 In silico docking analysis of aptamers with the extracellular domain of EGFR. (A) Visual representation of in-silico docking between the extracellular domain of human EGFR (green) and EGFR aptamers (red) or EGFR-5FU aptamers (red). The EGF binding sites are labeled by orange color. **(B)** Visual representation of in-silico docking between the extracellular domain of mouse Egfr (green) and EGFR aptamers (red) or EGFR-5FU aptamers (red). The Egf binding site is labeled by orange color.

4.4 Binding affinity of EGFR aptamers and EGFR-5FU aptamers

Affinity is the strength of the binding between a single molecule (e.g. protein or DNA) to its ligand. To explore the force of the binding interaction between aptamers and proteins, I performed a binding affinity assay. After recombinant human EGFR (with a His-tag) was attached to a 96-well plate, Cy3-coupled aptamers at indicated concentrations were added. After 30 min, the uncoupled aptamers were washed away and Cy3 fluorescence was measured. An experimental description of the binding affinity assay is summarized in **Figure 4.3 A**.

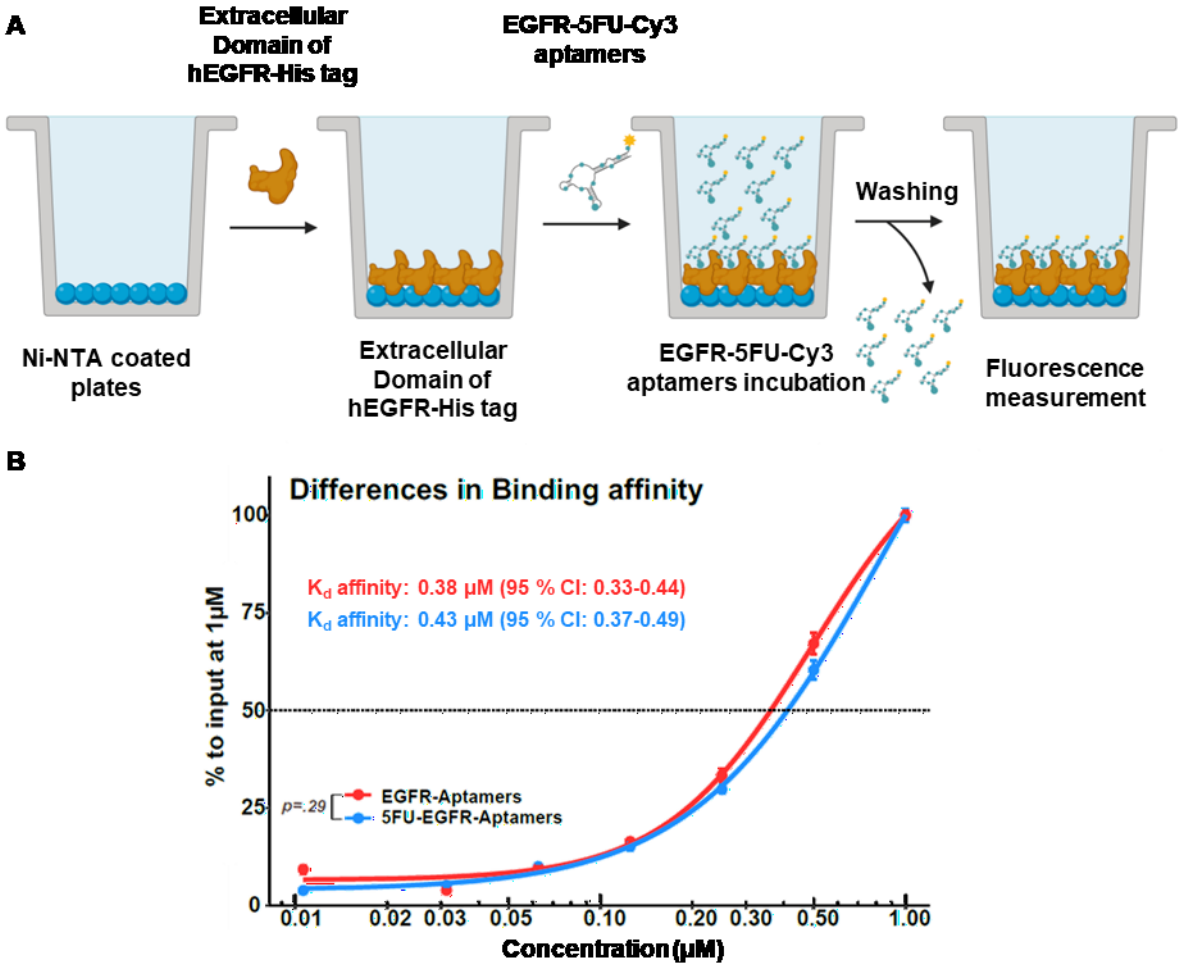

Figure 4.4: Binding affinity of EGFR aptamers and EGFR-5FU aptamers with human EGFR protein. (A) The scheme of binding affinity assay. **(B)** The binding affinity curves of EGFR aptamers and EGFR-5FU aptamers with human EGFR protein Data are expressed as mean ± SEM, n = 3 in each group. P-value was calculated by one-way analysis of variance (ANOVA).

The binding affinity of EGFR aptamers and EGFR-5FU aptamers to human EGFR is

displayed in **Figure 4.4 B.** The x-axis represents the concentrations of aptamers; the y-axis demonstrates the normalized relative fluorescence units (RFU). Since RFU reflects the amounts of aptamers binding to the protein, this figure shows the relationship between aptamer concentrations and the amounts of aptamers binding to protein. The results demonstrate that with increasing aptamer concentrations, more and more EGFR aptamers and EGFR-5FU aptamers were attached to the human EGFR. Binding affinity is usually quantified through the equilibrium dissociation constant (K_D). The lower K_D value represents the higher binding affinity of the aptamer for its target. After the calculation, the K_D value of EGFR aptamer binding to human EGFR was 0.38 μM (95 % confidence interval (CI): 0.33-0.44), whereas the K_D value of EGFR-5FU aptamer binding to human EGFR was 0.43 μM (95 % CI: 0.37-0.49). The difference between two curves was not significant (p = 0.29). This result was consistent with the prediction that EGFR aptamers and EGFR-5FU aptamers were equally efficient in binding with human EGFR (**Chapter 4.2, Figure 4.2.2 A-B**). In summary, the exchange of UTPs to 5FU-TPs in EGFR-5FU aptamers did not change the binding strength to human EGFR. EGFR-5FU aptamers showed the same efficient binding as EGFR aptamers against the extracellular domain of human EGFR.

4.5 EGFR aptamers inhibit EGFR signaling in human PDAC cells

When ligands, such as EGF, binds to the extracellular domain of EGFR, they can induce the formation of receptor homo or hetero dimers [76]. Subsequently, the kinase domain of EGFR (intracellular part of EGFR) is activated by phosphorylation so that it can trigger cellular signaling. EGFR phosphorylation activates several signaling pathways in cancer cells [77]. The RAS/RAF/MEK/ERK cascade is one of the most important reactions that promotes cell proliferation [41]. Extracellular regulated kinases 1 and 2 (ERK1/2) are crucial proteins in this cascade and are also activated by phosphorylation. Thus, the activation status of EGFR-related RAS/RAF/MEK/ERK singling pathway can be explored by checking the phosphorylation of EGFR and ERK1/2 protein.

Since EGFR aptamers and EGFR-5FU aptamers target the extracellular domain of

human and mouse EGFR, one of the major concerns was whether these aptamers trigger or inhibit EGFR signaling in PDAC cells. Thus, I examined the influence of EGFR aptamers on EGFR signaling by western blot (WB). I incubated PaTu-8988T cells (human PDAC cells) and DT6606PDA cells (mouse PDAC cells) with EGFR aptamers (30 nM) for 0 min, 5 min, 10 min, 20 min, 30 min and 60 min. PBS served as the negative control. Recombinant EGF served as the positive control. The status of EGFR signaling was detected by the phosphorylation of EGFR and ERK1/2.

The results of PaTu-8988T cells were displayed in **Figure 4.5.1**. pEGFR/EGFR ratios and pERK1/2/ERK1/2 ratios were shown in the middle of the blots at each time point. The control treatment demonstrated that pEGFR/EGFR ratios (range from 1.1 to 1.3) and pERK1/2/ERK1/2 ratios (range from 1.0 to 2.1) were not changed significantly over time (**Figure 4.5.1 A**). However, EGF treatment strongly activated the EGFR signaling after 5 min incubation (**Figure 4.5.1 B**, pEGFR/EGFR ratios: from 7.7 to 11.5; pERK1/2/ERK1/2 ratios: from 3.1 to 6.6). Notably, EGFR aptamer treatment did not activate EGFR signaling, EGFR and ERK1/2 were not phosphorylated after 60 min (pEGFR/EGFR ratios range from 0.8 – 1.0, pERK1/2/ERK1/2 ratios range from 1.3 - 1.8) (**Figure 4.5.1 C**). In addition, baseline phosphorylated EGFR and ERK1/2 were not dephosphorylated after this incubation. Therefore, short-time incubation with EGFR aptamers could not trigger or block intrinsic EGFR signaling in human PDAC cells.

The blots of DT6606PDA cells were displayed in **Figure 4.5.2**. Mouse Egf could activate Egfr signaling in mouse PDAC cells after 5 min incubation, whereas PBS could not (**Figure 4.5.2 A-B**). Egfr and Erk1/2 were not phosphorylated and phosphorylated Egfr and Erk1/2 were not dephosphorylated after incubation with EGFR aptamers over 60 min (pEgfr/Egf ratios range from 0.8 – 1.1, pErk1/2/Erk1/2 ratios range from 1.1 – 1.6) (**Figure 4.5.1 C**). Therefore, short-time incubation with EGFR aptamers could not trigger or block intrinsic Egfr signaling in mouse PDAC cells.

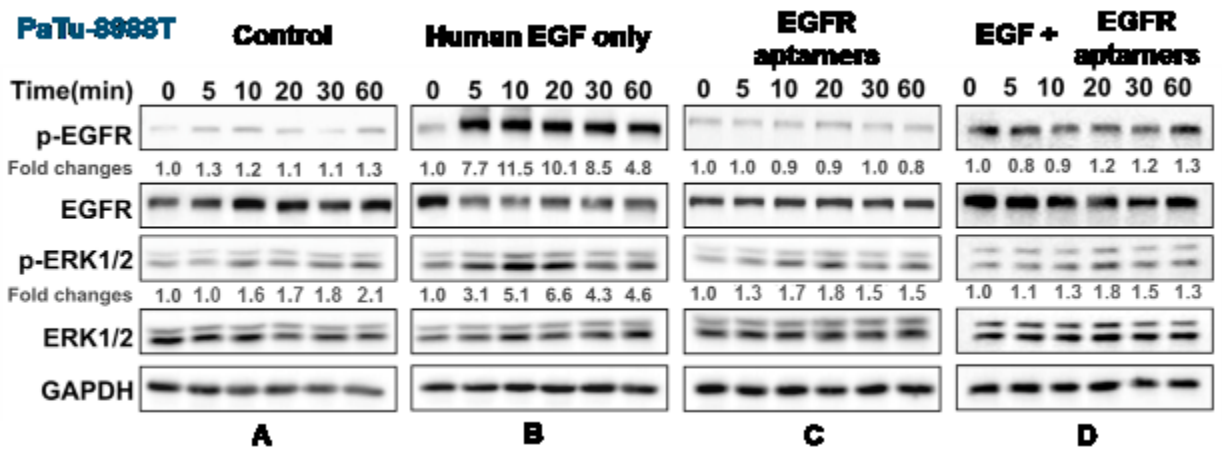

Figure 4.5.1: The effect of EGFR aptamers on EGFR signaling of PaTu-8988T cells. Western blots depict the phosphorylation of EGFR and ERK1/2 in PaTu-8988T cells after incubation with **(A)** PBS, **(B)** Human EGF (100 ng/ml), **(C)** EGFR aptamers (30 nM), **(D)** Human EGF (100 ng/ml) + EGFR aptamers (30 nM) for 0 min, 5 min, 10 min, 20 min, 30 min and 60 min. GAPDH is used for loading control.

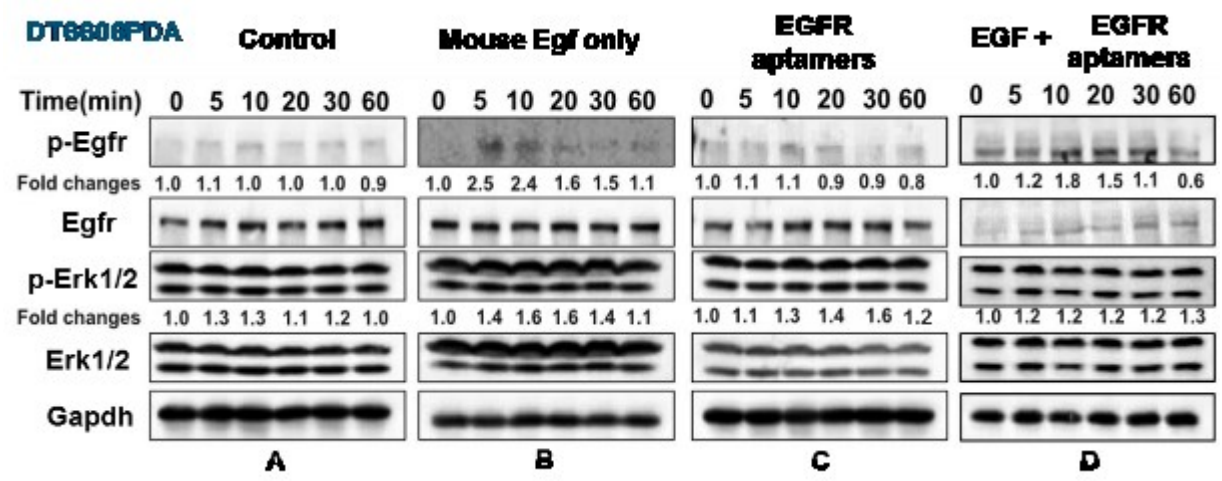

Figure 4.5.2: The effect of EGFR aptamers on Egfr signaling of DT6606PDA cells. Western blots depict the phosphorylation of Egfr and Erk1/2 in DT6606PDA cells after incubation with **(A)** PBS, **(B)** Mouse Egf (100 ng/ml), **(C)** EGFR aptamers (30 nM), **(D)** Human Egf (100 ng/ml) + EGFR aptamers (30 nM) for 0 min, 5 min, 10 min, 20 min, 30 min and 60 min. Gapdh is used for loading control.

The previous results of in-silico docking predicted that the aptamer interfered with the EGF binding pocket in human EGFR, whereas in mouse Egfr the aptamer did not. Thus, EGFR aptamers could be in principle human EGFR competitive inhibitors. To verify this prediction, I checked the phosphorylation of EGFR and ERK1/2 after co-incubation with human EGF and EGFR aptamers in PaTu-8988T cells (**Figure 4.5.1 D**). Compared to the positive control, in which EGFR signaling was activated after

incubation with EGF for 5 min (**Figure 4.5.1 B**), EGFR and ERK1/2 were not phosphorylated after co-incubation over 60 min (pEGFR/EGFR ratios range from 0.8 – 1.3, pERK1/2/ERK1/2 ratios range from 1.1 – 1.8) (**Figure 4.5.1 D**). This result led me to conclude that EGFR aptamers could act as human EGFR inhibitors.

I also checked the phosphorylation of Egfr and Erk1/2 after co-incubation with mouse Egf and EGFR aptamers in DT6606PDA cells (**Figure 4.5.2 D**). Compared to the positive control (**Figure 4.5.2 B**), Egfr could still be phosphorylated after co-incubation (**Figure 4.5.2 D**). This result led me to conclude that EGFR aptamers are no Egfr inhibitors in mouse cells. In summary, EGFR aptamers could not activate or inhibit intrinsic EGFR/ERK signaling in PDAC cells. EGFR aptamers could be human EGFR inhibitors, whereas they could not be mouse Egfr inhibitors.

4.6 EGFR-5FU aptamers are taken up by clathrin-dependent endocytosis

To monitor the uptake of EGFR-5FU aptamers, I performed time-lapsed live cell imaging with Cy3-conjugated EGFR-5FU aptamers on PaTu-8988T cells. First, the cell nuclei were tagged by DAPI (blue-fluorescent DNA stain). Then, cells were treated with 50 nM of Cy3-conjugated EGFR-5FU aptamers for 120 min at 37 °C. During the 2 h incubation, the fluorescent images were recorded every 5 min. Several parameters of images (e.g. fluorescent intensity) were also collected.

I found evident uptake of EGFR-5FU aptamers as early as 30 min compared to 0 min control (**Figure 4.6.1 A,** the first group of images in the horizontal direction). The continuous cellular uptake made the amount of EGFR-5FU aptamers increase gradually in PaTu-8988T cells over 2 h. This result proved that EGFR-5FU aptamers were indeed internalized by PaTu-8988T cells.

In order to evaluate whether the cellular uptake is EGFR-dependent, I incubated PaTu-8988T cells with cetuximab (EGFR monoclonal antibody) overnight before the treatment with Cy3-conjugated EGFR-5FU aptamers. I found a significant decrease in uptake compared to control experiments (**Figure 4.6.1 A**, the third group of images in the horizontal direction). Cetuximab pre-treatment blocked the EGFR, thus, rendering the cellular internalization of EGFR-5FU aptamers. In conclusion, the uptake of EGFR-

5FU aptamers into human PDAC cells is EGFR-dependent.

To assess the possible functional mechanism of uptake in human PDAC cells, I treated PaTu-8988T cells with clathrin-dependent endocytosis inhibitor, dynasore before the EGFR-5FU aptamers incubation. I found that endocytosis inhibition prevented EGFR-5FU aptamers uptake (**Figure 4.6.1 A**, the second group of images in the horizontal direction). I did not observe a marked decrease in uptake after pre-treatment with genistein (caveolin dependent inhibitor), herbimycin A (lipid raft inhibitor), fillipin III (Clathrin and caveolin independent inhibitors) or sodium ortho-vanadate (Na+/K+ ATPase inhibitor).

The uptake quantification was shown by time and percent of change in fluorescent intensity curves. The results shown in **Figure 4.6.1 B** displayed that EGFR-5FU aptamers were taken up by PaTu-8988T cells continuously within 120 min. Cetuximab, as well as dynasore (clathrin-dependent endocytosis inhibitor) pre-treatment, blocked the uptake of EGFR-5FU aptamers. These results led me to convince that the uptake of EGFR-5FU aptamers into human PDAC cells is EGFR dependent and the uptake mechanism is clathrin-dependent endocytosis.

To further explore the uptake of EGFR-5FU aptamers into mouse PDAC cells, I performed time-lapsed live cell imaging with Cy3-conjugated EGFR-5FU aptamers on DT6606PDA cells. I found evident uptake of EGFR-5FU aptamers into DT6606PDA cells (**Figure 4.6.1 C**, the first group of images in the horizontal direction). The continuous cellular uptake made Cy3 fluorescence increased gradually in DT6606PDA cells over 2 h. This result proved that DT6606PDA cells internalize EGFR-5FU aptamers.

To investigate the possible uptake mechanism in mouse PDAC cells, I hypothesized that the uptake of EGFR-5FU aptamers into mouse PDAC cells was also by clathrin-dependent endocytosis. To confirm this, I treated DT6606PDA cells with dynasore for 30 min before the EGFR-5FU aptamers incubation. I found that clathrin-dependent endocytosis inhibition ablated EGFR-5FU aptamer uptake (**Figure 4.6.1 C**, the second group of images in the horizontal direction).

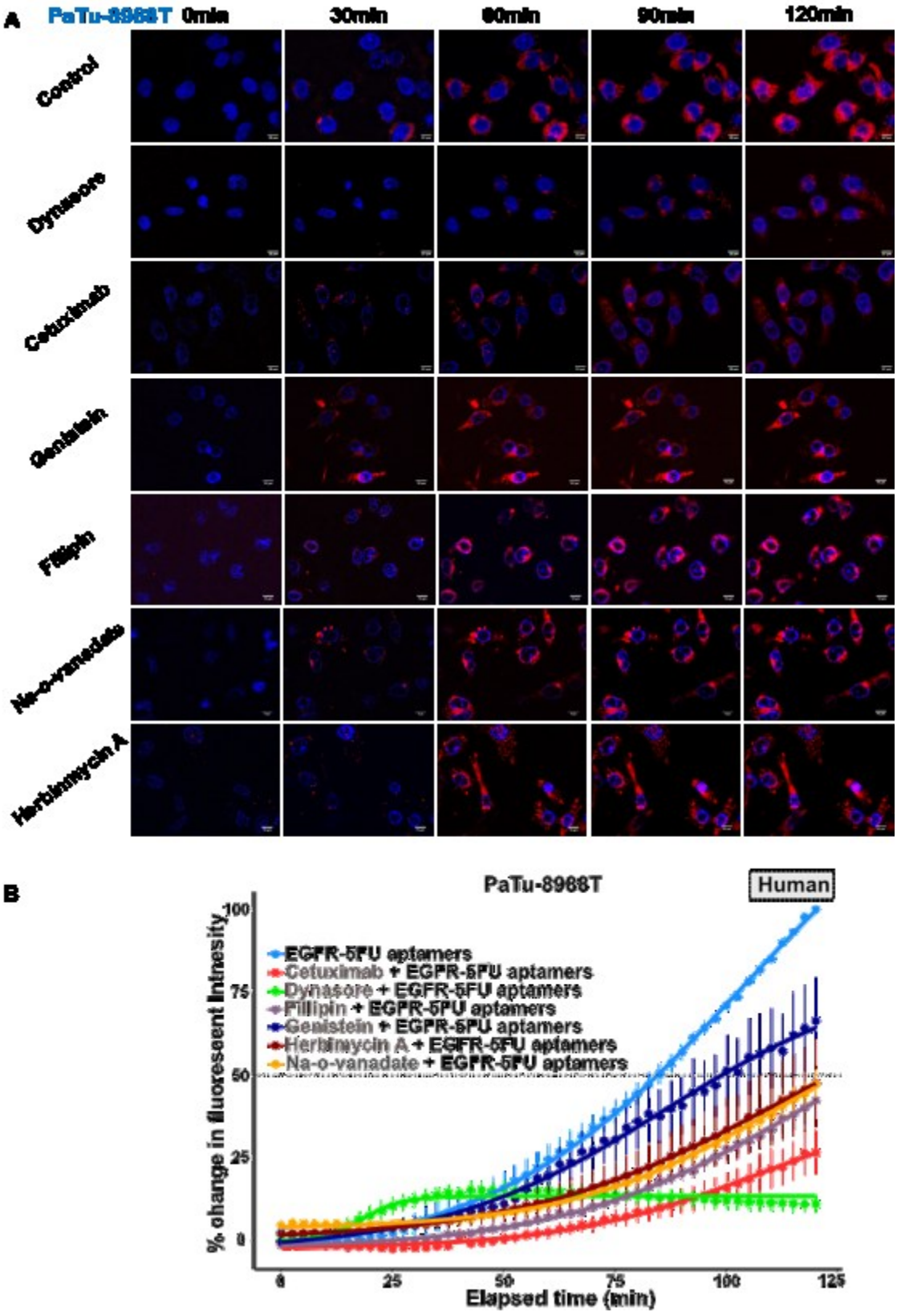
A
PaTu-8988T
0min
30min
60min
90min
120min
Control
Dynasore
Cetuximab
Genistein
Filipin
Na-o-vanadate
Herbimycin A
B
PaTu-8988T
Human
% change in fluoreseent Intnesity
Elapsed time (min)
EGFR-5FU aptamers
Cetuximab + EGFR-5FU aptamers
Dynasore + EGFR-5FU aptamers
Filipin + EGFR-5FU aptamers
Genistein + EGFR-5FU aptamers
Herbimycin A + EGFR-5FU aptamers
Na-o-vanadate + EGFR-5FU aptamers

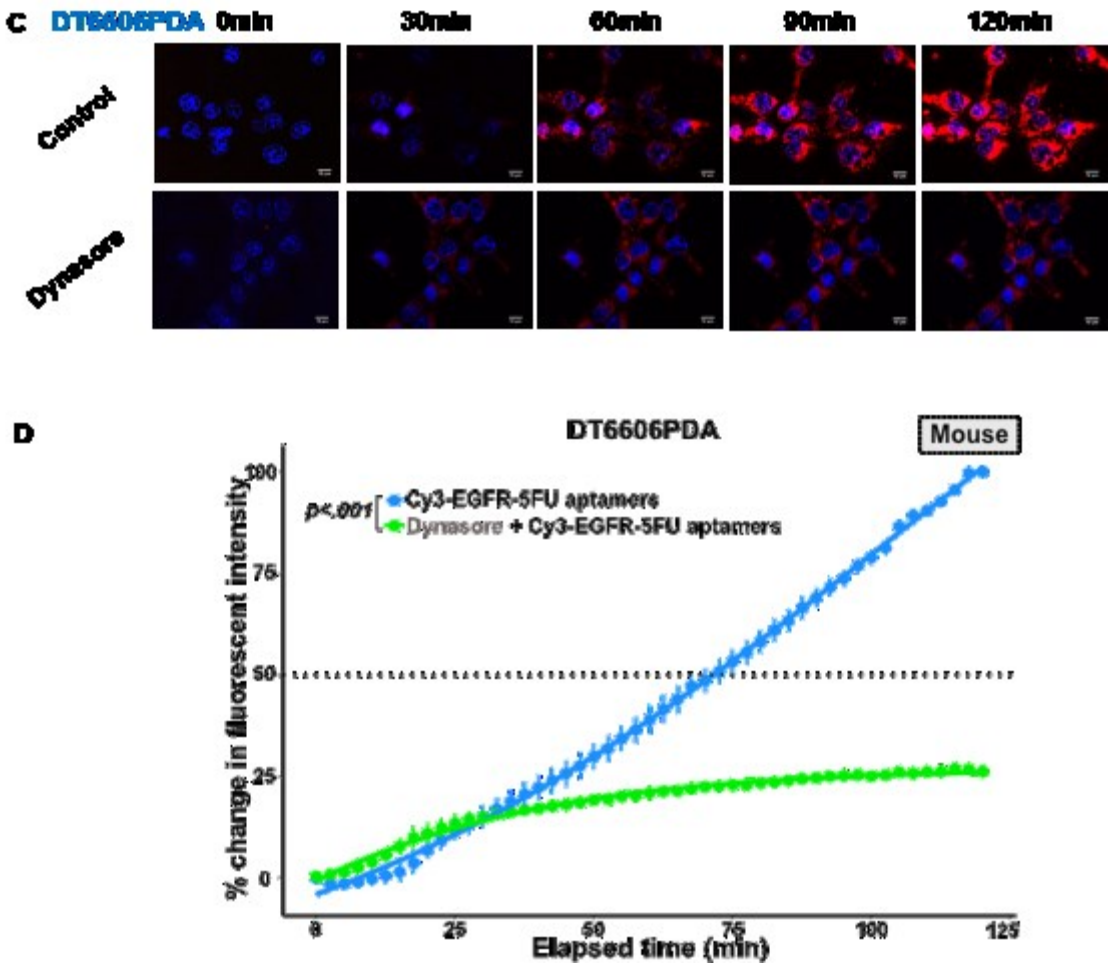

Figure 4.6.1 Cellular uptake of EGFR-5FU aptamers into PDAC cells. (A) Time-lapsed live cell imaging depicting the uptake of EGFR-5FU aptamers into PaTu-8988T cells after incubation for 0 min, 30 min, 60 min, 90 min and 120 min. Cells were pretreated with PBS (control), dynasore, cetuximab, genistein, fillipin, Na-o-vanadate, or herbimycin A. Cy3 fluorescence reflects EGFR-5FU aptamers, whereas blue fluorescence stains nuclei (DAPI). **(B)** Quantification of EGFR-5FU aptamers in PaTu-8988T cells (every 5 min over 120 min). Data are shown as time-normalized fluorescent intensity curves. **(C)** Time-lapsed live cell imaging depicts the uptake of EGFR-5FU aptamers into DT6606PDA cells over 120 min. Cells were pretreated with PBS (control) or dynasore. **(D)** Quantification of the EGFR-5FU aptamers in DT6606PDA cells (every 5 min over 120 min). Data are expressed as mean ± SEM, n = 3 in each group.

The quantification of Cy3 fluorescence in treated DT6606PDA cells reflected that EGFR-5FU aptamers were internalized continuously within 120 min. Dynasore pre-treatment blocked the uptake of EGFR-5FU aptamers into DT6606PDA cells (**Figure 4.6.1 D**). These results led me to conclude that the uptake of EGFR-5FU aptamers into mouse PDAC cells was also mediated by clathrin-dependent endocytosis.

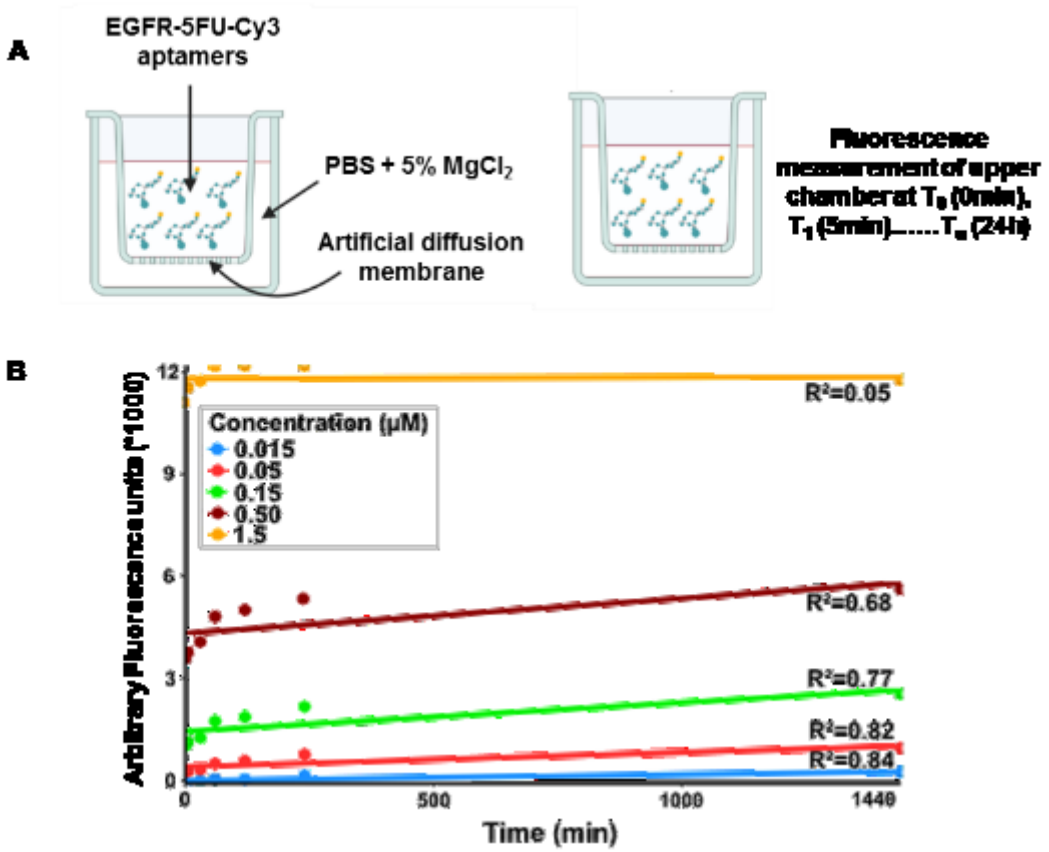

Figure 4.6.2: The parallel artificial membrane permeability of EGFR-5FU aptamers. (A) The scheme of parallel artificial membrane permeability assay (PAMPA). **(B)** The curves between Cy3 fluorescence and time depict the permeability of EGFR-5FU aptamers (concentration range from 0.015 μM to 1.5 μM) to the artificial diffusion membrane over 24 h incubation.

In addition to active cellular uptake mechanisms, I also assessed whether EGFR-5FU aptamers could be internalized into cancer cells by passive diffusion. Thus, the parallel artificial membrane permeability assay (PAMPA) was performed in the 96-well MultiScreen® IP Filter Plate (**Figure 4.6.2 A**). The spaces on both sides of the artificial membrane mimicked the pattern of inside and outside of the cell. Cy3-conjugated EGFR-5FU aptamers were added into the wells. During incubation at RT for 24 h, Cy3 fluorescence was measured. A decrease in fluorescence compared to the corresponding control depicted the amount of EGFR-5FU aptamers penetrating through the artificial membrane by diffusion.

Different concentrations (range from 0.015 μM to 1.5 μM) of EGFR-5FU aptamers were used. The results are shown as time-fluorescence curves. I noticed that no decreased

fluorescence intensity could be recorded over 24 h (**Figure 4.6.2 B**), which indicated that EGFR-5FU aptamers could not go through the artificial membrane by passive diffusion.

4.7 EGFR-5FU aptamers reduce the viability and colony-formation of PDAC cells

After investigating the binding affinity of aptamers, their influence on EGFR signaling, and their cellular uptake mechanism, I determined the impact of aptamers on the survival of cancer cells by MTT assay. I examined the viability of PDAC cells following the treatment of EGFR aptamers and EGFR-5FU aptamers. Because one molar EGFR-5FU aptamer incorporated 11 molar 5FU-TPs, I treated PDAC cells with 11 times higher concentrations of 5FU as controls. Obtained viability was normalized as percentages to the control without treatment. All viability data are displayed by dose-response curves.

The result of PaTu-8988T cells is shown in **Figure 4.7.1 A**. I observed that, compared to 5FU, there was a remarkable decrease in cell viability after incubation with EGFR-5FU aptamers for 72 h. The difference between these two dose-response curves was significant (p = 0.001). EGFR aptamers cannot inhibit the cell viability of PaTu-8988T cells. Notably, even a low concentration of EGFR-5FU aptamers (1 nM) can decrease the viability of PaTu-8988T cells by 50 %, whereas a high concentration of EGFR aptamers (300 nM) cannot impede the survival of human PDAC cells. Thus, EGFR-5FU aptamers have high cytotoxicity in human PDAC cells.

The result for DT6606PDA cells is shown in **Figure 4.7.1 B**. I observed that compared to 5FU, there was a strong decrease in cell viability after incubation with EGFR-5FU aptamers for 72 h. The difference between these two curves was significant (p < 0.0001). However, EGFR aptamers cannot inhibit the cell viability of DT6606PDA cells. Even a low concentration of EGFR-5FU aptamers (1 nM) could decrease the viability of DT6606PDA cells by 75 %, whereas high concentrations of EGFR aptamers (100 nM) cannot obstruct their survival. These results demonstrated that EGFR-5FU aptamers could also reduce the viability of mouse PDAC cells.

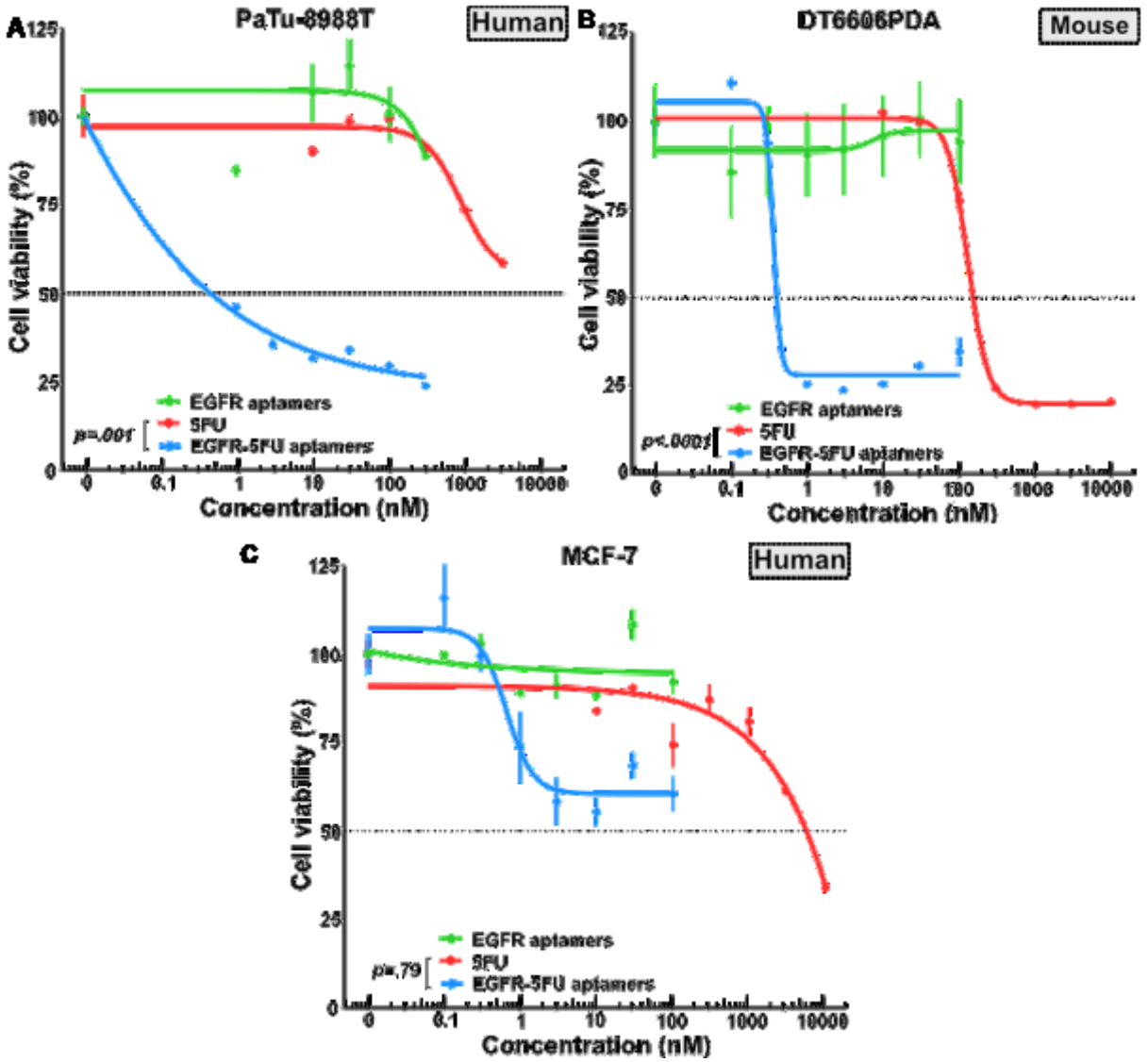

Figure 4.7.1: Effect of EGFR-5FU aptamers on the viability of PDAC cells. Comparison dose-response curves among the cell viability of **(A)** PaTu-8988T, **(B)** DT6606PDA, **(C)** MCF-7 after 72 h incubation with EGFR-5FU aptamers, EGFR aptamers or 5FU alone. Data are expressed as mean ± SEM, n = 3 in each group. P-value was calculated by one-way analysis of variance (ANOVA).

In addition, I performed an MTT assay to measure the viability of MCF7 cells with the treatment of EGFR-5FU aptamers, EGFR aptamers or 5FU alone (**Figure 4.7.1 C**). MCF7, a human breast adenocarcinoma cell-line have low levels of EGFR expression, and served as negative control. EGFR aptamers did not show any influence on the viability of MCF7 cells. Importantly, compared to 5FU, EGFR-5FU aptamers also did not show changes in the viability of MCF7 cells (p = 0.79), indicating lower cellular uptake of EGFR-5FU aptamers. This result demonstrated that the cytotoxicity of

EGFR-5FU aptamers is EGFR-dependent.

To further determine the influence of EGFR-5FU aptamers on colony-formation, I performed a long-term colony formation assay for PDAC cells. PaTu-8988T cells and DT6606PDA cells were incubated with EGFR-5FU aptamers or EGFR aptamers for 24 h. The 10-fold increased dose of 5FU served as control. After 10 days, colony formation was analyzed. The obtained results were normalized as percentages compared to no-treatment controls. All these results are presented as bar graphs.

The data of PaTu-8988T cells are displayed in **Figure 4.7.2 A**. I detected a big decrease in colony formation after treatment with EGFR-5FU aptamers compared to a 10-fold higher dose of 5FU. The difference between treatment with 10 nM EGFR-5FU aptamers and 100 nM 5FU was significant (p = 0.005). So was the difference in another treatment group (30 nM EGFR-5FU aptamers vs. 300 nM 5FU (p = 0.0001)). EGFR aptamers cannot inhibit the colony-formation of PaTu-8988T cells. These results implied that EGFR-5FU aptamer treatment strongly reduces the colony formation of human PDAC cells at 10 times lower doses compared to 5FU treatment.

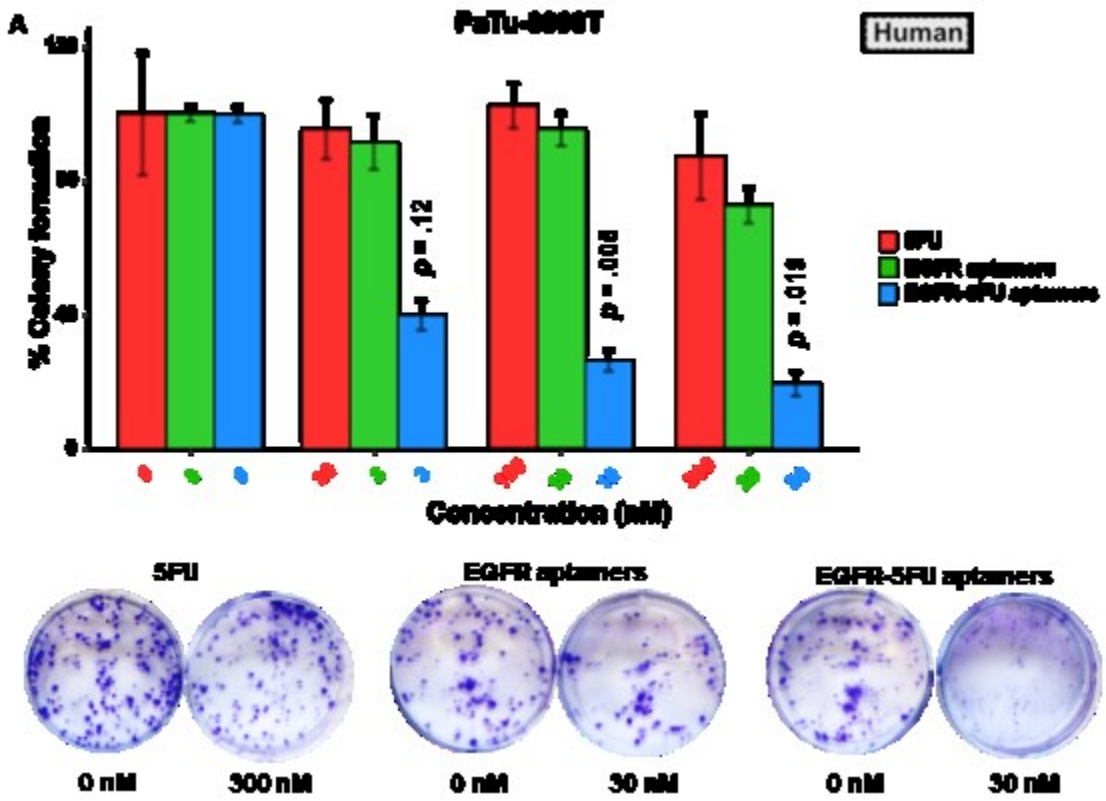

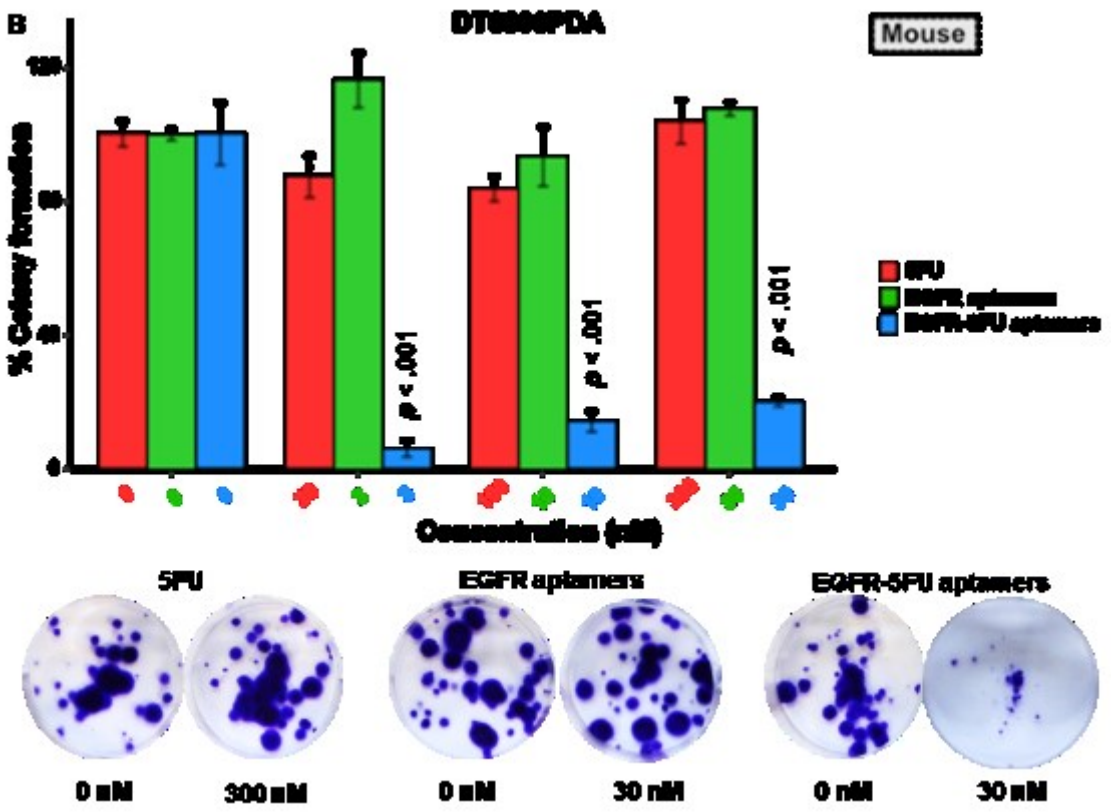

Figure 4.7.2: Effect of EGFR-5FU aptamers on colony formation of PDAC cells. Comparison bar graphs among the colony formation of **(A)** PaTu-8988T cells, **(B)** DT6606PDA cells after incubation with EGFR-5FU aptamers, EGFR aptamers or 5FU alone for 24 h. P-value was calculated by two-tailed, unpaired *t*-test. For each group, p-value was calculated compared to the result of 5FU treatment. Representative images of colony-forming are displayed below the bar graphs.

The results of DT6606PDA cells were shown in **Figure 4.7.2 B**. I identified a significant decrease in colony formation after treatment with EGFR-5FU aptamers compared to that of 10-fold increased dose of 5FU. The differences in all 3 groups between the treatment of EGFR-5FU aptamers and 5FU were significant ($p < 0.001$). However, EGFR aptamers cannot inhibit the colony-formation of DT6606PDA cells. Notably, even at low concentrations, EGFR-5FU aptamers (15 nM) could reduce colony formation of DT6606PDA cells by 90 %. This result demonstrated that EGFR-5FU aptamers reduce colony formation of mouse PDAC cells.

4.8 EGFR-5FU aptamers induce cell cycle arrest at the G1 phase

Several studies have reported that 5FU could induce G1 phase cell cycle arrest in

cancer cells [78, 79]. Thus, in the next step, the influence of EGFR-5FU aptamers on the cell cycle was investigated. Because 30 nM of EGFR-5FU aptamers could significantly inhibit the viability of PDAC cells (Chapter 4.7, Figure 4.7.1), I treated PaTu-8988T and DT6606PDA cells with EGFR-5FU aptamers at the concentration of 30 nM for 24 h. PBS served as a negative control. EGFR aptamers (30 nM) served as an unmodified aptamer control. Since 5FU at 11 times increased concentration (330 nM, the same amount of 5FU coupled in EGFR-5FU aptamers) did not affect the viability of PDAC cells (Chapter 4.7, Figure 4.7.1), I chose an overdose of 5FU (30 μM) as a positive control. After staining the treated cells with propidium iodide (PI, red-fluorescent DNA staining dye), the distribution of cell cycle phases was measured by fluorescence-activated cell sorting (FACS) analysis. The results were presented as histograms depicting the percentage of PDAC cells at different phases of the cell cycle. Differences (*p*-value) were calculated compared to PBS controls.

Cell cycle distribution of PaTu-8988T cells is shown in **Figure 4.8 A**. PBS-treated PaTu-8988T cells displayed that 55.97 % of cells were at G1 phase. The distribution of PaTu-8988T cells at G1 phase (74.05 %) was significantly increased after incubation with the excessive doses of 5FU (30 μM) for 24 h (p = 0.003). However, EGFR aptamers cannot increase the percentage of cells at the G1 phase (57.93 %). Interestingly, I found a strong accumulation of cells at the G1 phase (72.13 %) after EGFR-5FU aptamers treatment (p = 0.03). This result indicated that EGFR-5FU aptamers could induce G1 phase arrest in human PDAC cells.

Cell cycle distribution of DT6606PDA cells is shown in **Figure 4.8 B**. 56.90 % of PBS treated DT6606PDA cells were at G1 phase. A high dose of 5FU significantly increased the percentage of cells at the G1 phase (73.32 %) (p = 0.001). However, the distribution of DT6606PDA cells at the G1 phase (55.86 %) was not changed after 30 nM EGFR aptamers treatment. Importantly, I found a huge accumulation of cells at the G1 phase (70.24 %) after incubation with EGFR-5FU aptamers for 24 h (p = 0.005). This result showed that EGFR-5FU aptamers induced G1 phase arrest in mouse PDAC cells.

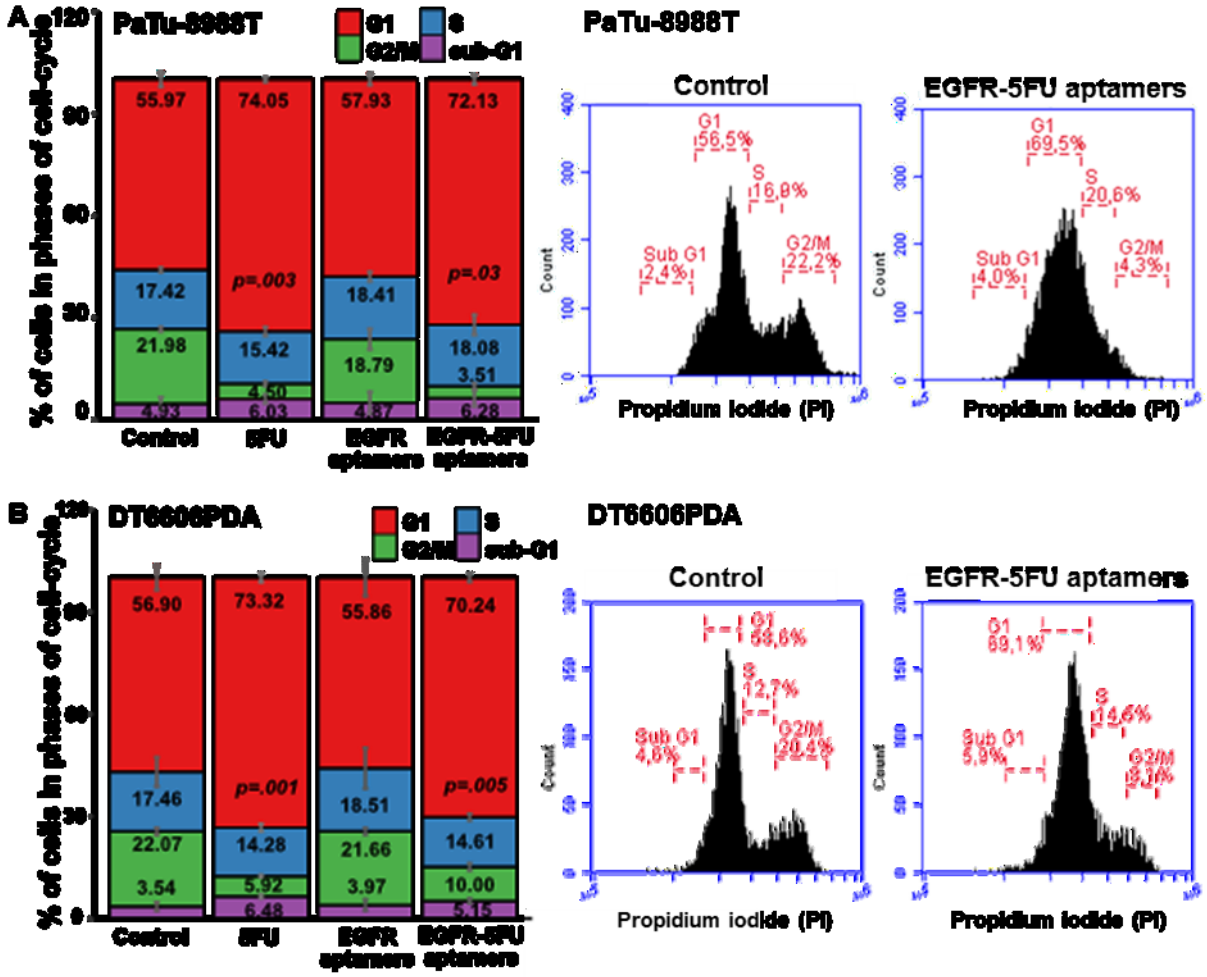

Figure 4.8: Effect of EGFR-5FU aptamers on the cell cycle of PDAC cells. Comparison histograms among the distribution of cell cycle phases in **(A)** PaTu-8988T cells, **(B)** DT6606PDA cells after incubation with PBS, overdoes of 5FU (30 µM), EGFR aptamers (30 nM) or EGFR-5FU aptamers (30 nM) for 24 h. Diagram in insert shows cell cycle peaks illustrating G1, S, G2/M and subG1 phase (red, green, blue and purple). P-value was calculated by two-tailed, unpaired *t*-test, compared to PBS controls. Representative images of FACS measurements were displayed on the right side of histograms.

In summary, EGFR-5FU aptamers and high doses of 5FU induced G1 cell cycle arrest in PaTu-8988T cells and DT6606PDA cells, whereas EGFR aptamers did not. Notably, even though the concentration of 5FU is 1000 times higher than that of EGFR-5FU aptamers, EGFR-5FU aptamer treatment exhibited a similar effect on inducing G1 phase arrest in PDAC cells. These data corroborated my earlier results that compared to 5FU, EGFR-5FU aptamers were highly efficient and cytotoxic to PDAC cells in-vitro.

4.9 EGFR antibody impedes the influence of EGFR-5FU aptamers on reducing the viability of PDAC cells

Specificity is an important aspect of targeted therapy. To investigate whether the cytotoxic effect of EGFR-5FU aptamers is EGFR dependent, I pretreated PaTu-8988T and DT6606PDAC cells with anti-human EGFR monoclonal antibody (cetuximab) or anti-mouse Egfr antibody overnight for EGFR blockage. Afterwards, I incubated these cells with EGFR-5FU aptamers (30 nM) or an equal loaded concentration of 5FU (330 nM) for 72 h. The results of normalized cell viability were displayed by bar graphs (**Figure 4.9**). In the control group (without antibody treatment), EGFR-5FU aptamers significantly decreased the viability of PaTu-8988T cells (p = 0.003). In contrast, in cetuximab pre-treated PDAC cells, EGFR-5FU aptamers failed to decrease cell viability (p = 0.58). The same effect was seen for DT6606PDA cells. I observed that Egfr blockade averted the cytotoxic effect of EGFR-5FU aptamers in mouse PDAC cells (p = 0.87). Thus, EGFR antibodies impeded the influence of EGFR-5FU aptamers on reducing the viability of PDAC cells. These data demonstrated that the effect of EGFR-5FU aptamers on decreasing the viability of PDAC cells was EGFR dependent.

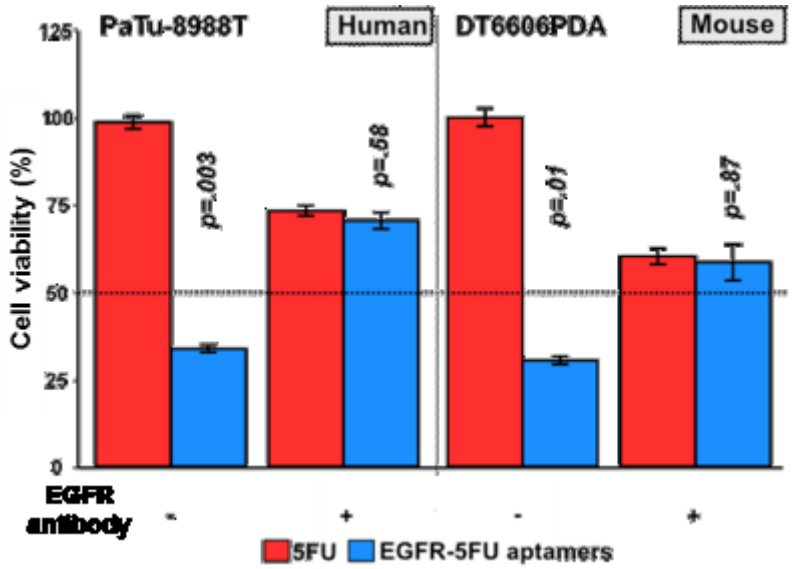

Figure 4.9: Influence of EGFR-5FU aptamers on the viability of EGFR antibody treated PDAC cells. Comparison bar graphs depict the viability between PBS treated and EGFR antibody treated PDAC cells after incubation with EGFR-5FU aptamers (30 nM) or the equimolar dose of 5FU (330 nM) for 72 h. Data are expressed as mean ±

SEM, n = 3 in each group. P-value was calculated by two-tailed, unpaired *t*-test.

4.10 Generation of CRISPR/Cas9-mediated *EGFR* KO cell lines

To further confirm the specificity of the EGFR-5FU aptamers, *EGFR* knock-out (KO) PaTu-8988T cell lines and *Egfr* KO DT6606PDA cell lines were generated with the help of the CRISPR/Cas9 genome editing system. The system included two kinds of plasmids, EGFR CRISPR-Cas9 KO plasmid and HDR repair plasmid. EGFR CRISPR-Cas9 KO plasmid consists of a pool of 3 plasmids (A, B and C for human; D, E and F for mouse), each encoding the Cas9 nuclease and a target-specific 20 nt guide RNA (gRNA). These gRNAs targeted different positions in the exons of EGFR gene, and can guide Cas9 to cut double-strand of DNA (**Figure 4.10 A-B**). HDR repair plasmid is able to repair these double-strand breaks and insert the puromycin resistance gene. Thus, the clones which were cut at the right position and had successfully inserted puromycin will survive the antibiotic selection procedure. Multiplex PCR was used to detect the insertion of puromycin selection cassette (**Figure 4.10 C**). Since one forward primer and two reverse primers were applied in one reaction, the PCR results of homozygous KO clones should display only one large band (longer products), compared to that of wild type (WT) control.

In my study, four single clones from PaTu-8988T cells (B8, D7, F5, F6) were selected. The results of multiplex PCR confirmed the homozygous insertion (**Figure 4.10 D**). B8, D7, F5 and F6 revealed PCR products of 678 bp for binding site A and 614 bp for binding site B, whereas PCR bands of WT cells were detected at 363 bp (A) and 311 bp (B). These results indicated that four clones had the homozygous insertion in the position where gRNA-A and gRNA-B are targeting. WT cells had no insertion in *EGFR* gene. However, the position where gRNA-A targeting was so closed to where gRNA-B targeting. Thus, it was not doubted that B8, D7, F5, F6 were all homozygous *EGFR* KO PaTu-8988T cell lines. The successful generation of homozygous *EGFR* KO PaTu-8988T cell lines was further confirmed by western blotting (**Figure 4.10 E**). The results demonstrated a loss of EGFR in clones B8, D7, F5 and F6, whereas WT cells showed EGFR expression.

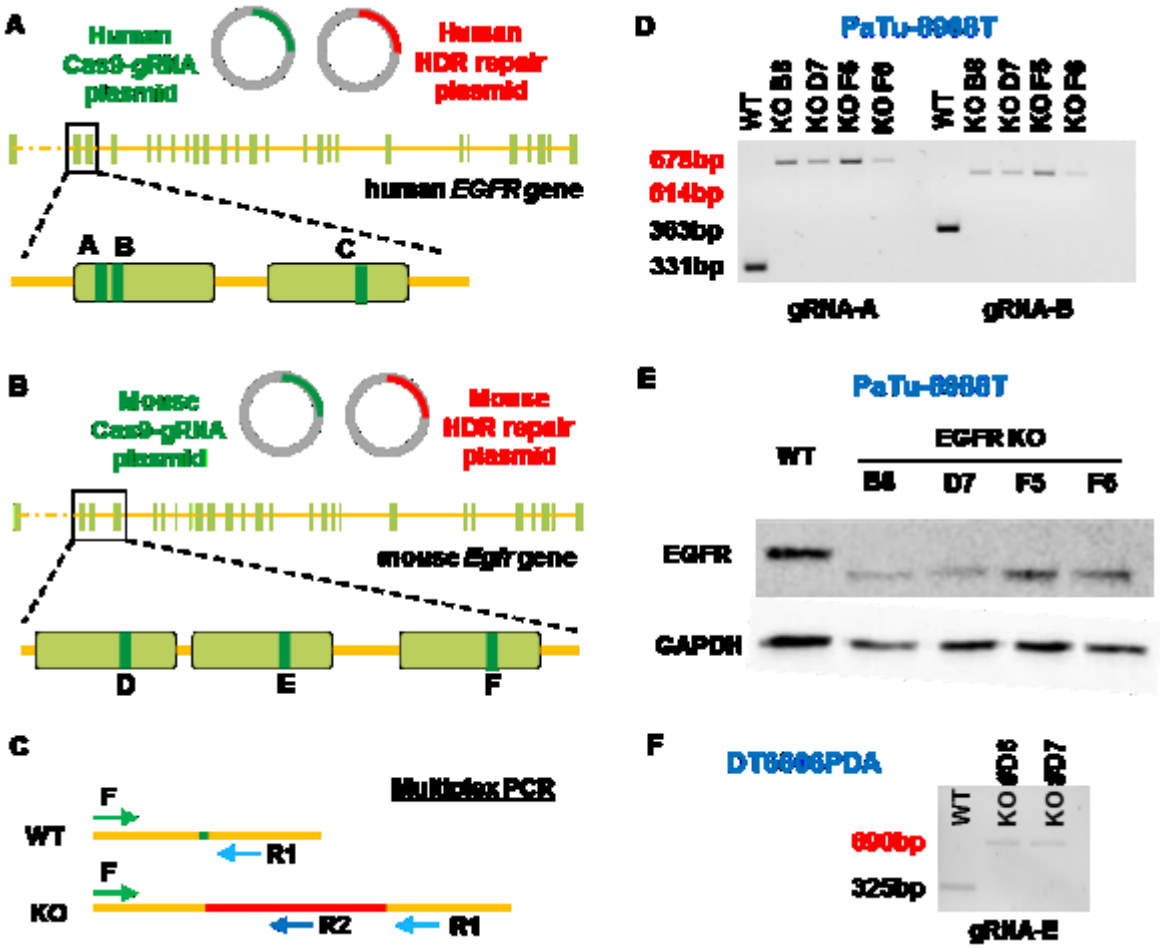

Figure 4.10: Generation of *EGFR* KO cell lines. (A) The scheme of the human *EGFR* gene and guide RNA (gRNA) targeting sites. gRNAs (transcription from plasmid A, B and C) targeted 3 different positions in 2 different exons in human *EGFR* gene. Dark green lines represent targeting positions for gRNAs. **(B)** The scheme of the mouse *Egfr* gene and gRNA targeting sites. gRNAs (transcription from plasmid D, E and F) targeted 3 different positions in 3 different exons in mouse *Egfr* gene. **(C)** The experimental design of multiplex PCR. One forward primer (F1, green) and two reverse primers (R1 and R2, blue) are used in one reaction. Yellow lines depict the original gene. The red line depicts the insertion gene. **(D)** Multiplex PCR of PaTu-8988T and 4 selected clones (B8, D7, F5 and F6). **(E)** Western blot of EGFR in PaTu-8988T and *EGFR* KO cell clones. GAPDH is used as the loading control. **(F)** Multiplex PCR data in DT6606PDA and *Egfr* KO clones (#D6, #D7).

Two single clones from DT6606PDA cells (#D6, #D7) were selected. The results of multiplex PCR confirmed the homozygous insertion (**Figure 4.10 F**). #D6, #D7 showed PCR products of 690 bp, whereas the PCR band of WT cells was detected at 325 bp. These results revealed that two clones had a homozygous insertion in the positions where gRNA-E is targeting. DT6606PDA WT cells had no insertion in *Egfr* gene.

4.11 EGFR-5FU aptamers do not influence the viability of *EGFR* KO cells

An *EGFR* knock-out (KO) cell line is an ideal model to investigate the specificity of EGFR-target drugs. To further explore the specificity of EGFR-5FU aptamers, I determined the viability of PaTu-8988T and *EGFR* KO PaTu-8988T cells, as well as the viability of DT6606PDA and *Egfr* KO DT6606PDA cells under EGFR-5FU aptamers (30 nM) treatment. The results were normalized as percentages compared to no-treatment controls. The viability is presented as bar graphs (**Figure 4.11**). EGFR-5FU aptamers decreased the viability of PaTu-8988T significantly. In contrast, EGFR-5FU aptamers failed to reduce the viability of *EGFR* KO PaTu-8988T cells. The difference between the viability of PaTu-8988T and *EGFR* KO PaTu-8988T cells was significant ($p < 0.001$). The same effect was seen for mouse PDAC cells. I observed that EGFR-5FU aptamers failed to inhibit the viability of *Egfr* KO DT6606PDA cells. And there was a big difference ($p < 0.001$) between the viability of DT6606PDA cells and that of *Egfr* KO DT6606PDA cells after 72 h incubation with EGFR-5FU aptamers. Thus, without functional EGFR protein, EGFR-5FU aptamers are not cytotoxic for PDAC cells. This result corroborated my findings that cetuximab impeded the influence of EGFR-5FU aptamers on reducing the viability of PDAC cells (**Chapter 4.9**). Together, the cytotoxicity of EGFR-5FU aptamers in PDAC cells is EGFR dependent.

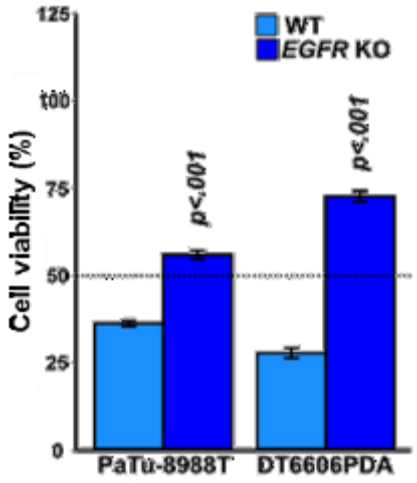

Figure 4.11: Influence of EGFR-5FU aptamers on the viability of *EGFR* KO PaTu-8988T cells and *Egfr* KO DT6606PDA cells. Bar graphs depict the viability of control and *EGFR* KO PDAC cells after incubation with EGFR-5FU aptamers (30 nM) for 72 h. Data are expressed as mean ± SEM, n = 3 in each group. P values were calculated by two-tailed, unpaired *t*-test.

4.12 EGFR-5FU aptamers are efficient in 5FU resistant PDAC cells

After showing a high treatment efficacy of EGFR-5FU aptamers in 5FU sensitive tumor cells, I wanted to evaluate the influence of EGFR-5FU aptamers on the viability of 5FU resistant PDAC cells. 5FU-resistant PaTu-8988T cells were previously established and selected from PaTu-8988T cells after a long-term (6 months) 5FU treatment. I treated 5FU-resistant PaTu-8988T and PaTu-8988T cells with EGFR-5FU aptamers or 5FU. The cell survival was normalized as percentages to untreated controls. The half-maximal inhibitory concentration (IC_{50}) was calculated and is shown as bar graphs **Figure 4.12.1**. I detected a significant decrease of the IC_{50} value for EGFR-5FU aptamer treatment compared to 5FU (p = 0.003) in PaTu-8988T cells. Notably, even though 5FU-resistant PaTu-8988T cells were extremely resistant to 5FU, EGFR-5FU aptamer treatment could strongly reduce the cell viability, which was confirmed by highly different IC_{50} values (p = 0.01). Importantly, when I compared the IC_{50} values of EGFR-5FU aptamer treatment in PaTu-8988T cells and 5FU-resistant PaTu-8988T cells, I noticed that there was no difference (p = 0.32). Thus, I uncovered that EGFR-5FU aptamers were as effective in 5FU-resistant PaTu-8988T cells as in corresponding control cells, whereas 5FU failed to show any effect at the therapeutic dose.

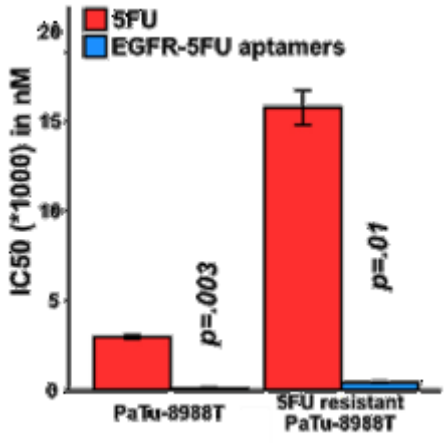

Figure 4.12.1: Effect of EGFR-5FU aptamers on the viability of 5FU resistant cancer cells. Bar graphs depicting the IC_{50} of EGFR-5FU aptamers and 5FU against PaTu-8988T cells and 5FU resistant PaTu-8988T cells after 72 h incubation. Data are expressed as mean ± SEM, n = 3 in each group.

Next, to identify the specificity of EGFR-5FU aptamers to 5FU resistant PDAC cells,

5FU resistant PaTu-8988T cells were treated with cetuximab followed by incubation with EGFR-5FU aptamers (30 nM) or the equimolar of 5FU (330 nM). The cell viability was normalized as percentages to untreated controls and is shown as bar graphs in **Figure 4.12.2**. Compared to 5FU, EGFR-5FU aptamer treatment significantly decreased the viability of 5FU-resistant PaTu-8988T cells (p = 0.009), I observed EGFR blockade by cetuximab averted the cytotoxic effect of EGFR-5FU aptamers in 5FU-resistant PaTu-8988T cells. The treatment efficacy of EGFR-5FU aptamers was not different compared to 5FU in cetuximab pre-treated 5FU-resistant PaTu-8988T cells (p = 0.33). Therefore, the influence of EGFR-5FU aptamers on the cell viability of 5FU-resistant PaTu-8988T cells was EGFR dependent.

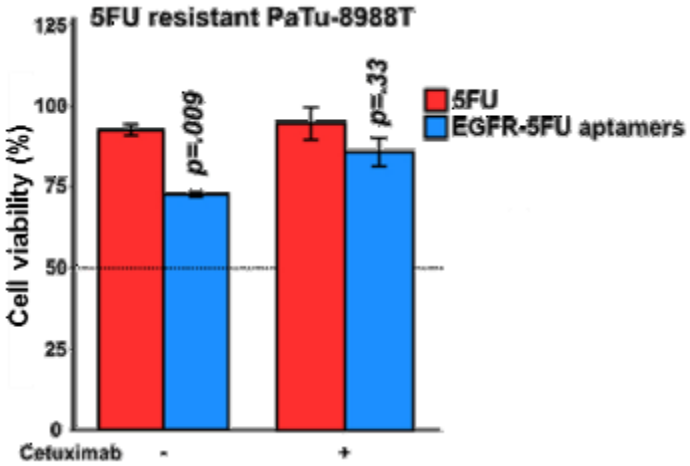

Figure 4.12.2: Influence of EGFR-5FU aptamers on the viability of cetuximab treated 5FU-resistant cancer cells. Bar graphs depict the viability between PBS pre-treated and cetuximab pre-treated 5FU resistant PaTu-8988T cells after incubation with EGFR-5FU aptamers (30 nM) or the equimolar dose of 5FU (330 nM) for 72 h. Data are expressed as mean ± SEM, n = 3 in each group. P values were calculated by two-tailed, unpaired *t*-test.

5. Discussion

Therapeutic options of pancreatic ductal adenocarcinoma (PDAC) are limited: systematic chemotherapy is only of transient benefit [80], and additional targeted therapies have not shown significant improvements in survival [12]. Thus, developing new strategies to increase local concentrations of cytotoxic drugs combined with targeted treatment may help to overcome chemoresistance and promote the outcome of therapy. In the present study, I generated and characterized a novel aptamer (EGFR-5FU aptamer) for targeted delivery of 5-fluorouracil (5FU) into EGFR overexpressing pancreatic cancer cells. My results demonstrated that the EGFR-5FU aptamer is highly specific for human and mouse EGFR protein. During EGFR binding, the EGFR-5FU aptamer occupied the side of EGF targeting and blocked the activation of EGFR signaling in human PDAC cells. Consequently, the aptamer had the capability of silencing EGF-induced EGFR signaling in human PDAC cells. In mouse PDAC cells, the aptamer bound to another Egfr protein domain and was therefore not able to inhibit Egf-mediated signaling. Notably, the aptamers were selectively internalized into PDAC cells by clathrin-dependent endocytosis. Due to the improved 5FU delivery process, EGFR-5FU aptamers elicited a cytotoxic response at very low concentrations in-vitro. Importantly, EGFR-5FU aptamers were highly efficient in promoting cytotoxicity in 5FU-sensitive and in 5FU-resistant cells. Therefore, EGFR-5FU aptamers exhibit a high potential to overcome PDAC chemoresistance in the future.

Since EGFR is overexpressed in several types of cancer, and the activation of EGFR signaling enhances uncontrolled proliferation [81-83], EGFR has emerged as a useful biomarker and a therapeutic target in different cancers. Aptamers are a class of single-stranded RNAs or DNAs that can specifically target proteins by their unique three-dimensional structures [53]. Because of their high tissue penetrability, rapid production, low synthesis cost, reduced immunogenicity, great thermal stability and ease of labeling, aptamers are popular ligands for targeted therapies [55]. The first human EGFR targeted RNA aptamer (E07) was selected in 2011 by targeting recombinant human EGFR-Fc receptor fusion protein [66]. It has a high affinity to human EGFR. In

addition, it also targets mouse Egfr. After binding to the receptor, the aptamer was internalized into EGFR-expressing cells [66]. These features provide E07 with the potential to deliver anti-tumor agents specifically into EGFR-expressing cancer cells. Moreover, Ray and colleagues proved that the aptamer E07 was an excellent carrier for targeted PDAC therapy, since EGFR is overexpressed in 90 % of PDAC cases [39, 84]. One of the standard chemotherapeutic reagents for PDAC is gemcitabine [12]. Notably, gemcitabine is a nucleotide analog, and Ray et al. used gemcitabine triphosphate (dFdCTP) as a replacement of CTP in EGFR-targeted aptamers [39, 84]. This novel process helped to deliver gemcitabine-containing aptamers into PDAC cells, which inhibited cell proliferation in-vitro. Thus, E07 was an outstanding carrier in targeted therapy. Furthermore, this approach provided a novel targeted strategy to incorporate multiple nucleotide analogs in aptamers for targeted drug delivery into EGFR-expressing cells.

Based on the published EGFR-targeted RNA aptamer E07 [66], I generated a novel 5FU-incorporated EGFR-targeted aptamer (EGFR-5FU aptamer) and tested it for selectivity, specificity and treatment efficacy in-vitro. The idea was to utilize 5-fluorouridine triphosphate (5FU-TP) instead of uridine triphosphate (UTP) to generate an intrinsically 5FU-incorporated EGFR-targeted RNA nucleotide. In 5FU, the hydrogen at the C-5 position of uracil is substituted with fluorine (F) (**Figure 5A**). A replacement of UTP with 5FU-TP in the RNA does not interfere with the structure of the pentose sugars (**Figure 5B)**. Since T7 RNA polymerase catalyzes the formation of RNA (phosphoester bonds between the 3' carbon atom of one sugar molecule and the 5' carbon atom of another) in the 5'→ 3' direction according to the DNA template [85], it was no problem to generate 5FU-TP-incorporated aptamers by in-vitro transcription with T7 RNA polymerase.

I synthesized EGFR-5FU aptamers and EGFR aptamers, whereby 11 5FU-TPs were successfully incorporated into one EGFR-5FU aptamer. Besides the aptamer monomers, dimers and tetramers of the aptamer were also created during the in-vitro transcription. Hydrophobic interaction of RNA was considered as a reason for aptamer dimerization and tetramerization. I was unsure if the three-dimensional structures of

these multimers are able to recognize EGFR, thus, I choose only the monomer of the EGFR-5FU aptamer and EGFR aptamer for further investigation.

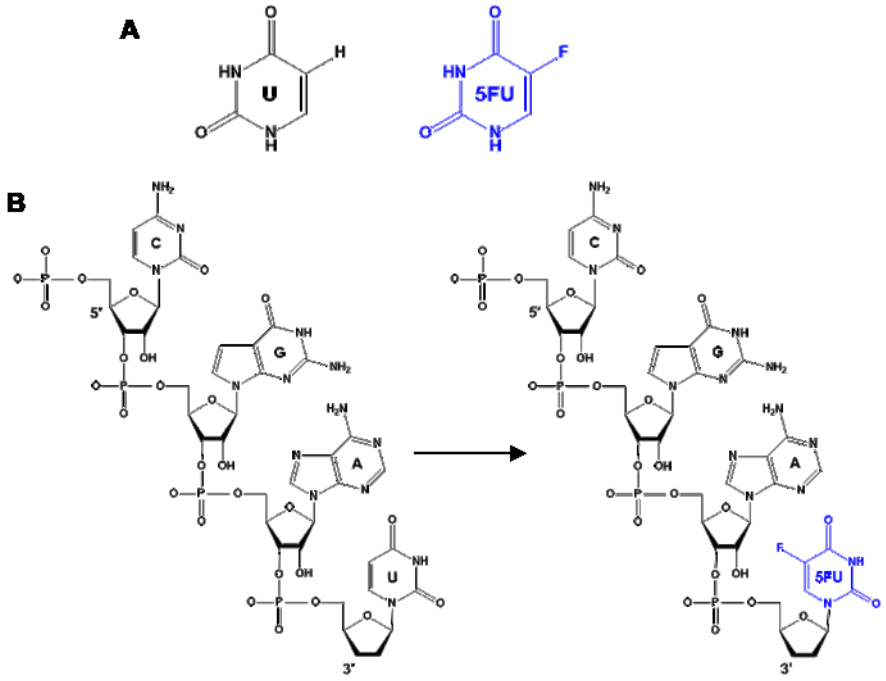

Figure 5: Chemical structures of nucleotides. (A) The structure of uracil (U) and 5-fluorouracil (5FU). **(B)** RNA structure and 5FU incorporated RNA structure in the 5'→ 3' direction (from up to down). Replacement of UTPs to 5FU-TPs does not interfere with the structure of pentose sugars. Abbreviations: A, adenine; C, cytosine; G, guanine; U, uracil; 5FU, 5-fluorouracil.

Highly selective and effective binding is an essential prerequisite for targeted drug delivery. EGFR-5FU aptamers had a low K_d value to human EGFR protein, which displays their high targeting efficiency in human PDAC cell treatment. Moreover, the replacement of UTP with 5FU-TP in the RNA did not change the aptamer binding strength to human EGFR. One plausible explanation can be that the EGFR-5FU aptamer and EGFR aptamer have the same primary, secondary, and tertiary structure. In-silico docking of the human extracellular domain of EGFR with EGFR aptamer and EGFR-5FU aptamer further demonstrated that EGFR aptamers and its 5FU-incorporated counterpart stipulated equivalent and excellent binding affinity. Thus, with the effective binding, EGFR-5FU aptamer could be used for human EGFR-targeted drug delivery.

Interestingly, my data showed that EGFR aptamers and EGFR-5FU aptamers were functional on human and mouse PDAC cells. One explanation is that the extracellular domain of human and mouse EGFR share a sequence homology of around 97 %. However, I observed that co-incubation with EGF and EGFR aptamer blocked EGFR cell signaling in human PDAC cells, but not in mouse PDAC cells. One plausible cause was that the EGFR aptamer and EGFR-5FU aptamer bind to different protein pockets in the extracellular domain of human and mouse EGFR. Even though EGFR aptamer and EGFR-5FU aptamer had a similar binding affinity, the aptamer binding location interferes with EGF binding sites in the extracellular domain of human EGFR, but not in mouse Egfr. Several studies demonstrated that EGFR inhibitors could not block the mutant KRAS-related ERK or PI3K signaling in PDAC cells [86, 87]. Since neither EGFR monoclonal antibodies (mAbs) nor EGFR tyrosine kinase inhibitors (TKIs) improve the survival of PDAC patients [46, 47], it is believed that continuous activation of mutant KRAS is responsible for the treatment failure of EGFR-targeted therapies. The continuous ERK pathway activation due to mutant KRAS provokes among others undirected cancer proliferation [88]. In my study, I confirmed that EGFR aptamers act as EGFR inhibitors on human cancer cells (Chapter 4.5, Figure 4.5.1). Although EGFR aptamers showed an inhibition of the EGFR/ERK signaling in human PDAC cells, the pathway blockage is only achieved during acute EGF stimulation. However, no changes in the baseline EGFR/ERK signaling activity were detected after EGFR aptamer treatment of PDAC cells. Therefore, EGFR aptamers do not influence baseline EGFR/ERK signaling in PDAC cells. Moreover, my results demonstrated that EGFR aptamers cannot reduce the viability of cancer cells (Chapter 4.7.1). In line with these data, it is reported that even high doses of EGFR aptamers did not induce growth inhibition of human PDAC cells [49].

One aim of my study was to deliver concentrated therapeutic agents into cancer cells for targeted PDAC therapy. To confirm that EGFR-5FU aptamers, like EGFR aptamers, are internalized into EGFR-overexpressing cells [66], I performed time-lapsed live cell imaging. I observed a significant accumulation of EGFR-5FU aptamers into PDAC cells and subsequently assessed the uptake specificity of the aptamers. The blockage of

the EGFR through cetuximab pretreatment revealed that aptamer internalization is receptor-mediated and depends on the expression of EGFR. The cellular uptake can be divided into active and passive mechanisms, based on energy consumption. Since cells usually take up foreign materials through an active and energy-dependent process [89], I assumed that EGFR-5FU aptamers were actively transported into PDAC cancer cells. To further investigate the exact uptake mechanisms, I incubated the cells with specific inhibitors to prevent active channel transport, clathrin-dependent endocytosis, caveolin-dependent endocytosis, clathrin- and caveolin-independent endocytosis and lipid raft formation. Notably, the short incubation time and a low concentration of aptamers were used to minimize non-specific cellular uptake of unbound aptamers, which occurs via non-specific mechanisms of endocytosis (macro-pinocytosis) when treating the cells with high concentrations of aptamers [89, 90]. I uncovered that dynasore pre-treatment inhibited the uptake of EGFR-5FU aptamers into PDAC cells. This data showed that the EGFR-5FU aptamers uptake into PDAC cancer cells was driven by clathrin-mediated endocytosis.

Several studies have proven that the cellular uptake of aptamers is via receptor-dependent and clathrin-mediated endocytosis [91]. In addition, once internalized, aptamers are distributed to early endosomes, late endosomes and lysosomes [92]. Endosomal escape is an essential way to deliver aptamers into the cytoplasm for achieving therapeutic activity [93]. Besides, nucleoside transporters, such as ENT3 are located on lysosomes and can act as cargos to deliver degraded nucleosides to the cytoplasm [94]. Therefore, degraded 5FU-TPs could be released from lysosomes by nucleoside transporters to induce cytotoxic effects as well. To further investigate the mechanisms of drug release, the subcellular distribution of EGFR-5FU aptamers can be explored, especially the co-localization analysis of aptamers with endosomes and lysosomes. Moreover, since the change in lysosomal pH (from acid to alkali) indicated the cargo release [95], monitoring lysosomal pH after the cellular uptake of EGFR-5FU aptamers can be performed to detect this process. To exclude the possibility that cellular uptake of EGFR-5FU aptamers was via passive transport, I measured the amount of EGFR-5FU aptamers that went through an artificial membrane. Notably,

different concentrations of aptamers (from low to high) were used to set a concentration gradients between two membrane sides. I observed no EGFR-5FU aptamers could pass the membrane. This result demonstrated that the internalization process did not occur through passive diffusion of EGFR-5FU aptamers.

Having confirmed that EGFR-5FU aptamers could effectively target EGFR protein on the membrane of PDAC cells followed by cellular internalization, the treatment efficacy is the next important issue to investigate. 5FU anti-tumor effects are introduced only after cellular conversion into several active metabolites [28]. Importantly, the loaded cargos on the EGFR-5FU aptamers were multiple 5FU-TPs and not 5FUs. Therefore, 5FU-TP, one of the active metabolites of 5FU, was the actual therapeutic reagent delivered into target cells.

I explored the cytotoxic effect of EGFR-5FU aptamers by generating dose-response curves. I detected that, compared to 5FU, EGFR-5FU aptamer treatment decreased the survival of PDAC cells significantly. Notably, EGFR-5FU aptamers loaded the same amount of 5FU as 5FU alone, but at a 10-fold lower dose. This high 5FU delivery efficacy allowed EGFR-5FU aptamers to elicit an increased treatment potency in human and mouse PDAC cell lines. Ray et al. generated gemcitabine contained EGFR aptamers by the replacement of CTP to gemcitabine triphosphate (dFdCTP) [84]. This aptamer was loaded with seven molar gemcitabine in one molar aptamers. Compared to gemcitabine-loaded EGFR aptamers, which could inhibit 35 % viability of PDAC cells at the concentration of 100 nM, my EGFR-5FU aptamers were able to obstruct over 70 % survival of PDAC cells at the same concentration. This comparison further revealed that EGFR-5FU aptamers have a high treatment efficacy in PDAC.

The high metastatic potential of PDAC contributes to the poor outcome [96]. Even in tumors that are sensitive to chemotherapy, metastases are often a major reason for treatment failures [97]. The potential of tumor cells to form colonies, and thus metastases, under EGFR-5FU aptamer treatment conditions was investigated in vitro by performing colony-forming assays. Here, I detected that a very low dose of EGFR-5FU aptamers strongly inhibited colony formation of PDAC cells. With the feature of high effective impediment in colony formation, EGFR-5FU aptamers are more

conceivable to benefit the treatment in PDAC targeted therapy.

Several studies have found that 5FU induces G1/S cell cycle arrest in cancer cells, which results in DNA/RNA damage [78, 79, 98] and causes "cellular suicide" through programmed cell death [99]. My data confirmed that high-dose 5FU treatment leads to a cell cycle arrest in PDAC cells (Chapter 4.8). Interestingly, compared to the high dose of 5FU, a low dose of EGFR-5FU aptamers could induce increased G1 phase arrest in PDAC cells. This result revealed the extreme influence of EGFR-5FU aptamers on the PDAC cell cycle. It also implicates that EGFR-5FU aptamers have a similar cytotoxic mechanism as 5FU. More experiments, such as the expression of apoptosis markers, need to be performed in the future to identify the cell death pathway after EGFR-5FU aptamers treatment.

The big influence of EGFR-5FU aptamer on reducing proliferation, decreasing colony-forming, and inducing significant G1 arrest reflected its high treatment efficacy. However, it is not enough. A good specificity is important to bypass healthy cells and produce fewer side effects in targeted therapy. To assess the specificity of EGFR-5FU aptamers in targeted PDAC treatment, EGFR protein was blocked via incubation with EGFR monoclonal antibodies or the *EGFR* gene was deleted in PDAC cells. Cetuximab interacted exclusively with domain III of soluble human EGFR, partially occupying the ligand-binding region and sterically preventing the receptor from dimerization [100]. Anti-Egfr antibody-targeted the extracellular domain of mouse Egfr and inhibited mouse Egfr phosphorylation. CRISPR/Cas9 system helped to generate *EGFR* gene KO PDAC cells so that no functional EGFR proteins could express on the membrane. I observed that EGFR antibodies could prevent EGFR-5FU aptamer-mediated cytotoxicity in PDAC cells. Similarly, EGFR-5FU aptamers failed to induce cell death of *EGFR* KO PDAC cells. Therefore, EGFR-5FU aptamers are specific to EGFR-overexpressing cancer cells. MCF-7 cells, which express reduced levels of EGFR receptors [101], were also used to evaluate the specificity of aptamers. EGFR-5FU aptamer treatment did not show an impact on cell survival of MCF-7 cells. Thus, EGFR-5FU aptamers do not exhibit cytotoxic effects on EGFR-low-expressing cells.

However, EGFR-non-expressing and EGFR-low-expressing cells are rare. The

majority of normal cells express normal levels of EGFR to sustain their physiological function [41]. Although normal cells only express no more than one-tenth of receptors in comparison to cancer cells (4×10^4 - 10^5 receptors per cell vs. more than 10^6 receptors per cell), EGFR-5FU aptamers can be in principle internalized into normal cells and induce undesired cytotoxicity. The influence of EGFR-5FU aptamers on normal cells needs to be investigated in the future.

Chemoresistance is a major complication in PDAC therapy [102]. Several factors are involved in 5FU resistance. One of the important mechanisms is the low expression of vital intracellular enzymes in cancer cells [103]. Since 5FU itself has no cytotoxic effects, low expression of enzymes such as thymidine synthase (TS) fails to generate active metabolites of 5FU in target cells and leads to 5FU resistance [104]. Thus, direct delivery of active 5FU metabolites may help to skip the drug activation step and sensitize the cancer cells. Notably, my novel designed EGFR-5FU aptamers loaded the therapeutic reagent 5FU-TP and not 5FU. 5FU-TP is just one of the active metabolites of 5FU, which induces RNA and DNA damage in target cells [28]. Thus, successful delivery of EGFR-5FU aptamer could help to directly transfer an abundant amount of active 5FU metabolites and to improve its cellular cytotoxicity. To investigate this probability, I checked the treatment efficacy of EGFR-5FU aptamers in 5FU-resistant PDAC cells. I detected that EGFR-5FU aptamers were equally efficient in 5FU-resistant cells and 5FU-sensitive cells. This exciting result indicated that treatment with EGFR-5FU aptamers could be an effective strategy to target 5FU-resistant cells. Therefore, this strategy had the possibility to overcome the difficulty of 5FU resistance in PDAC.

To summarize, I successfully generated EGFR-5FU aptamers, which are highly specific for EGFR protein binding and could be selectively taken up by PDAC cells via clathrin-dependent endocytosis. With the high 5FU delivery efficiency, EGFR-5FU aptamer could induce significant cytotoxicity in 5FU-resistant and 5FU-sensitive PDAC cells. Thus, EGFR-5FU aptamers have the potential to improve PDAC therapy and might suspend chemoresistance in the future.

6. Conclusion

This is the first experiment to treat pancreatic ductal adenocarcinoma (PDAC) cells with an EGFR-targeted RNA aptamer that has intrinsically incorporated 5FU (EGFR-5FU aptamer). This novel designed aptamer is able to target EGFR and deliver abundant active metabolites of 5FU into EGFR-overexpressing PDAC cells. In addition, it blocks EGF-activated EGFR signaling in human PDAC cells. EGFR-5FU aptamers are highly specific to cancer cells, overcome 5FU resistance and represent a successful treatment option for PDAC. Thus, I believe that my study represents an important new step toward the application of aptamers as both carriers and inhibitors in cancer-targeted therapy. Moreover, this targeted treatment strategy has the potential to solve the problem of chemoresistance in the future. Furthermore, it provides an efficient approach and in principle could be tested in other EGFR overexpressing cancers.

7. References

1. Yadav, D. and A.B. Lowenfels, *The epidemiology of pancreatitis and pancreatic cancer.* Gastroenterology, 2013. **144**(6): p. 1252-61.
2. Ferlay, J., M. Colombet, I. Soerjomataram, T. Dyba, et al., *Cancer incidence and mortality patterns in Europe: Estimates for 40 countries and 25 major cancers in 2018.* Eur J Cancer, 2018. **103**: p. 356-387.
3. Bray, F., J. Ferlay, I. Soerjomataram, R.L. Siegel, et al., *Global cancer statistics 2018: GLOBOCAN estimates of incidence and mortality worldwide for 36 cancers in 185 countries.* CA Cancer J Clin, 2018. **68**(6): p. 394-424.
4. Siegel, R.L., K.D. Miller and A. Jemal, *Cancer statistics, 2020.* CA Cancer J Clin, 2020. **70**(1): p. 7-30.
5. Kamisawa, T., L.D. Wood, T. Itoi, and K. Takaori, *Pancreatic cancer.* The Lancet, 2016. **388**(10039): p. 73-85.
6. Huang, L., L. Jansen, Y. Balavarca, E. Molina-Montes, et al., *Resection of pancreatic cancer in Europe and USA: an international large-scale study highlighting large variations.* Gut, 2019. **68**(1): p. 130-139.
7. Oneda, E. and A. Zaniboni, *Are We Sure that Adjuvant Chemotherapy is the Best Approach for Resectable Pancreatic Cancer? Are We in the Era of Neoadjuvant Treatment? A Review of Current Literature.* J Clin Med, 2019. **8**(11).
8. Conroy, T., P. Hammel, M. Hebbar, M. Ben Abdelghani, et al., *FOLFIRINOX or Gemcitabine as Adjuvant Therapy for Pancreatic Cancer.* N Engl J Med, 2018. **379**(25): p. 2395-2406.
9. Hall, B.R., A. Cannon, P. Atri, C.S. Wichman, et al., *Advanced pancreatic cancer: a meta-analysis of clinical trials over thirty years.* Oncotarget, 2018. **9**(27): p. 19396.
10. Conroy, T., F. Desseigne, M. Ychou, O. Bouché, et al., *FOLFIRINOX versus gemcitabine for metastatic pancreatic cancer.* 2011. **364**(19): p. 1817-1825.
11. Goldstein, D., R.H. El Maraghi, P. Hammel, V. Heinemann, et al., *Updated survival from a randomized phase III trial (MPACT) of nab-paclitaxel plus gemcitabine versus gemcitabine alone for patients (pts) with metastatic adenocarcinoma of the pancreas*. 2014, American Society of Clinical Oncology.
12. Neoptolemos, J.P., J. Kleeff, P. Michl, E. Costello, et al., *Therapeutic developments in pancreatic cancer: current and future perspectives.* Nat Rev Gastroenterol Hepatol, 2018. **15**(6): p. 333-348.
13. Uson Junior, P.L.S., E.T. Rother, F.C. Maluf, and D.D.G. Bugano, *Meta-analysis of Modified FOLFIRINOX Regimens for Patients With Metastatic Pancreatic Cancer.* Clin Colorectal Cancer, 2018. **17**(3): p. 187-197.
14. Zeng, S., M. Pottler, B. Lan, R. Grutzmann, et al., *Chemoresistance in Pancreatic Cancer.* Int J Mol Sci, 2019. **20**(18).
15. Amrutkar, M. and I.P. Gladhaug, *Pancreatic Cancer Chemoresistance to Gemcitabine.* Cancers (Basel), 2017. **9**(11).

16. Xie, D. and K. Xie, *Pancreatic cancer stromal biology and therapy.* Genes & Diseases, 2015. **2**(2): p. 133-143.
17. Adamska, A., O. Elaskalani, A. Emmanouilidi, M. Kim, et al., *Molecular and cellular mechanisms of chemoresistance in pancreatic cancer.* Adv Biol Regul, 2018. **68**: p. 77-87.
18. Saiki, Y., Y. Yoshino, H. Fujimura, T. Manabe, et al., *DCK is frequently inactivated in acquired gemcitabine-resistant human cancer cells.* Biochem Biophys Res Commun, 2012. **421**(1): p. 98-104.
19. Ohhashi, S., K. Ohuchida, K. Mizumoto, H. Fujita, et al., *Down-regulation of deoxycytidine kinase enhances acquired resistance to gemcitabine in pancreatic cancer.* 2008. **28**(4B): p. 2205-2212.
20. Tang, K., Z. Zhang, Z. Bai, X. Ma, et al., *Enhancement of gemcitabine sensitivity in pancreatic cancer by co-regulation of dCK and p8 expression.* Oncol Rep, 2011. **25**(4): p. 963-70.
21. Ohmine, K., K. Kawaguchi, S. Ohtsuki, F. Motoi, et al., *Quantitative Targeted Proteomics of Pancreatic Cancer: Deoxycytidine Kinase Protein Level Correlates to Progression-Free Survival of Patients Receiving Gemcitabine Treatment.* Mol Pharm, 2015. **12**(9): p. 3282-91.
22. Sierzega, M., R. Pach, P. Kulig, J. Legutko, et al., *Prognostic Implications of Expression Profiling for Gemcitabine-Related Genes (hENT1, dCK, RRM1, RRM2) in Patients With Resectable Pancreatic Adenocarcinoma Receiving Adjuvant Chemotherapy.* Pancreas, 2017. **46**(5): p. 684-689.
23. Mameri, H., I. Bieche, D. Meseure, E. Marangoni, et al., *Cytidine Deaminase Deficiency Reveals New Therapeutic Opportunities against Cancer.* Clin Cancer Res, 2017. **23**(8): p. 2116-2126.
24. Bjanes, T.K., L.P. Jordheim, J. Schjott, T. Kamceva, et al., *Intracellular Cytidine Deaminase Regulates Gemcitabine Metabolism in Pancreatic Cancer Cell Lines.* Drug Metab Dispos, 2020. **48**(3): p. 153-158.
25. Frese, K.K., A. Neesse, N. Cook, T.E. Bapiro, et al., *nab-Paclitaxel potentiates gemcitabine activity by reducing cytidine deaminase levels in a mouse model of pancreatic cancer.* Cancer Discov, 2012. **2**(3): p. 260-269.
26. Heidelberger, C., N. Chaudhuri, P. Danneberg, D. Mooren, et al., *Fluorinated pyrimidines, a new class of tumour-inhibitory compounds.* Nature, 1957. **179**(4561): p. 663-666.
27. Vodenkova, S., T. Buchler, K. Cervena, V. Veskrnova, et al., *5-fluorouracil and other fluoropyrimidines in colorectal cancer: Past, present and future.* Pharmacol Ther, 2020. **206**: p. 107447.
28. Longley, D.B., D.P. Harkin and P.G. Johnston, *5-fluorouracil: mechanisms of action and clinical strategies.* Nat Rev Cancer, 2003. **3**(5): p. 330-8.
29. Miura, K., M. Kinouchi, K. Ishida, W. Fujibuchi, et al., *5-fu metabolism in cancer and orally-administrable 5-fu drugs.* Cancers (Basel), 2010. **2**(3): p. 1717-30.
30. Motoi, F. and M. Unno, *Adjuvant and neoadjuvant treatment for pancreatic adenocarcinoma.* Jpn J Clin Oncol, 2020.

31. Neoptolemos, J.P., D.H. Palmer, P. Ghaneh, E.E. Psarelli, et al., *Comparison of adjuvant gemcitabine and capecitabine with gemcitabine monotherapy in patients with resected pancreatic cancer (ESPAC-4): a multicentre, open-label, randomised, phase 3 trial.* 2017. **389**(10073): p. 1011-1024.
32. Unno, M., F. Motoi, Y. Matsuyama, S. Satoi, et al., *Randomized phase II/III trial of neoadjuvant chemotherapy with gemcitabine and S-1 versus upfront surgery for resectable pancreatic cancer (Prep-02/JSAP-05)*. 2019, American Society of Clinical Oncology.
33. Burris, H.r., M.J. Moore, J. Andersen, M.R. Green, et al., *Improvements in survival and clinical benefit with gemcitabine as first-line therapy for patients with advanced pancreas cancer: a randomized trial.* Journal of clinical oncology, 1997. **15**(6): p. 2403-2413.
34. Wang, W.B., Y. Yang, Y.P. Zhao, T.P. Zhang, et al., *Recent studies of 5-fluorouracil resistance in pancreatic cancer.* World J Gastroenterol, 2014. **20**(42): p. 15682-90.
35. Wigle, T.J., E.V. Tsvetkova, S.A. Welch, and R.B. Kim, *DPYD and Fluorouracil-Based Chemotherapy: Mini Review and Case Report.* Pharmaceutics, 2019. **11**(5).
36. Kurata, N., H. Fujita, K. Ohuchida, K. Mizumoto, et al., *Predicting the chemosensitivity of pancreatic cancer cells by quantifying the expression levels of genes associated with the metabolism of gemcitabine and 5-fluorouracil.* Int J Oncol, 2011. **39**(2): p. 473-82.
37. Nambaru, P.K., T. Hubner, K. Kock, S. Mews, et al., *Drug efflux transporter multidrug resistance-associated protein 5 affects sensitivity of pancreatic cancer cell lines to the nucleoside anticancer drug 5-fluorouracil.* Drug Metab Dispos, 2011. **39**(1): p. 132-9.
38. Yarden, Y., *The EGFR family and its ligands in human cancer: signalling mechanisms and therapeutic opportunities.* European journal of cancer, 2001. **37**: p. 3-8.
39. Ueda, S., S. Ogata, H. Tsuda, N. Kawarabayashi, et al., *The correlation between cytoplasmic overexpression of epidermal growth factor receptor and tumor aggressiveness: poor prognosis in patients with pancreatic ductal adenocarcinoma.* 2004. **29**(1): p. e1-e8.
40. Grapa, C.M., T. Mocan, D. Gonciar, C. Zdrehus, et al., *Epidermal Growth Factor Receptor and Its Role in Pancreatic Cancer Treatment Mediated by Nanoparticles.* Int J Nanomedicine, 2019. **14**: p. 9693-9706.
41. Wee, P. and Z. Wang, *Epidermal Growth Factor Receptor Cell Proliferation Signaling Pathways.* Cancers (Basel), 2017. **9**(5).
42. Yamaoka, T., M. Ohba and T. Ohmori, *Molecular-Targeted Therapies for Epidermal Growth Factor Receptor and Its Resistance Mechanisms.* Int J Mol Sci, 2017. **18**(11).
43. da Cunha Santos, G., F.A. Shepherd and M.S. Tsao, *EGFR Mutations and Lung Cancer.* Annual Review of Pathology: Mechanisms of Disease, 2011. **6**(1): p. 49-69.

44. Cremolini, C., M. Schirripa, C. Antoniotti, R. Moretto, et al., *First-line chemotherapy for mCRC-a review and evidence-based algorithm.* Nat Rev Clin Oncol, 2015. **12**(10): p. 607-19.
45. Agarwal, V., A. Subash, R.C. Nayar, and V. Rao, *Is EGFR really a therapeutic target in head and neck cancers?* J Surg Oncol, 2019. **119**(6): p. 685-686.
46. Chiramel, J., A.C. Backen, R. Pihlak, A. Lamarca, et al., *Targeting the Epidermal Growth Factor Receptor in Addition to Chemotherapy in Patients with Advanced Pancreatic Cancer: A Systematic Review and Meta-Analysis.* Int J Mol Sci, 2017. **18**(5).
47. Ottaiano, A., M. Capozzi, C. De Divitiis, A. De Stefano, et al., *Gemcitabine mono-therapy versus gemcitabine plus targeted therapy in advanced pancreatic cancer: a meta-analysis of randomized phase III trials.* Acta Oncol, 2017. **56**(3): p. 377-383.
48. Lanfredini, S., A. Thapa and E. O'Neill, *RAS in pancreatic cancer.* Biochem Soc Trans, 2019. **47**(4): p. 961-972.
49. Mann, K.M., H. Ying, J. Juan, N.A. Jenkins, et al., *KRAS-related proteins in pancreatic cancer.* Pharmacol Ther, 2016. **168**: p. 29-42.
50. Singh, A., J. Xu, G. Mattheolabakis, and M. Amiji, *EGFR-targeted gelatin nanoparticles for systemic administration of gemcitabine in an orthotopic pancreatic cancer model.* Nanomedicine, 2016. **12**(3): p. 589-600.
51. Santos-Rebelo, A., P. Kumar, V. Pillay, Y.E. Choonara, et al., *Development and Mechanistic Insight into the Enhanced Cytotoxic Potential of Parvifloron D Albumin Nanoparticles in EGFR-Overexpressing Pancreatic Cancer Cells.* Cancers (Basel), 2019. **11**(11).
52. McDaid, W.J., M.K. Greene, M.C. Johnston, E. Pollheimer, et al., *Repurposing of Cetuximab in antibody-directed chemotherapy-loaded nanoparticles in EGFR therapy-resistant pancreatic tumours.* Nanoscale, 2019. **11**(42): p. 20261-20273.
53. Bayat, P., R. Nosrati, M. Alibolandi, H. Rafatpanah, et al., *SELEX methods on the road to protein targeting with nucleic acid aptamers.* Biochimie, 2018. **154**: p. 132-155.
54. Zhang, Y., B.S. Lai and M. Juhas, *Recent Advances in Aptamer Discovery and Applications.* Molecules, 2019. **24**(5).
55. Nimjee, S.M., R.R. White, R.C. Becker, and B.A. Sullenger, *Aptamers as Therapeutics.* Annu Rev Pharmacol Toxicol, 2017. **57**: p. 61-79.
56. Banerjee, J. and M. Nilsen-Hamilton, *Aptamers: multifunctional molecules for biomedical research.* J Mol Med (Berl), 2013. **91**(12): p. 1333-42.
57. Ali, M.H., M.E. Elsherbiny and M. Emara, *Updates on Aptamer Research.* Int J Mol Sci, 2019. **20**(10).
58. Takakura, K., A. Kawamura, Y. Torisu, S. Koido, et al., *The Clinical Potential of Oligonucleotide Therapeutics against Pancreatic Cancer.* Int J Mol Sci, 2019. **20**(13).
59. Zhu, G. and X. Chen, *Aptamer-based targeted therapy.* Adv Drug Deliv Rev, 2018. **134**: p. 65-78.

60. Nuzzo, S., G. Roscigno, A. Affinito, F. Ingenito, et al., *Potential and Challenges of Aptamers as Specific Carriers of Therapeutic Oligonucleotides for Precision Medicine in Cancer.* Cancers (Basel), 2019. **11**(10).
61. Soldevilla, M.M., D. Meraviglia-Crivelli de Caso, A.P. Menon, and F. Pastor, *Aptamer-iRNAs as Therapeutics for Cancer Treatment.* Pharmaceuticals (Basel), 2018. **11**(4).
62. Yoon, S., B. Armstrong, N. Habib, and J.J. Rossi, *Blind SELEX Approach Identifies RNA Aptamers That Regulate EMT and Inhibit Metastasis.* Mol Cancer Res, 2017. **15**(7): p. 811-820.
63. Kim, Y.H., H.J. Sung, S. Kim, E.O. Kim, et al., *An RNA aptamer that specifically binds pancreatic adenocarcinoma up-regulated factor inhibits migration and growth of pancreatic cancer cells.* Cancer Lett, 2011. **313**(1): p. 76-83.
64. Dua, P., S. S, S. Kim, and D.K. Lee, *ALPPL2 Aptamer-Mediated Targeted Delivery of 5-Fluoro-2'-Deoxyuridine to Pancreatic Cancer.* Nucleic Acid Ther, 2015. **25**(4): p. 180-7.
65. Yoon, S., K.W. Huang, V. Reebye, D. Spalding, et al., *Aptamer-Drug Conjugates of Active Metabolites of Nucleoside Analogs and Cytotoxic Agents Inhibit Pancreatic Tumor Cell Growth.* Mol Ther Nucleic Acids, 2017. **6**: p. 80-88.
66. Li, N., H.H. Nguyen, M. Byrom, and A.D. Ellington, *Inhibition of cell proliferation by an anti-EGFR aptamer.* PLoS One, 2011. **6**(6): p. e20299.
67. van Zundert, G.C.P., J. Rodrigues, M. Trellet, C. Schmitz, et al., *The HADDOCK2.2 Web Server: User-Friendly Integrative Modeling of Biomolecular Complexes.* J Mol Biol, 2016. **428**(4): p. 720-725.
68. Ogiso, H., R. Ishitani, O. Nureki, S. Fukai, et al., *Crystal structure of the complex of human epidermal growth factor and receptor extracellular domains.* 2002. **110**(6): p. 775-787.
69. Schots, A., B.J. Van der Leede, E. De Jongh, and E. Egberts, *A method for the determination of antibody affinity using a direct ELISA.* Journal of immunological methods, 1988. **109**(2): p. 225-233.
70. Mayor, S. and R.E. Pagano, *Pathways of clathrin-independent endocytosis.* Nat Rev Mol Cell Biol, 2007. **8**(8): p. 603-12.
71. Poynton, F.E., S.A. Bright, S. Blasco, D.C. Williams, et al., *The development of ruthenium(ii) polypyridyl complexes and conjugates for in vitro cellular and in vivo applications.* Chem Soc Rev, 2017. **46**(24): p. 7706-7756.
72. Li, Y., L. Gao, X. Tan, F. Li, et al., *Lipid rafts-mediated endocytosis and physiology-based cell membrane traffic models of doxorubicin liposomes.* Biochim Biophys Acta, 2016. **1858**(8): p. 1801-11.
73. Crowley, L.C., M.E. Christensen and N.J. Waterhouse, *Measuring Survival of Adherent Cells with the Colony-Forming Assay.* Cold Spring Harb Protoc, 2016. **2016**(8).
74. Darzynkiewicz, Z., G. Juan and E. Bedner, *Determining cell cycle stages by flow cytometry.* Current protocols in cell biology, 1999. **1**(1): p. 8.4. 1-8.4. 18.

75. Ma, Y., L. Zhang and X. Huang, *Genome modification by CRISPR/Cas9.* FEBS J, 2014. **281**(23): p. 5186-93.
76. Wang, Z., *ErbB receptors and cancer*, in *ErbB Receptor Signaling*. 2017, Springer. p. 3-35.
77. Oda, K., Y. Matsuoka, A. Funahashi, and H. Kitano, *A comprehensive pathway map of epidermal growth factor receptor signaling.* Mol Syst Biol, 2005. **1**: p. 2005 0010.
78. Li, M.-H., D. Ito, M. Sanada, T. Odani, et al., *Effect of 5-fluorouracil on G1 phase cell cycle regulation in oral cancer cell lines.* Oral Oncology, 2004. **40**(1): p. 63-70.
79. Liu, H.C., G.G. Chen, A.C. Vlantis, B.C. Leung, et al., *5-fluorouracil mediates apoptosis and G1/S arrest in laryngeal squamous cell carcinoma via a p53-independent pathway.* 2006. **12**(6): p. 482-493.
80. Regel, I., J. Mayerle and U.M. Mahajan, *Current Strategies and Future Perspectives for Precision Medicine in Pancreatic Cancer.* Cancers (Basel), 2020. **12**(4).
81. Moore, M.J., D. Goldstein, J. Hamm, A. Figer, et al., *Erlotinib plus gemcitabine compared with gemcitabine alone in patients with advanced pancreatic cancer: a phase III trial of the National Cancer Institute of Canada Clinical Trials Group.* J Clin Oncol, 2007. **25**(15): p. 1960-6.
82. Tobita, K., H. Kijima, S. Dowaki, H. Kashiwagi, et al., *Epidermal growth factor receptor expression in human pancreatic cancer: Significance for liver metastasis.* 2003. **11**(3): p. 305-309.
83. Ghaneh, P., A. Kawesha, J.D. Evans, and J.P.J.J.o.h.-b.-p.s. Neoptolemos, *Molecular prognostic markers in pancreatic cancer.* 2002. **9**(1): p. 1-11.
84. Ray, P., M.A. Cheek, M.L. Sharaf, N. Li, et al., *Aptamer-mediated delivery of chemotherapy to pancreatic cancer cells.* Nucleic Acid Ther, 2012. **22**(5): p. 295-305.
85. Tabor, S., *Expression using the T7 RNA polymerase/promoter system.* Current protocols in molecular biology, 1990. **11**(1): p. 16.2. 1-16.2. 11.
86. Blasco, M.T., C. Navas, G. Martin-Serrano, O. Grana-Castro, et al., *Complete Regression of Advanced Pancreatic Ductal Adenocarcinomas upon Combined Inhibition of EGFR and C-RAF.* Cancer Cell, 2019. **35**(4): p. 573-587 e6.
87. Diersch, S., M. Wirth, C. Schneeweis, S. Jors, et al., *Kras(G12D) induces EGFR-MYC cross signaling in murine primary pancreatic ductal epithelial cells.* Oncogene, 2016. **35**(29): p. 3880-6.
88. Drosten, M. and M. Barbacid, *Targeting the MAPK Pathway in KRAS-Driven Tumors.* Cancer Cell, 2020. **37**(4): p. 543-550.
89. Porciani, D., L.N. Cardwell, K.D. Tawiah, K.K. Alam, et al., *Modular cell-internalizing aptamer nanostructure enables targeted delivery of large functional RNAs in cancer cell lines.* Nat Commun, 2018. **9**(1): p. 2283.
90. Juliano, R.L.J.N.a.r., *The delivery of therapeutic oligonucleotides.* 2016. **44**(14): p. 6518-6548.

91. Yoon, S. and J.J. Rossi, *Aptamers: Uptake mechanisms and intracellular applications.* Adv Drug Deliv Rev, 2018. **134**: p. 22-35.
92. Yoon, S., K.W. Huang, P. Andrikakou, D. Vasconcelos, et al., *Targeted Delivery of C/EBPalpha-saRNA by RNA Aptamers Shows Anti-tumor Effects in a Mouse Model of Advanced PDAC.* Mol Ther Nucleic Acids, 2019. **18**: p. 142-154.
93. Dowdy, S.F., *Overcoming cellular barriers for RNA therapeutics.* Nat Biotechnol, 2017. **35**(3): p. 222-229.
94. Baldwin, S.A., S.Y. Yao, R.J. Hyde, A.M. Ng, et al., *Functional characterization of novel human and mouse equilibrative nucleoside transporters (hENT3 and mENT3) located in intracellular membranes.* J Biol Chem, 2005. **280**(16): p. 15880-7.
95. Wang, C., T. Zhao, Y. Li, G. Huang, et al., *Investigation of endosome and lysosome biology by ultra pH-sensitive nanoprobes.* Adv Drug Deliv Rev, 2017. **113**: p. 87-96.
96. Le Large, T.Y.S., M.F. Bijlsma, G. Kazemier, H.W.M. van Laarhoven, et al., *Key biological processes driving metastatic spread of pancreatic cancer as identified by multi-omics studies.* Semin Cancer Biol, 2017. **44**: p. 153-169.
97. Qian, C.N., Y. Mei and J. Zhang, *Cancer metastasis: issues and challenges.* Chin J Cancer, 2017. **36**(1): p. 38.
98. Sun, X.X., M.S. Dai and H. Lu, *5-fluorouracil activation of p53 involves an MDM2-ribosomal protein interaction.* J Biol Chem, 2007. **282**(11): p. 8052-9.
99. Evan, G.I. and K.H.J.N. Vousden, *Proliferation, cell cycle and apoptosis in cancer.* 2001. **411**(6835): p. 342-348.
100. Li, S., K.R. Schmitz, P.D. Jeffrey, J.J. Wiltzius, et al., *Structural basis for inhibition of the epidermal growth factor receptor by cetuximab.* Cancer Cell, 2005. **7**(4): p. 301-11.
101. Mamot, C., D.C. Drummond, U. Greiser, K. Hong, et al., *Epidermal growth factor receptor (EGFR)-targeted immunoliposomes mediate specific and efficient drug delivery to EGFR-and EGFRvIII-overexpressing tumor cells.* 2003. **63**(12): p. 3154-3161.
102. Grasso, C., G. Jansen and E. Giovannetti, *Drug resistance in pancreatic cancer: Impact of altered energy metabolism.* Crit Rev Oncol Hematol, 2017. **114**: p. 139-152.
103. Zhang, N., Y. Yin, S.J. Xu, and W.S. Chen, *5-Fluorouracil: mechanisms of resistance and reversal strategies.* Molecules, 2008. **13**(8): p. 1551-69.
104. Mader, R.M., M. Müller and G.G. Steger, *Resistance to 5-fluorouracil.* General Pharmacology: The Vascular System, 1998. **31**(5): p. 661-666.

8. Appendix

8.1 List of tables

8.2 List of figures

9. Acknowledgments

I would like to dedicate my paper to all those who have offered me tremendous assistance during the three years in Munich.

Firstly, I would like to express my sincere gratitude to my supervisor Prof. Julia Mayerle for the continuous support of my study and related research. Her profound insight, valuable suggestions and constant encouragement taught me so much that they are engraved on my heart. Her meticulous attitude towards research manifests the personalities and qualities I should cultivate as a qualified scholar. I give my most genuine gratitude to her for her generous help and teaching.

Besides my supervisor, I would like to thank my co-supervisor Ph.D. Ujjwal M. Mahajan for his patience, motivation, and immense knowledge. His guidance helped me in all the time of research and writing of this thesis. Whenever we discussed problems during experiments, he always gave me precious suggestions that improved my critical thinking a lot.

Moreover, I would like to extend my gratitude to Ph.D. Ivonne Regel, M.D. Georg Beyer, Ahmed Alnatsha, Lisa Fahr and all my labmates in the lab of Department of Medicine 2, Hospital of University of Munich-Grosshadern. They have taught me many critical approaches and broadened my horizons and enriched my knowledge in this study. Their conscientious teaching will always be of great value to my future academic research.

Finally, I would like to extend my sincere gratefulness to my family and dear friends who have helped me and shared my worries, frustrations, and happiness. Their love is always the source of my strength during all my life. They taught me how to balance study and rest. Their encouragement and support have made my accomplishments possible.

LMU LUDWIG-MAXIMILIANS-UNIVERSITÄT MÜNCHEN

Dean's Office
Faculty of Medicine

MMRS

Affidavit

Li, Qi
Surname, first name

Marchioninistr.15 (IV E 00 309)
Street

81377, München
Zip code, town

Germany
Country

I hereby declare, that the submitted thesis entitled

Tumor-specific delivery of 5FU incorporated EGFR targeted aptamers induce cytotoxicity in pancreatic cancer cells

is my own work. I have only used the sources indicated and have not made unauthorised use of services of a third party. Where the work of others has been quoted or reproduced, the source is always given.

I further declare that the submitted thesis or parts thereof have not been presented as part of an examination degree to any other university.

Beijing , 24/05/2021
Place, date

Li Qi 李琦
Signature doctoral candidate